Kinetics of Gas Hydrate Nucleation and Growth

by

Hailu Kebede Abay

Thesis submitted in fulfilment of the
requirements for the degree of

DOCTOR OF PHILOSOPHY
(PhD)

University of
Stavanger

Faculty of Science and Technology
Department of Petroleum Engineering

2011

University of Stavanger
NO-4036 Stavanger
NORWAY
www.uis.no

Copyright © 2011 Hailu Kebede Abay

ISBN: 978-82-7644-463-6
ISSN: 1890-1387

Preface

My PhD dissertation comprises of six papers published in international journals and proceedings. Three of the six papers are published in the Journal of Energy & Fuels and the rest three in the proceedings of the 7th International Conference on Gas Hydrates. All these papers are preceded by a review followed by proposed future work. The papers are enumerated in chronological order based on the the dates of publication. I have used Roman numerals in listing and referencing the papers.

In Paper I, effect of ultralow concentration of methanol on methane hydrate formation is presented.
In Paper II, multicomponent gas hydrate nucleation and the effect of cooling rate and gas composition is presented. The methods of paper I has been employed.
In Paper III, effect of gas composition on structure II hydrate growth kinetics has been extended from the nucleation study of paper II.
In Paper IV, a time-dependent kinetic rate model has been proposed for the kinetics of methane hydrate formation.
In Paper V, promotional effect of PVCap on the nucleation of structure II hydrates is presented.
In Paper VI, the effect of PVCap on methane hydrate nucleation and growth is presented.

Most of these papers are definitely of great interest from both scientific and commercial perspectives as they have bearing on production and gas pipeline blockage issues. The methods I used are also important for further fundamental research on other similar systems especially for those who are interested on gas hydrate nucleation and growth processes.

Acknowledgments

I would like to express my sincere thanks to my supervisor Dr. Thor Martin Svartaas for his continuous supervision and valuable feedbacks. I would like to thank my co-supervisor Dr. Rune Time for his positive attitude for a help. NFR is also greatly acknowledged for the financial support of all my work through a PhD research fellow position.

All my studies were carried out at Stavanger University, Department of Petroleum Engineering. The Department has provided me a motivating environment during my study and I would like to thank all the academic and administrative staff members of the Department who supported me during the course of my study.

I would like also to thank Dr. Helge Hodne for his kind support in providing me the latex format for writing this dissertation. I would like to thank all the technicians of the Department of Petroleum Engineering, especially Sivert B. Drangeid, Svein Myhren, and Ola K. Siqveland, for their technical support in laboratory work and Latex writing.

I would like also to thank all my friends who encouraged me both academically and socially. Special thanks go to Desalegn Yeshitila and Ke Wei.

Last, but not least, I would like to thank my wife Yimegnushal Abebe, and two of my daughters, Hermella Hailu and Mariana Hailu, for their love and care. Without their support, I would have not been successful in my study and research.

List of papers

The following six papers are internationally published. All copies of the papers are enclosed in the appendix and referenced by their Roman numerals in this dissertation as follows:

I Hailu K. Abay and Thor M. Svartaas, *Effect of Ultralow Concentration of Methanol on Methane Hydrate Formation*, Energy & Fuels, **24**, 752-757, (2010).

II Hailu K. Abay and Thor M. Svartaas, *Multicomponent Gas Hydrate Nucleation: The Effect of the Cooling Rate and Composition*, Energy & Fuels, **25**, 42-51, (2011).

III Hailu K. Abay, Thor M. Svartaas and Ke Wei, *Effect of Gas Composition on sII Hydrate Growth Kinetics*, Energy & Fuels, **25**, 1335-1341, (2011).

IV Hailu K. Abay and Thor M. Svartaas, *On the Kinetics of Methane Hydrate Formation: A Time-dependent Kinetic Rate Model*, Proceedings of the 7th International Conference on Gas Hydrates, Edinburgh, United Kingdom, July 17-21, 2011.

V Hailu K. Abay, Eirik Hovring and Thor M. Svartaas, *Does PVCap Promote Nucleation of Structure II Hydrate?* Proceedings of the 7th International Conference on Gas Hydrates, Edinburgh, United Kingdom, July 17-21, 2011.

VI Hailu K. Abay, Jonas Hovland and Thor M. Svartaas, *The Effect of PVCap on Methane Hydrate Nucleation and Growth*, Proceedings of the 7th International Conference on Gas Hydrates, Edinburgh, United Kingdom, July 17-21, 2011.

Nomenclature

AAs	Antiagglomerants	
c_1	Concentration of component 1	
C_{kj}	Langmuir constant of species k in cavity j	
$D_{1,2}$	Interdiffusion coefficient of component 1 in component 2	
f_{gk}	Fugacity of gas component k	
Δg	Driving force for a critical nucleus	
J	Rate of nucleation	min^{-1}
J_q	Heat flux	
J_1	Mass flux of component 1	
k	Boltzmann constant	
k	Kinetic rate	min^{-1}
KHIs	Kinetic hydrate inhibitors	
LDHIs	Low dosage hydrate inhibitors	
MEG	Monoethylene glycol	
MeOH	Methanol	
M_w	Weight average molecular weight	
mL	Milliliter	
N	Average number of nuclei	
n	Number of moles of gas consumed	
Δn	Amount of gas hydrates formed	
n_w	Number of water molecules in unit cell	
p	Probability of nucleation	
P	Pressure	bar
P_{eq}	Equilibrium pressure	bar
P_m	Probability of forming m nuclei	
ΔP	Pressure drop	bar
PVCap	polyvinylcaprolactum	
PVP	Polyvinylpyrrolidone	
R	Average growth rate	

R	Universal gas constant	
rpm	Revolution per minute	
SNG	Synthetic natural gas	
T	Temperature	^{o}C
ΔT	Degrees of subcooling	^{o}C
$\Delta\mathrm{T}$	Hydrate depression temperature	^{o}F
THIs	Thermodynamic hydrate inhibitors	
t	Induction time	min
$\Delta\mathrm{t}$	Time interval in forming a nuclei	
V	Volume of gas	
V	Unit volume of N nuclei	
v_j	Number of type j cavities per water molecule	
v_w	Molar volume of water molecule in solution	
v_{hw}	Molecular volume of water molecule in hydrate	
W	Weight % of inhibitor	
W^*	Second derivative of activation energy at the critical size	
x	wt% of methanol	
y	Composition in gas phase	
y_1	Activity coefficient	
z	Compressibility factor	
τ	Lag time	min
θ_{kj}	Fractional filling of cavity j by molecule k	
$\Delta\varphi^*$	Activation energy for the formation of a critical size cluster	
λ	Eigenvalue of the product of growth matrix	
μ	Chemical potential	
σ	Entropy production	

Contents

Preface **iii**

Acknowledgments **v**

List of papers **vii**

Nomenclature **ix**

Contents **xi**

1 Introduction **1**
- 1.1 Gas Hydrates 1
- 1.2 Hydrate Formation 2
  - 1.2.1 Nucleation of Gas Hydrates 2
  - 1.2.2 Growth of Gas Hydrates 7
- 1.3 Gas Hydrate Issues 9
  - 1.3.1 Gas Hydrates as Threats 9
  - 1.3.2 Gas Hydrates as Opportunities 10
  - 1.3.3 Gas Hydrates as Nuisance 10

2 Objective **15**

3 Experimental Setup and Procedure **17**
- 3.1 Experimental Setup 17
- 3.2 Experimental Procedure 18

4 Main Results and Discussion **23**
- 4.1 Effect of MeOH, PVP and PVCap on Nucleation and Growth . . 23

4.2 Effect of Cooling Rate and Gas Compositions on Nucleation and Growth . . . 28
4.3 Time-dependent Kinetic Rate Model for Single-component Hydrate Growth . . . 33

5 Conclusion 37

6 Proposed Future Work 39

Bibliography 41

Appendix 50

A Paper I 51

B Paper II 61

C Paper III 75

D Paper IV 85

E Paper V 99

F Paper VI 107

Chapter 1

Introduction

1.1 Gas Hydrates

Gas hydrates are ice-like crystalline compounds that are composed of water molecules (host) with encaged gas molecules (guests). Despite gas hydrates look like ice, they are quite different from ice as they can exist at temperatures well above the ice point and also with their structures. The most common gas hydrate crystal structures are structure I (sI, cubic), structure II (sII, cubic), and structure H (sH, hexagonal) of which sII is the commonest. Physical and chemical properties of these structures are different [1]. The present work focuses only on sI and sII hydrates. Generally, these structures are composed of cavities formed from hydrogen-bonded water molecules where the guest molecule is trapped in the host. A specific number of water molecules is associated with each gas molecule due to the framework of the crystal type. For example, the ideal cubic unit cell of sI hydrate consists of two small pentagonal dodecahedron (5^{12}) cavities and six large tetrakaidecahedron ($5^{12}6^{2}$) cavities with a total of 46 water molecules. SII hydrate is composed of 16 small (5^{12}) cavities and 8 large hexakaidecahedron ($5^{12}6^{4}$) cavities with a total of 136 water molecules. Each cavity is formed from hydrogen-bonded water molecules. Fig. 1.1 shows 5^{12}, $5^{12}6^{2}$ and $5^{12}6^{4}$ cavities of sI and sII hydrates. The smallest cavity can accommodate one guest molecule of suitable size and shape but the largest cavity can accommodate two guests of suitable combination in size. At high pressures and at lower temperatures, the process of filling these cages by a guest molecule starts when hydrates begins to nucleate and grow which is called the process of hydrate formation.

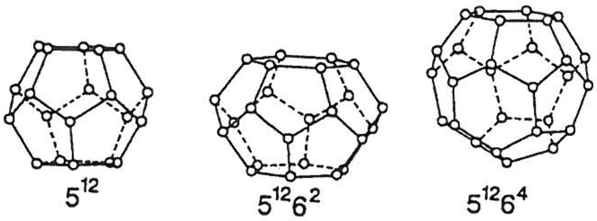

Figure 1.1: *Three different cavities of sI and sII hydrates.*

1.2 Hydrate Formation

Hydrate formation processes starts with encaging a guest into a host under suitable low temperature and high pressure conditions. Hydrate formation is physical rather than chemical in nature. The physical conditions required to form gas hydrates are guests and hosts with the correct conditions of low temperatures and high pressures. No strong chemical bonds are formed between the guest and the host. In fact, the guest molecule is free to rotate within the void spaces of the host. The process of hydrate formation has two major stages, nucleation and growth.

1.2.1 Nucleation of Gas Hydrates

Nucleation in general is a complex process especially before reaching a steady-state regime [2, 3, 4, 5, 6] where a steady-state nucleation occurs. Besides, it is a stochastic process [7] requiring many experiments to be performed on a system with the same experimental condition. Prediction of hydrate onset and deterministic approach on the process of nucleation is unlikely. Attempts in predicting when and where hydrate plugs form in flow lines [8] or limiting the stochastic nature of gas hydrate crystallization and increase data repeatability [9] have been made on hydrate formation processes. Induction time measurements for water droplets with hydrate memory could be shorter than the droplets without hydrate memory [10, 11] in sII hydrates. In fact, during a search for memory effect study in sI hydrates [12], it was proved that there was no evidence of a significant difference between the structure of water before and after the hydrate formation, nor in the water around the guest. Induction period was also shortened by the memory effect on the study [13] on the kinetics of sH hydrates. A recent investigation [14] also showed that a significant improvement in the reproducibility of induction times can be obtained by adding small amounts of impurities to the hydrate-forming system. However, the appearance of a critical nucleus from fresh water experiments is a very random process that cannot be predicted. For such random process of nucleation, probabilistic approach is more appropriate than deterministic approach due to the nature of the system.

The probability P_m of forming exactly m nuclei within a time interval Δt is given by the Poisson distribution law [15, 16]:

$$P_m = \frac{N^m exp(-N)}{m!} \tag{1.1}$$

where N(t) is the expected average number of nuclei within the interval Δt. From this equation, the probability P_0 to form $m = 0$ nuclei is $P_0 = exp(-N)$, the probability to form exactly 1 nucleus ($m = 1$) is $P_1 = Nexp(-N)$. Thus, the probability $P_{\geq m}$ to form at least m, i.e., m or more than m, nuclei within the interval Δt is:

$$P_{\geq m} = 1 - P_0 - P_1 - P_2 - ... - P_{m-1} = 1 - \sum_{0}^{m-1} P_i \tag{1.2}$$

Hence from Eqs. 1.1 and 1.2, we have:

$$P_{\geq m} = 1 - exp(-N) \sum_{i=0}^{i=m-1} \frac{N^i}{i!} \tag{1.3}$$

Employing Eq. 1.3, the probability $P_{\geq 1}$ that at least 1 nucleus has appeared in the time interval Δt is given by:

$$P_{\geq 1} = 1 - P_0 = 1 - e^{-N} \tag{1.4}$$

Now, the average number of nuclei N appeared in the time interval Δt and volume V is related to the stationary nucleation rate J as [17]:

$$N = JV\Delta t \tag{1.5}$$

Inserting the right hand side expression of Eq. 1.5 into Eq. 1.4, the probability $P'(\Delta t)$ that at least 1 nucleus has appeared in the time interval Δt becomes:

$$P'(\Delta t) = 1 - e^{-JV\Delta t} \tag{1.6}$$

Experimental detection of a nuclei requires that the formed nuclei in a solution have to grow to a detectable size which could result in a continuous intake of gas molecules into the solution. This causes a delay called the lag time τ between the time Δt of appearance of a nucleus and the time t of detection called the induction time. Thus, $\Delta t = t - \tau$, and inserting this expression into Eq. 1.6, the probability $P(t)$ of detecting hydrate crystals per unit volume at time t that were nucleated at earlier time becomes:

$$P(t) = 1 - e^{-J(t-\tau)} \tag{1.7}$$

Eq. 1.7 is called the nucleation probability distribution function where J the rate of nucleation, t is the induction time and τ is the corresponding lag time, which is the measure of the time necessary for the nucleation rate to attain a steady-state value. Before attaining the steady-state regime, the rate of nucleation has a transient regime that corresponds to the time required to attain a steady-state distribution of nuclei [18]. The probability distribution function of Eq. 1.7, could be applied to analyze nucleation experiments of crystals in general and gas hydrates in particular [19, 20, 21]. Other methods could also be applied. For example, the rate of nucleation could be determined by counting the total number of particles detected by cameras [22] or the method of laser light scattering by measuring the intensity of the scattered light during hydrate nucleation [23].

Nucleation is a microscopic phenomenon involving many molecules and too difficult to observe it experimentally. Despite the existence of alternative methods in studying nucleation, the method based on induction time measurement has a better advantage as induction time measurement bridges nucleation theory and experimental investigation [24]. This experimentally accessible induction time is the measure of the ability of a system to remain in the state of metastable equilibrium and contains valuable information about the kinetics of nucleation [25].

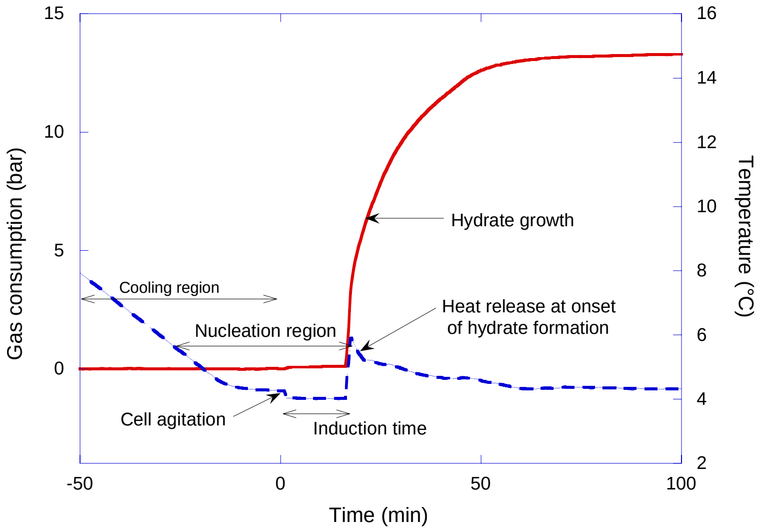

Figure 1.2: *Experimental measurement of induction time* t. *The solid red curve is the gas consumption in bars and the broken blue curve is the temperature of the system in* ^oC.

Thus, induction time experiments require careful measurements. Fig. 1.2 shows how an experimental induction time could be measured carefully from both gas consumption curve and the temperature pulse during hydrate formation. Before time zero, a system is allowed to cool down to the desired experimental temperature and pressure. At time zero, start of stirring or cell agitation is introduced to initiate hydrate formation. After some time, the hydrates start to grow which is detected by gas consumption rise accompanied by a temperature pulse as hydrate formation is an exothermic reaction that releases heat energy. The time taken by the system from the start of stirring to the onset of hydrate formation is the induction time. The nucleation stage may occur before the start of cell agitation during the cooling sequence [Paper I] in the overlapping region of Fig. 1.2 between the cooling and nucleation regions.

During the nucleation stage, reactant molecules start clustering before reaching a critical nuclei. Fig. 1.3 shows a conceptual figure showing some molecules rearranging themselves to form a critical nuclei. A detailed mathematical derivation on nucleation kinetics of multicomponent systems has been presented [26] based on cluster dynamics. Phase field theory of nuclei could also be applied in study-

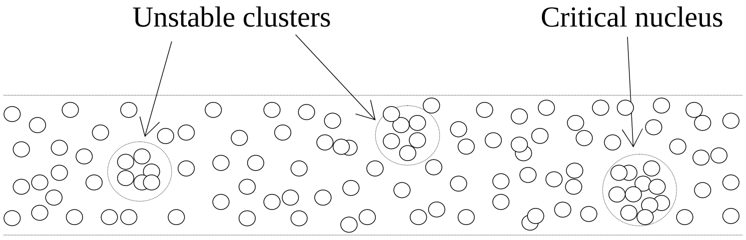

Figure 1.3: *Dynamics of reactant molecules during the formation of a critical nuclei [paper II].*

ing the kinetics of hydrate formation [27]. The cluster of a multicomponent critical nuclei generally contains a few hundred molecules [28], and the deriving force per unit cell for a multicomponent critical hydrate nucleus is give by [29]:

$$\Delta g = n_w[(v_w - v_{hw})(P - P_{eq}) - kT\sum_j v_j ln(\frac{1-\sum_k \theta_{kj}(T,P,y)}{1-\sum_k \theta_{kj}(T,P_{eq},y)})] \quad (1.8)$$

where n_w is the number of water molecules in a unit cell, v_w is the molar volume of water molecule in a solution, v_{hw} is the molecular volume of water in the hydrate (hydrate unit cell volume divided by the number of water molecules in the unit cell), P is pressure, T is temperature, k is the Boltzmann constant, v_j is the number of type j cavities per water molecule, y is the composition in the gas phase, and θ_{kj} is the fractional filling of cavity j by a type k molecule expressed as

$$\theta_{kj} = \frac{C_{kj} f_{gk}}{1+\sum_i C_{ij} f_{gj}} \quad (1.9)$$

where C_{kj} is the Langmuir constant for species k in cavity j, f_{gk} is the fugacity of gas component k in the gas phase in equilibrium with the hydrate, and the summation is for all species except water. The driving force for nucleation of multicomponent gas hydrates depends on hydrate phase composition [30] besides temperature, pressure, and gas phase composition. Theoretical papers [31, 32, 33, 34] have discussed how to evaluate the work of formation of the critical nucleus, the size of the nucleus and the thermodynamics of crystal nucleation in multicomponent systems. The rate of nucleation is related with the nucleation work [35] which derives the system to start forming and filling the cavities. Once the system starts filling of the cavities continuously in accordance with Eq. 1.9, then the nucleation stage starts transforming to the hydrate growth region shown in Fig. 1.2 after the onset point.

1.2.2 Growth of Gas Hydrates

The hydrate growth stage is an immediate process that follows the nucleation stage. A very simple but powerful method of studying and analyzing growth experiments is by using the real gas equation:

$$PV = znRT \tag{1.10}$$

where P is pressure, V is gas volume, z is the compressibility factor, n is the number of moles, R is the universal gas constant and T is the temperature of the gas. For an isochoric system, where the principle of mass conservation holds true, the pressure drop in the gas phase caused by hydrate growth gives an estimation of the amount of hydrates formed in the liquid phase. Thus, Eq. 1.10 yields:

$$\Delta n = \frac{V}{zRT}\Delta P \tag{1.11}$$

where Δn is the amount of gas consumed during hydrate formation (amount of hydrates formed) and ΔP is the measured experimental pressure drop caused by hydrate formation. Approximating the term $\frac{V}{zRT}$ as the constant of proportionality which does not change significantly, we have:

$$\Delta n \propto \Delta P$$

indicating that the amount of gas consumed in the liquid phase and the pressure drop in the gas phase are directly proportional with each other. This concept could be employed to estimate the amount of gas hydrates formed in filling the cavities of Fig. 1.1 for sI and sII systems when the systems meet the appropriate conditions for gas hydrate growth.

Growth processes are very fast reactions specially during the early growth periods. It involves coupled mass and heat transfer since the nucleation stage.

Primarily it is limited by mass transfer of the reactants to the growing crystal and a simultaneous removal of heat away from the growing crystal. Such coupled heat and mass transfer is a complex process to explain especially for a multicomponent system. A two-component coupled heat and mass transfer process is the simplest system to describe mathematically. Assuming transport of heat and mass in a radial direction, the entropy production in a two-component system is given by [36]:

$$\sigma = J_q \frac{\partial}{\partial r}(\frac{1}{T}) + J_1(-\frac{1}{T}\frac{\partial \mu_{1,T}}{\partial r}) \tag{1.12}$$

where J_q is heat flux, J_1 is mass flux of component 1 and $\mu_{1,T} = \mu_1^0 + RTln(c_1 y_1)$ is chemical potential with a reference state μ_1^0, c_1 is concentration of component 1 with y_1 as its activity coefficient. Heat is transported in the system by convection and conduction. The radial flux-force relations for measurable heat flux and molar flux are given by:

$$J_q = l_{qq}\frac{\partial}{\partial r}(\frac{1}{T}) + l_{qu}(-\frac{1}{T}\frac{\partial \mu_{1,T}}{\partial r}) \tag{1.13}$$

and

$$J_1 = l_{uq}\frac{\partial}{\partial r}(\frac{1}{T}) + l_{uu}(-\frac{1}{T}\frac{\partial \mu_{1,T}}{\partial r}) \tag{1.14}$$

where $\frac{\partial}{\partial r}(\frac{1}{T})$ and $(-\frac{1}{T}\frac{\partial \mu_{1,T}}{\partial r})$ describe the forces. From Onsager's reciprocity relations [37, 38], the coefficient l_{qu} is equal to the coefficient l_{uq} and are used to describe the diffusive transport of heat and mass. If temperature is constant, then:

$$\frac{\partial}{\partial r}(\frac{1}{T}) = 0 \tag{1.15}$$

and hence Eq. 1.14 becomes:

$$J_1 = -l_{uu}\frac{1}{T}\frac{\partial \mu_{1,T}}{\partial c_1}\frac{\partial c_1}{\partial r} \tag{1.16}$$

which could be reexpressed as:

$$J_1 = -D_{1,2}\frac{\partial c_1}{\partial r} \tag{1.17}$$

where $D_{1,2}$ is the interdiffusion coefficient of component 1 (the solute) in component 2 (the solvent) which could be measured by spectroscopic and analytical techniques. Because hydrate nucleation and growth require transport of a solute in a solvent towards the growing hydrate crystal, diffusion of molecules play an important role both in the nucleation and growth stages. But, mass transport by diffusion in n-component mixture is described by n(n-1)/2 diffusion coefficients, and hence multicomponent systems are too difficult to explain as compared to the simplest two-component system described by Eq. 1.17. Such application of irreversible thermodynamics with more accurate flux equations is very important in modeling of chemical processes [39].

1.3 Gas Hydrate Issues

Generally, gas hydrate issues could be categorized into three groups depending on where the hydrates are located and on the nature of the hydrate formation. Gas hydrates are threats for the environmental researchers, opportunities for others as they are the future energy source and a means of gas storage and transport, and nuisance for the oil and gas industries.

1.3.1 Gas Hydrates as Threats

Gas hydrates, containing mostly methane, have been formed naturally in the earth and exist in vast quantities in the permafrost and subsea sediments in the Arctic, the Antarctic, the tropical and subtropical oceans [40, 41, 42]. Despite the difference of reports on the amount of gas hydrates in nature amongst researchers, it is believed that 10^{16} m^3 of methane gas exists in solid hydrate form [43]. A more recent study [44] estimated a total volume of 1.2 $\times 10^{17}$ m^3 of methane gas that is globally distributed in ocean sediments which is larger than worldwide conventional natural gas reserves. This enormous amount of methane gas in the hydrate state in the earth could easily be released into the atmosphere if triggered by geological phenomenon such as earth quakes. Gas hydrates, containing primarily methane which is a strong greenhouse gas, are thus environmental threats as they have the potential to change the earth's climate leading to increased global warming.

1.3.2 Gas Hydrates as Opportunities

Contrary to the environmental threat, the enormous reserve of methane gas in the hydrate state is considered as the future energy source. The estimates of the volume of methane gas contained in gas hydrate state is double that of known fossil-fuel resources [45]. Besides, the ability of gas hydrates to contain 150-180 volumes of gas/volume of hydrate [46] makes them to be considered as a means for natural gas storage and transport. However, practical exploitation of this opportunity requires an ability to preserve the hydrate in a predictable and controllable manner [47]. Storage of CO_2 in natural gas hydrate reservoirs and at the same time releasing the hydrocarbon gas trapped in the hydrate state could be considered as double opportunities [48]. Thus, being fuel for the future and means of transporting and storing natural gases, gas hydrates are opportunities to alleviate problems related with these issues. In fact, getting the gas out of the natural hydrate state or storing the gas in a hydrate state is a challenge that has attracted many researchers. Gas storage and transportation based on hydrate technology has been a focus for many researchers [49, 50, 51, 52, 53]. Specially storing hydrogen molecule in semi-clathrate hydrates with an energy density comparable to the current fossil fuel has become an opportunity for hydrogen powered vehicles [54, 55, 56, 57].

1.3.3 Gas Hydrates as Nuisance

Gas hydrate as a nuisance in the petroleum industry by plugging oil and gas production pipelines and causing costly operations was first discovered and reported by Hammerschmidt [58]. Since then, the industrial hydrate concerns have been in flow assurance which is the major technical problem in offshore development, production, and transportation. Besides production pipelines, the well and the platform are also susceptible portions of the system where hydrate plugs occur [59]. With regard to flow assurance, the focus has then become in inhibiting hydrate formation before hydrates form and block pipelines. If hydrates form and block pipelines, then dissociating them in a safe way is also a challenge as hydrates possess an enormous amount of gas which could cause a hydrate projectile that may endanger human life.

In preventing hydrate blockage, thermodynamic hydrate inhibitors (THIs) and low dosage hydrate inhibitors (LDHIs) have been successfully used. THIs are divided into three classes: alcohols, glycols and salts of which methanol (MeOH, CH_3OH) and monoethylene glycol (MEG, $HOCH_2CH_2OH$) are the most widely used inhibitors in the gas and oil fields due their effectiveness. The wellhead jumpers and flow lines are parts of the system where, for example methanol, is being added to inhibit the formation of hydrates [60]. When used in large amounts, THIs prevents hydrate crystallization by shifting the phase boundary thermodynamically to the lower temperature and higher pressure. To approximate the hydrate depression temperature for several THIs in the aqueous liquid, the industry uses the original Hammerschmidt equation [61]:

$$\Delta T = \frac{2335W}{M_w(100 - W)} \tag{1.18}$$

where ΔT is the hydrate depression in ^oF, M_w is the molecular weight of alcohol or glycol, and W is the $wt\%$ of the inhibitor in the liquid. From Eq. 1.18, the molecular weight of THIs is the key parameter for the inhibition performance. Thus, MeOH is a better inhibitor than MEG as it has a lower molecular weight which could result in a higher performance of inhibition. Hammerschmidt provided also a modification of the molecular weight M when salts were used as inhibitors. Later study [62] showed that the Hammerschmidt equation applies only to methanol concentrations less than 0.2 mol fraction, and presented the following equation as an improved version applicable for a wider range as large as 0.8 mol fraction:

$$\Delta T = -129.6ln(1 - x_{MeOH}) \tag{1.19}$$

where ΔT is the hydrate temperature depression below the uninhibited condition in ^oF. All these equations are used for prevention methods before the hydrates form and plug pipelines.

Once the hydrate is formed, it could be dissociated either by depressurization or heating methods. Fig. 1.4 shows three possible mechanisms of moving the red circular point, which is within the hydrate forming region (left of the equilibrium curve), into the hydrate free region (right of the equilibrium curve). The method of inhibition by shifting the phase boundary across the red circular point leaves that specific point to be on the right side of the hydrate equilibrium curve. This method is the method how THIs prevent hydrate formation provided that THIs are used in large amounts.

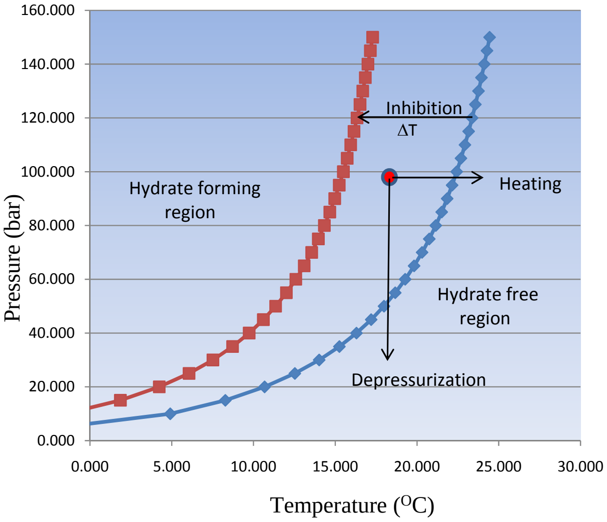

Figure 1.4: *An equilibrium curve showing the hydrate forming region with three possible ways of moving a particular initial condition, represented by the red spot, out of the hydrate forming region. The data has been generated using CSMGem with 0 and 15 wt% MeOH, where the presence of methanol caused the equilibrium curve to shift to the left.*

Unlike the conventional THIs which acts in shifting the phase boundary to low temperature and high pressure regions, a recent method of retarding crystal growth were achieved by using LDHIs [63] that do not significantly affect the thermodynamics but the kinetics of hydrate formation. LDHIs are divided into two classes, kinetic hydrate inhibitors (KHIs or simply KIs) and antiagglomerants (AAs). KIs are low molecular weight water-soluble polymers such as polyvinylpyrrolidone (PVP) and polyvinylcaprolactum (PVCap), and AAs are surfactants (surface acting chemicals). KIs prevent nucleation and growth of hydrate crystals, whereas AAs do not prevent formation rather they prevent the agglomeration and deposition of hydrate crystals and the consequent hydrate blockage while a transportable hydrate slurry is formed. Both KIs and AAs do not always inhibit hydrate blockage. Studies on KIs [64] and AAs [65, 66, 67] showed that KIs and AAs sometimes promote hydrate formation depending on the concentration of the chemicals used along with other system conditions. It was reported [68] that AAs property decreases in the presence of salt water which indicates that the efficiency of additives in general may depend also on the water salinity.

Another alternate method of addressing hydrate problems in pipelines without using chemicals such as THIs, KHIs, and AAs or without the help of heating methods or heat-retention schemes is the cold flow technology [69, 70, 71, 72]. Cold flow technology is emerging as a good candidate for actual field implementation and alleviating hydrate blockage problems in an uninsulated pipelines. In cold flow methods, inert hydrate particles are readily transportable in cold regions, say 4 ^oC, without deposition or agglomeration surviving long shut-ins and restarts without plugging pipelines during flow conditions favoring hydrate formations. The basic concept of cold flow technology is mixing hot reservoir fluid coming out of the wellhead with a recirculating cold stream of hydrate particles acting as seed crystals. This converts all fresh water into inert hydrates enabling the inhibited water not to form sticky hydrates and hence yielding hydrate particles which are dry, non-depositing, and non-agglomerating.

Chapter 2

Objective

The knowledge of the dynamics of gas hydrate formation, nucleation and growth, is very important in determining the parameters for production of gas hydrates and in understanding plug conditions in oil and gas production pipelines [73]. This has drawn a considerable attention in the petroleum industry and in research institutes as hydrate plugging on production pipelines causes costly operations. In spite of many attempts in understanding nucleation and growth kinetics, still little is known about the process as compared to hydrate thermodynamics. The main reason is that hydrate nucleation and growth is a time-dependent processes that is challenging with regard to measurement and modeling [74] and hence the kinetics of hydrate nucleation and growth is much less understood than the thermodynamics [75]. Thus, the objective of the present study has been achieving a better understanding of nucleation and growth processes, and identifying the key factors that are involved in the kinetics. For this, multicomponent hydrate formation has been given much intention in the study as single-component hydrate studies [76, 77, 78, 79, 80, 81, 82] have been addressed well as compared to the multicomponent studies. This is essential in strengthening the knowledge of multicomponent hydrate formation processes as these processes, specifically sII hydrate nucleation and growth, are the processes encountered in the oil and gas production pipelines. Single-component studies have also been covered, and a new time-dependent model has been proposed for the formation process. The interpretation of nucleation and growth measurements made in the laboratory and presented in this dissertation are believed to help others to understand the most challenging processes of nucleation and growth kinetics.

Chapter 3

Experimental Setup and Procedure

3.1 Experimental Setup

The schematic experimental setup used for testing all the nucleation and growth experiments of this review is shown in Fig. 3.1. Similar high-pressure isochoric apparatus was discussed previously for kinetic hydrate inhibitor (KHI) performance test [83]. The cylindrical cell was made of titanium with inner volume of 145 ml from which 50 ml of the cell volume was filled with distilled water (DIW) with or without additives depending on the the objective of the experiment. The rest 95 ml of the cell volume was filled with synthetic natural gas (SNG). Temperature and pressure sensors had direct access to the inner part of the cell where the sample fluid was present. A 1/10 DIN Pt100 element of accuracy 0.03 ^{o}C was connected to a digital signal transmitter for temperature measurements. A Rosemount 3051 TA absolute pressure transmitter was used for pressure readings. The accuracy of the transmitted temperature and pressure signals were $\pm$ 0.1 ^{o}C and $\pm$ 0.2 bar, respectively. In some of the experiments, two temperature sensors were used, one in the vapor phase and the other in the aqueous phase. This enabled us to track the temperature pulse both in the vapor phase and in the aqueous phase during gas consumption and hydrate growth.

The cell was equipped with a cylindrical cooling cap, and water from a refrigerated circulator passed through this cap to control the cell temperature. The

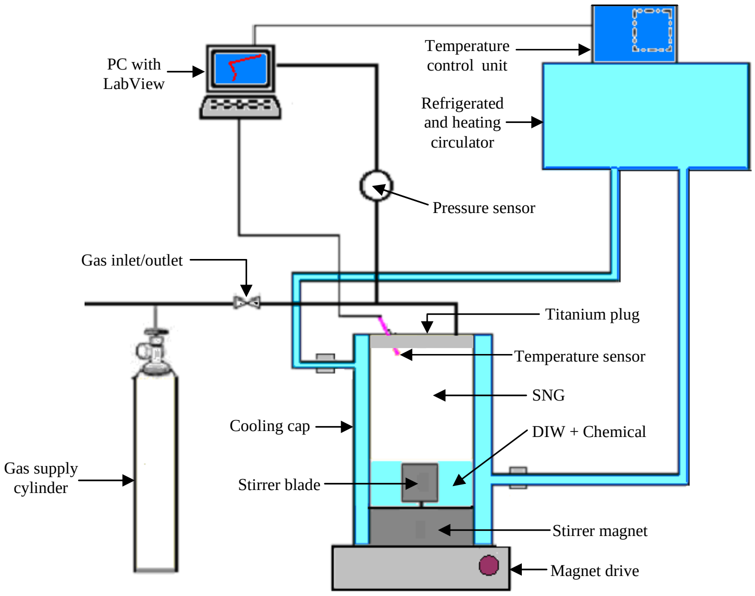
Temperature control unit
PC with LabView
Refrigerated and heating circulator
Pressure sensor
Gas inlet/outlet
Titanium plug
Temperature sensor
SNG
Cooling cap
DIW + Chemical
Gas supply cylinder
Stirrer blade
Stirrer magnet
Magnet drive

Figure 3.1: *Experimental setup drawing.*

refrigerated and heating circulator used was Julabo F34 HL "High Tech" series with integrated programmer and temperature stability of ± 0.01 ^{o}C. The temperature profiles were handled by the integrated programmer, and the internal bath temperature could be logged via an RS 232 interface connection. LabView was used to collect system pressure and temperature data points and PT plots were continuously updated by the PC on the LCD screen during the experiment.

3.2 Experimental Procedure

More or less similar procedures have been used in all the experiments by changing operating P and T conditions. Some of the procedures are without any chemicals and some with chemicals depending on the objective of the experiment. For those experiments with chemicals in solution, three different chemicals, MeOH (liquid), PVP (dry powder, Mw ∼ 15,000) and PVCap (dry powder, Mw ∼ 6,000) were selected and dissolved in distilled water to the desired concentrations in ppm (parts per million by weight). 100 ppm corresponds to 3.12×10^{-3} mol/litre of MeOH or 1.67×10^{-5} mol/litre of PVCap or 6.67×10^{-6} mol/litre

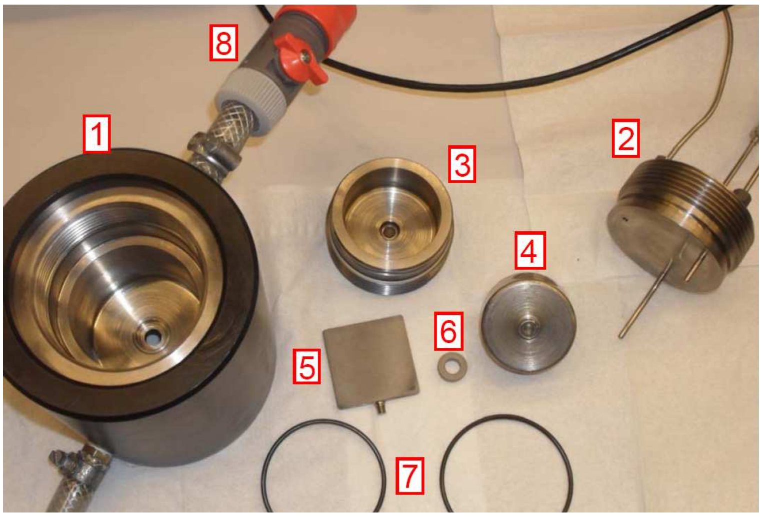

Figure 3.2: *Components of the inside part of the autoclave cell. 1 is main cell body with cooling cap, 2 is top lid with two T sensors, 3 is magnet housing (cell bottom), 4 is magnet holder, 5 is stirrer blade, 6 is sliding bearing for balance of stirrer blade and magnet holder when mounted, 7 are o-ring sealing for top lid (2) and magnet housing (3) and (8) are quick-fit connections for cooling water with closing valve (Gardena type).*

of PVP. Pure water was considered as 0 ppm baseline for comparison.

Fig. 3.2 shows the inside part of the autoclave cell and the inside cell components. Referring to the figure, the stirrer blade (5) and the magnet holder (4) were connected through the hole for the connecting axle at the cell bottom. The magnet housing (3) was filled with a desired solution to displace all dead volume air in the gap between the magnet housing and the magnet holder during mounting of this section. Excess water solution displaced from the magnet housing into the experimental cell section during this mounting was removed prior to filling the desired amount of solution into the cell. Thereafter, the top lid (2) was mounted and the cell was closed and centered on the magnet drive as shown in Fig. 3.3. This figure shows a photograph of the experimental setup which was represented schematically by Fig. 3.1. The cooling bath was connected via the quick-fit connections (8) and their valves were opened to allow in and out flow of cooling water around the main cell body (1). The bath was adjusted to a desired initial temperature of an experiment, which was kept constant at the

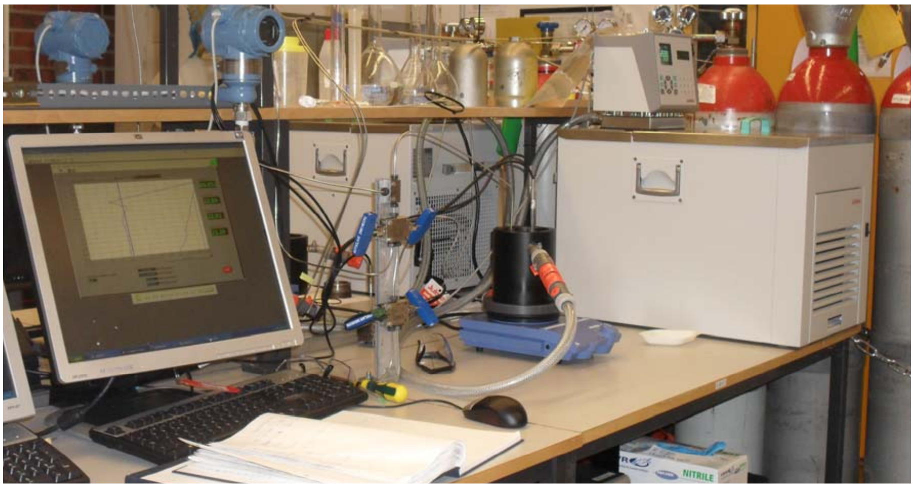

Figure 3.3: *Photograph of experimental apparatus.*

desired level during the preparation of the experiment. After mounting, the cell was purged twice with 40 bar gas to remove residual air from the cell yielding 40 × 40 = 1600 × dilution. Totally, three different gas supply cylinders with three different synthetic natural gases (SNGs) were used for the study of the present work. Molar compositions of each SNG are given in Table 3.1.

Table 3.1: *Gas compositions of SNGs used in mole percentage.*

Gas component	SNG1 (mol%)	SNG2 (mol%)	SNG7 (mol%)
CH_4 (methane)	99.9995	92.51	80.40
C_2H_6 (ethane)	0	0	10.30
C_3H_8 (propane)	0	7.49	5.00
i-C_4H_{10} (*i*-butane)	0	0	1.65
n-C_4H_{10} (*n*-butane)	0	0	0.72
CO_2 (carbon dioxide)	0	0	1.82
N_2 (nitrogen)	0	0	0.11

After dilution, the cell was stirred for a while to purge residual air that is present in the water solution. The amount of gas used was controlled by two pressure gauges, one gauge from the gas cylinder and another gauge connected to the inlet at the top of the cell. After purging was completed, the cell was pressurized to a desired pressure based on the objective of the experiment. The system was left without stirring and cooling for the temperature and pressure values to stabilize. At this time, pressure leak test was done simultaneously. The stabilized filling pressure and temperature values were taken as the initial condition of the system. The initial condition of temperature and pressure lies in the hydrate free region for all experiments. As thermal history of water affects the induction time measurement [84], the distilled water used in all experiments were fresh and initially at room temperature with the same thermal history prior to loading of the cell. After loading, the cell was then cooled down without stirring to a desired temperature using a certain cooling rate depending on the type of the experiment and the bath was programmed to keep the desired temperature level throughout the continuing part of the experiment. Having obtained a stable temperature and pressure at the desired level, cell agitation was introduced by the start of the stirrer at 750 rpm.

A stirring rate of 750 rpm was used in all the experiments as induction time is affected by stirring rate [85]. The start of stirring was considered as the start of the experiment at time zero. Induction time and formation rate are also dependent on the degree of subcooling in both uninhibited and underinhibited systems [86]. Thus, the same degree of subcooling was maintained during the experiments after stabilized values of temperature and pressure were attained. The stabilized values of temperature and pressure remained constant from time zero to the onset of hydrate formation. After onset of hydrate formation, all experiments were given enough time to complete the hydrate growth process before the experiments were terminated by heating the system and dissociating the hydrates in the cell. Prior to the next series of experiments, all the components of the autoclave cell were disassembled as shown in Fig. 3.2 and cleaned twice with distilled water and dry air.

Chapter 4

Main Results and Discussion

The kinetics of hydrate nucleation and modeling of hydrate growth required a lot of experiments to be performed. The following results and discussions are based on many experimental data with an extensive theoretical discussions and fitting of the observed experimental results. To be able to evaluate the kinetics of nucleation and growth, the stochastic approach of classical nucleation theory and the real gas equations have been employed primarily. To obtain sufficient statistical accuracy, a minimum number of 6 experiments are required for nucleation study. In the present PhD work, a total number of 6 to 10 parallel experiments were normally run at each condition during nucleation studies. The main results of the thesis on the kinetics of gas hydrate formation are presented in three parts, nucleation and growth studies with chemicals, without chemicals and modeling.

4.1 Effect of MeOH, PVP and PVCap on Nucleation and Growth

The effect of MeOH on hydrate formation has been studied on sI methane hydrates. As there was no question on the inhibition effect of MeOH at high concentrations, the system in question was studied for low concentrations of MeOH. Low concentrations of MeOH studies have attracted researchers especially from the report [87] that underinhibition using methanol at low concentrations enhanced the rate and amount of hydrates formed in a multicomponent fluid.

	number of experiments				
concentration (ppm)	done (< 36 h)	terminated (> 36 h)	ΔP (±std dev[a])	J (min^{-1})	τ_o (min)
0	7	0	35.13 (±2:00)	2.28×10^{-3}	−53
1.5	10	2	31.26 (±0:44)	2.71×10^{-3}	61.18
5	8	1	32.79 (±2:38)	2.43×10^{-3}	27.6
10	10	0	31.49 (±0:53)	3.09×10^{-3}	−32.26
20	6	5	31.08 (±1:09)	6.54×10^{-3}	247.9

[a] Standard deviation.

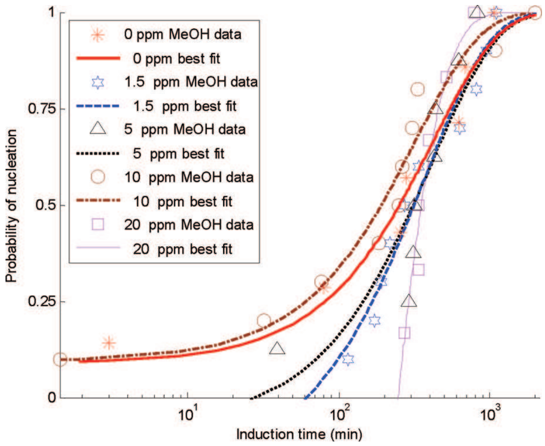

Figure 4.1: *Nucleation probabilities vs induction time for ultralow concentration of methanol. The above table shows the pressure drop, nucleation rate, and induction time for each concentration [paper I]*

Low concentration of methanol was initially assumed to stabilize both sI and sII structures but later studies verified no sign of encaging methanol molecule [88, 89]. Another study [90] on thin-film vapor deposits of methanol with water showed that methanol can readily form mixed clathrate hydrates within a certain temperature range. Further study [91] on MeOH showed that low concentration of methanol in aqueous solution increased hydrate stabilization. However, other experimental studies indicated that thermodynamic stability did not increase with the presence of small amounts of methanol but inhibiting effect was observed [92]. Promotional effects of deuterated methanol were also clearly observed on the kinetics of hydrate formation [93]. Our investigation on methanol also supports both inhibition and promotion effects on methane hydrate formation [paper I]. The role of MeOH on hydrate crystallization could be due to three possible mechanisms: lattice defects, temperature dependent forces, and surface tension effect.

Excluding 1.5 and 5 ppm MeOH the results showed that the nucleation rate increases with increasing concentration of MeOH at this ultra low concentration level refereing to the table associated with Fig. 4.1. At 20 ppm MeOH the lag time showed significant increase. The negative lag times observed for pure water and 10 ppm MeOH could be due to nucleation taking place during the cooling sequence or non ideal fit of experimental values to the probability distribution function. Boundary conditions could be set to eliminate negative lag times, but nucleation could occur prior to defined time zero for the experiment at start of stirring.

The hydroxyl group of methanol has an effect by hydrogen bonding with water molecules, whereas the methyl group tends to organize the water molecules in direct competition for a hydrate guest. This may cause a lattice defect as lattice defects caused by guest-water hydrogen bonding in other systems have been reported [94] and a distorted lattice structure may enhance diffusion that could possibly affect hydrate formation process. Another possible explanation of methanol effect on the kinetics could be through the temperature-dependent attractive and repulsive forces that could disturb the system's behavior. In a dilute aqueous solution of alcohols, a study [95] showed that alcohol molecules have temperature-dependent attractive and repulsive forces, that affect the activity coefficient of alcohol and water. This may have an effect on the kinetics of sII hydrate formation since the kinetic rate is dependent on the temperature of the system described by the Arrhenius equation. Methanol molecules could also be easily taken up into hydrogen bonding network of water to form substitution-type clusters [96]. Surface tension effects could also be a third possible mechanism. During a molecular dynamics study [97] on methanol-water mixtures, it was observed that the surface tension of the solution was greatly reduced by adding a small amount of methanol to water. As hydrate formation requires transporting of guest molecules from the gas phase to the growing cluster in the liquid phase, the reduction in surface tension may have an effect on the formation process. Trace amounts of other classes of alcohols such as ethanol have been reported [98] in optimizing formation rates of, for example, methane hydrate aggregates.

The effects of the KIs (PVP and PVCap) we used have shown a clear effect on the nucleation and growth kinetics. Experimental [99, 100] and simulation [101, 102] studies have reported the good performance of PVCap as compared to PVP. PVCap has a better attachment to the surface of a growing crystal resulting in retardation of hydrate formation. In fact, the optimal performance of PVCap depends on a certain concentration at a given pressure [103] i.e., increasing concentration of PVCap does not always increase inhibition performance. The growth inhibition by PVCap is a result of polymer adsorption to an active growing crystal surface where the adsorbed molecule is acting as a barrier for further growth [104]. PVP does not adsorb to the surface of a hydrate crystal, but only increases the surface energy of the interfacial region [105]. Because transporting the reactants to the growing product is a significant factor [106] for hydrate growth kinetics, PVP could easily affect this factor by increasing the surface energy of the interfacial region and PVCap by binding to an actively growing structure and result in delay for the growth process. But inhibiting effect of PVCap is at high concentration and promotional effects could be observed at low concentrations depending on system pressure and volume. For example, in our study [paper V] on sII system at 90 bars, PVCap was found to be a good promoter in the range 50−500 ppm, and a good inhibitor in the range 1000−3000 ppm as shown in Fig. 4.2.

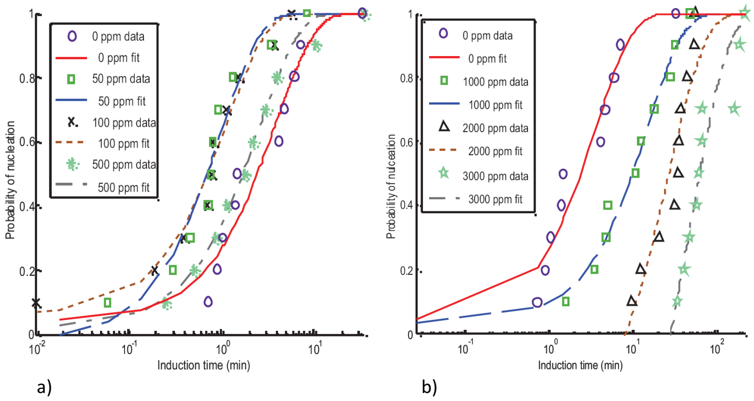

a) b)

Figure 4.2: *Probability of nucleation versus induction time for: a) 0, 50, 100 and 500 ppm and b) 0, 1000, 2000 and 3000 ppm PVCap [paper V].*

Fig. 4.3 indicated that nucleation rate has a minimum in the region between 1000 and 2000 ppm PVCap and that the lag time (induction time) was relatively short until the concentration exceeded 1000 ppm. A significant increase in lag time was observed for 2000 and 3000 ppm PVCap, while nucleation rate

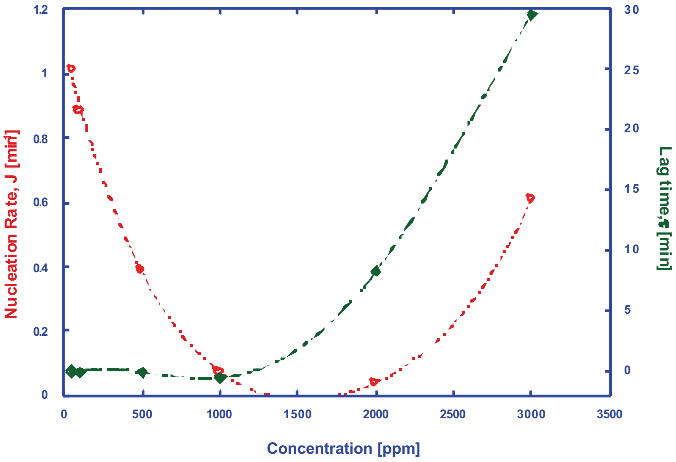

Figure 4.3: *Nucleation rate (left axis, red curve), and lag time (right axis, green curve) as function of PVCap concentration [paper V].*

showed a significant increase in the region between 2000 and 3000 ppm. At concentrations less than 1000 ppm, catastrophic fast growth (i.e. fast, exothermic reaction) occurred immediately after onset. At 1000 ppm the initial growth rate was considerably reduced and the catastrophic growth was delayed by approximately 1 minute. At 2000 ppm the catastrophic growth was delayed by approximately 10 minutes and at 3000 ppm catastrophic growth was not reached within the normal duration of the experiments (between 15 and 24 hours). In one experiment with 3000 ppm run over a weekend catastrophic growth occurred after 67.8 hours. In other words, increasing concentration from 2000 ppm to 3000 ppm, doesn't increase inhibition performance with respect to nucleation, but there was a tremendous increase in the prevention of growth. In a previous study [103] on effective inhibitors for natural gas hydrates, it was reported that optimal performance of PVCap depends on a certain concentration at a given pressure. On other systems such as sI hydrates, the promotion or inhibition effects of PVCap were primarily dependent on the random nature of newly born critical nuclei that could trigger the PVCap start acting on the system [paper VI].

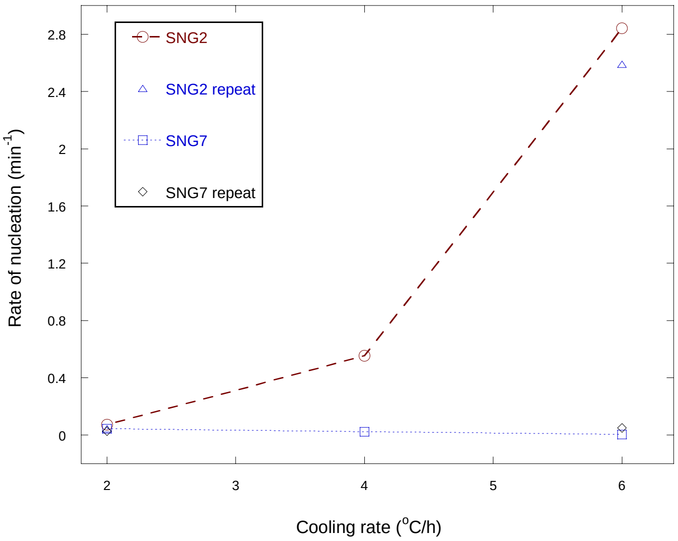

Figure 4.4: *Rate of nucleation versus cooling rate for SNG2 and SNG7 [paper II].*

4.2 Effect of Cooling Rate and Gas Compositions on Nucleation and Growth

The effects of THIs and KHIs on the kinetics of hydrate formation have been a focus whereas gas composition itself as a kinetic parameter has never been investigated with and without additives. While the main focus is investigating the effect of gas composition on sII hydrate growth kinetics, we also studied the effects of low concentrations of MeOH, PVP, and PVCap on the kinetics. Hence, another goal of this PhD study was to investigate the effect of cooling rate and gas compositions on nucleation and growth of gas hydrates without additives. Such findings on system responses are very important for a reliable evaluation of the effect of additives on hydrate formation processes. SNG2 and SNG7 of Table 3.1 have been used in studying the effect of gas composition on the kinetics of sII hydrate formation and on the stochastic nature of nucleation. For cooling rate effects, three different cooling rates of 2, 4 and 6 °C/h have been used, keeping other parameters that could affect the kinetics the same for both SNG2 and SNG7. The result of the effect of gas composition and cooling rates on nucleation is plotted in Fig. 4.4. The experimental results showed that the rate of nucleation is dependent on gas composition, and different gas compositions responded differently on the same cooling rate. For the slower cooling rate of 2 °C/h, the rates of nucleation in both systems were of comparable magnitude at the selected P and T conditions. However, for the faster cooling rate of 6 °C/h, SNG2 gave increased nucleation rate while the nucleation rate was reduced for SNG7.

The observed results of Fig. 4.4 could be explained in three ways: the dependence of the critical size on temperature and gas composition, chemical oscillations due to solubility change of individual gas components, and coupled mass and heat fluxes during cooling. It is known that some molecules saturate the liquid water at the experimental temperature and pressure and hence the liquid in equilibrium with hydrate is not pure water [107]. Natural gases actively dissolve in water and solubility of natural gases decrease with increasing molecular weight of hydrocarbons. The presence of inorganic gases like carbon dioxide and nitrogen could affect the solubility of the natural gas in water. The presence of the acid gas CO_2 in SNG7 increases the solubility of the hydrocarbon gases in water, whereas the presence of the other inorganic gas N_2 decreases the gas solubility in water [108]. In our SNG7, the N_2 content is very low (0.11 %) and effects of nitrogen on solubility can most probably be neglected. The system pressure also changes in accordance with the real gas equation when the temperature changes. The change in the temperature and pressure of the system induces a change in the solubility of the components in both SNG2 and SNG7. The main reason is that solubility of gas in water depends on temperature, the partial pressure of the gas over the liquid water, the nature of the solvent and the nature of the gas from Henry's solubility law. The hydrate formation process could change the solubility of the organic gases and may show divergence from the normal Henry's law of solubility [109]. Inorganic gases may also change the solubility trend in the presence of hydrates. Solubility of CO_2 increases with decreasing temperature in the absence of gas hydrate but this trend gets reversed in the presence of gas hydrates i.e., solubility of CO_2 decreases with decreasing temperature in the hydrate formation region [110].

The chemical potential of each molecule in the cluster will also affect the solute concentration at which the n-sized cluster can coexist with the solution which is called cluster solubility [111]. The dynamics of clusters play a major role in the kinetics of nucleation [112]. All these conditions make SNG7 difficult to equilibrate the system easily as compared to SNG2, where only two hydrocarbon molecules are present. Since hydrate formation in the bulk water is like "vacuuming" of dissolved gas from the water phase to the region of the growing

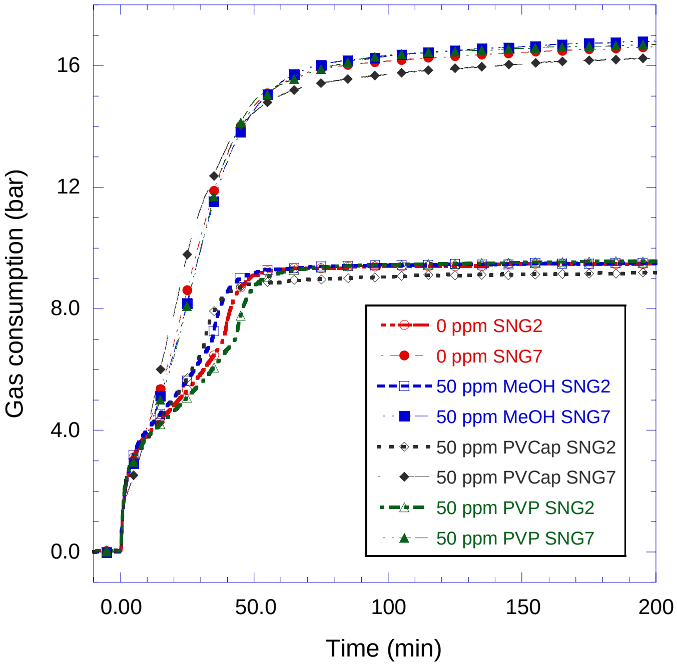

Figure 4.5: *Gas consumption vs time for 50 ppm additives. The amount of sII hydrate formed from SNG7 (filled symbols) is nearly double that of SNG2 (open symbols), regardless of the additives [paper III].*

cluster in the water phase, solubilities of SNG2 and SNG7 play the major role for the rate of nucleation. Besides, hydrate nucleation rate in the water phase is determined mainly by the flux of dissolved gas to the surface of a growing cluster in the water phase. These dissolved gases may show oscillating reaction during nucleation. Chemical oscillations involving nucleation and growth of bubbles from a solution in other systems were reported [113] and their mechanisms were discussed. Chemical oscillations due to solubility of components in SNG7 could possibly result in a reduced nucleation rate as compared to SNG2.

It is also possible that the cooling rate as well as the individual concentration of components at the site of nucleation affect the critical size during nucleation. In a study [114] of heating rate effects on transient nucleation problems, the survival size dependence on heating rate has been discussed. In the discussion, it is pointed out that a critical size depends on temperature. Besides cooling, the

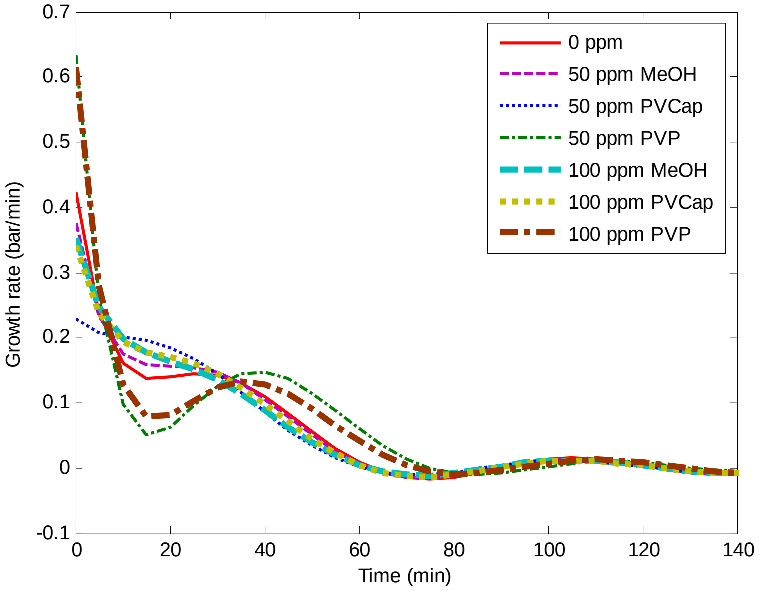

Figure 4.6: *Growth rate versus time curves of SNG2 experiments for 50 and 100 ppm concentrations of MeOH, PVP and PVCap [paper III].*

presence of an additive could also change solubility of gas species [115] which in turn may affect the rate of nucleation in the region of the growing cluster leading to even a more complex processes that are challenging to describe. The effect of composition difference on the growth process is more simple to explain as compared to the nucleation process. For example, Eq. 1.11 could easily be employed in analyzing the results of Fig. 4.5. One can clearly see that the amount of sII hydrates formed from SNG7 was nearly twice of the amount of hydrate formed from SNG2 with and without the additives. Similar difference was observed for experiments with 100 ppm additives in solution implying that difference in gas composition matters for the amount of hydrate formation. The main reason why SNG7 produced more hydrates than SNG2 and thus gave greater pressure drop could be explained by the gas compositions and the individual content of large cavity preferring components in the mixtures. Both systems are water excess and the conversion of water into sII hydrate is limited by the amount of sII formers available.

Fig. 4.6 shows the growth rate curves of sII hydrates produced from SNG2.

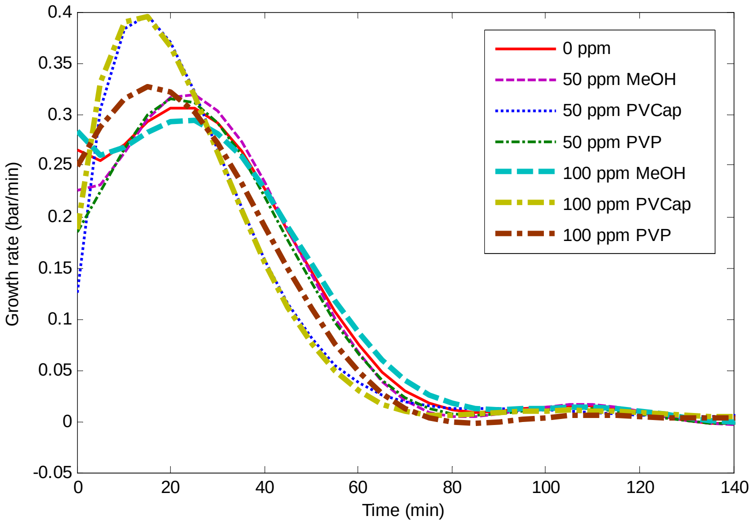

Figure 4.7: *Growth rate versus time curves of SNG7 experiments for 50 and 100 ppm concentrations of MeOH, PVP and PVCap [paper III].*

Time zero represents onset for hydrate formation. For SNG2 maximum growth rate occurred at onset, and then growth rates for all SNG2 systems decayed over the next 18−20 min after onset. In this period, the rates showed fluctuations before finally decaying towards zero value at the end of the process. The structure of the growth curves of SNG7 was also different as compared to the structure of the growth curves of SNG2. As shown in Fig. 4.7, the growth rates of sII hydrate produced from SNG7 initially increased to attain a maximum value, and then decreased to zero. Such differences in growth patterns for the same hydrate structure could be considered as a finger print of the effect of gas composition on growth kinetics. These sII hydrate growth curve structures were unique for each SNG, and the effects of the additives on these growth curves were shifting the curves up or down based on the concentration and type of the chemicals used while the unique structure remained the same. The increased initial growth rate of sII hydrate produced from SNG2 as compared to the hydrate produced from SNG7 could be due to the large number of critical nuclei in SNG2 as compared to SNG7. In a multicomponent gas hydrate nucleation study [116] of sII hydrates from both SNG2 and SNG7, it was shown that SNG2 system nucleates more easily than SNG7 system. Moreover, as discussed before on the difference of the total amount of hydrate formation from SNG2/SNG7, more options of guest molecules for $5^{12}6^4$ cage fillings may contribute to an increased overall hydrate formation. Despite its promotion on hydrate formation, more options of guest molecules available in SNG7, however, may reduce the growth rate, especially during the starting period of the growth process. With abundant guest molecules in both SNGs for $5^{12}6^4$ cage fillings, $5^{12}6^4$ cage fillings may become the rate-limiting step in hydrate formation. The multiple $5^{12}6^4$ cage filling molecules (ethane, propane, *i*-butane, *n*-butane, carbon dioxide and nitrogen) in SNG7 may compete with each other in occupying $5^{12}6^4$ cages and thus reduce the initial growth rate in an observable manner. Ethane as the main large cavity filling gas was discussed previously [117, 118, 119, 120].

4.3 Time-dependent Kinetic Rate Model for Single-component Hydrate Growth

The growth rate is expressed as the rate by which the amount of gas molecule is converted to hydrate [121]. Another goal in this dissertation is thus investigating the dependence of growth rates on the driving force and modeling hydrate formation. A comprehensive review [122] on modeling of hydrate formation kinetics showed that growth models considered a constant kinetic rate parameter for many reasons. The reason for having time-dependent kinetic rate could be explained in terms of the driving force of the system. The driving force could be the difference in chemical potential [123, 124, 125] or the degree of subcooling. In fact, the degree of subcooling does not represent the real driving force in all systems, but in systems with one type of guest molecule, single-component systems, the driving force for hydrate formation is proportional to the degree of subcooling over a wide pressure range [126].

Though the degree of subcooling is a good representative of the driving force, it is not constant during the whole growth period of hydrates as shown in Fig. 4.8. The figure shows the PT path from onset of hydrate growth at an initial subcooling of $\Delta \mathrm{T}_{initial} = 4$ °C, to the end of the growth process in the vicinity of the hydrate equilibrium curve at $\Delta T_{final} = 0$ °C. The rate of hydrate growth is a function of the degree of subcooling while the degree of subcooling is not actually constant during growth. A study [127] on methane hydrate formation indicated that formation rates are dependent on the degree of subcooling. Methane hydrate film growth studies [128, 129, 130, 131] on the rate of formation also showed the dependence of the rate of hydrate growth on the degree of subcooling used. A flow loop experiment study [132] also used the degree of subcooling as the driving force for hydrate formation, and the formation rate was found proportional to the driving force. In addition to these studies, a heat transfer modeling study [133] showed an explicit dependence of the rate of methane hydrate formation on the degree of subcooling. Such time-dependent driving force may suggest a time-dependent kinetic rate $k(t)$, which could be derived from PVT relation as:

$$k_3 = \frac{-1}{t} ln(\frac{PV}{zn_oRT}) \tag{4.1}$$

where n_o is the initial number of moles of the free gas, k_3 is a kinetic rate constant in the late growth region (region 3 of Fig. 4.8), and t is the time. This gives the kinetic rate of single-component hydrate formation at any time for the first-order reaction in the late growth region.

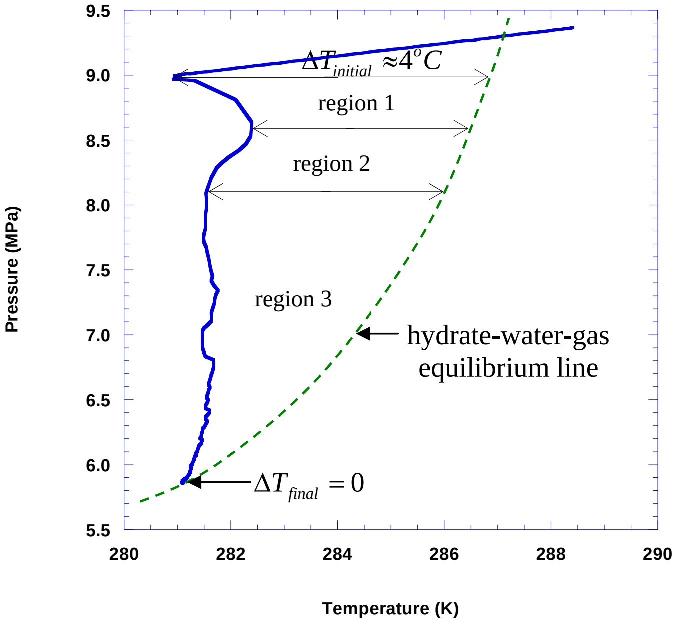

Figure 4.8: *Variation of the degree of subcooling during hydrate growth [paper IV].*

Originally, the kinetic rate parameter based on the theories of crystallization and mass transfer at a gas-liquid interface [134] accounts for the combined diffusion and reaction of the guest molecule during the modeling of hydrate formation. Another paper [135] indicated that changing the magnitude of the kinetic rate parameter has an effect on the rate and gas consumption. During a mechanistic model studies [136] for hydrate formation, different rate constants within a single experiment were reported. Hence, a good advantage of the proposed model may be that it gives information about the kinetic rate from the easily accessible thermodynamic conditions of the system at any time during hydrate formation. However, the present model was tested for a stirring rate of 750 rpm, and it does not include the effect of rpm on the rate constant. It is reported [137, 138] that stirring rate has an effect on the rate of methane hydrate crystallization. The inverse time dependence of Eq. 4.1 shows that the kinetic rate decreases as time increases, which could be explained by the reduction in the driving force with time. One, thus, could express the decreasing hydrate growth in the liquid water phase by employing the time-dependent rate as

$$r = -n_o k_3 \tag{4.2}$$

where k_3 is given by Eq. 4.1. This model, Eq. 4.2, predicts the hydrate growth rate for the pure water reference and for systems with THIs and KIs in solution. The model still requires to be certified and/or improved on other systems at different operating P and T conditions.

Chapter 5

Conclusion

My PhD research was focused on the kinetics of sI and sII hydrate formation mainly nucleation and growth. Both single and multicomponent systems have been considered in studying the nucleation and growth processes. The effect of methanol on the kinetics of sI hydrate has been studied from pure methane gas (SNG1). The effects of chemicals (MeOH, PVP, PVCap) and gas composition on the kinetics of sII hydrate formation have been investigated by using two different multicomponent gases, SNG2 and SNG7. Other factors that could affect the kinetics such as initial degree of subcooling, operating T and P, stirring rate, type and molecular weights of the chemicals were all kept constant to examine the effect of the gas composition alone.

The nucleation probability distribution function, the real gas equation, and the principle of irreversible thermodynamics have been employed in an attempt to understand the experimental results. The most important results can be concluded as follows: The dependence of the critical size on temperature and gas composition, chemical oscillations due to solubility change of individual gas components and coupled mass and heat fluxes during cooling were the possible explanation for the reason that the two-component system (SNG2) nucleated easily as compared to the seven-component system (SNG7). However, on the process of hydrate formation after nucleation, SNG7 favored the growth of sII hydrate as compared to SNG2. For all aqueous solutions, the amount of hydrate formed from SNG7 was twice the amount of hydrate formed from SNG2 due to concentration differences in the large $5^{12}6^4$ cavity preferring gas components in the mixtures.

The effects of the additives MeOH, PVP, and PVCap on the structure of the growth curves have also been studied. Growth rate curves of sII hydrates produced from SNG2 and SNG7 were different. The additives only shifted the growth curves of sII hydrates formed from both SNG2 and SNG7. The growth curves of SNG2 and SNG7 were unique for each composition, and this unique curve structure was not affected by the presence of the additives confirming that gas composition itself played a major role in sII hydrate growth kinetics.

Promotion and inhibition effects of thermodynamic (MeOH) and kinetic (PVCap) inhibitors were also studied in underinhibited systems for both sI and sII hydrates. Concentration dependent effects on the nucleation of sI hydrate was not observed on both chemicals when the chemicals were used in small amounts due to the stochastic nature of nucleation besides other factors such as temperature-dependent long-range forces, lattice defects and surface tension effects. The effect of PVCap on growth was clear and concentration dependent up to a certain limit. However, increasing concentration did not increase growth inhibition as the chemical had an optimal performance at a certain concentration as at a given pressure. A time-dependent kinetic rate model has been proposed for the formation of sI hydrate crystals. Both MeOH and PVCap have been tested on the model and the model reflects the effects of the chemicals on sI hydrate growth. The model could be utilized for testing the effect of other additives.

Chapter 6

Proposed Future Work

Despite its importance, researchers have been focusing on effects of chemicals for studying the kinetics of hydrate formation. Through measurements and intensive theoretical studies, we have confirmed that difference in gas composition affects nucleation and growth kinetics. Such effects are very important for a reliable evaluation of the effects of THIs and KHIs on hydrate formation kinetics. The effect of gas composition studies on nucleation and growth kinetics were done by using only two types of gases with a specific molar composition requiring further studies on different systems.

Different types of gases with different molar compositions would be of great interest in continuing further investigation of gas composition effects and hence determining the role of each molecule by carefully selecting the types of molecules which may affect the kinetics strongly. Changing experimental conditions and the method of the procedures used in this study would also be a good future work. Temperature dependent processes are unpredictable and changing the operating P and T conditions and the degrees of subcooling may give a clue for a novel research. The proposed time-dependent kinetic rate model could also be proved or disproved on different systems in different operating conditions.

Bibliography

[1] Sloan E. D. *Energy Fuels.* **1998**, *12*, 191-196.

[2] Frade, J. R.; Kharton, V. V.; Lopez, D. M.; Nunez, P.; Abrantes, J. C. C. *Thermochim. Acta* **2005**, *435*, 85-91.

[3] Kelton, K. F.; Geer, A. L.; Thompson, C. V. *J. Chem. Phys.* **1983**, *79*, 6261.

[4] Kelton, K. F.; Narayan, K. L.; Levine, L. E.; Cull, T. C.; Ray, C. S. *J. Non-Cryst. Solids* **1996**, *204*, 13-31.

[5] Davis, M. J. *J. Am. Ceram. Soc.* **2001**, *84*, 492-496.

[6] Frade, J. R.; Queiroz, C. M.; Fernandes, M. H. *J. Non-Cryst. Solids* **2004**, *333*, 271-277.

[7] Wilson P. W.; Lester, D.; Haymet, A. D. J. *Chem. Eng. Sci.* **2005**, *60*, 2937-2941.

[8] Boxall, J.; Davies, S.; Koh, A.; Sloan, E. D. *Predicting when and where hydrate plugs form in oil-dominated flowlinws*, SPE 129538, Offshore Technology Conference, Houston, 5-8 May 2008, pp 80-86.

[9] Duchateau, C.; Peytavy, J. L.; Glenat, P.; Pou, T. E.; Hidalgo, M.; Dicharry, C. *Energy Fuels.* **2009**, *23*, 962-966.

[10] Sarshar, M.; Esmaeilzadeh, F.; Fathikaljahi, J. *Oil and Gas Science Technology - Rev. IFP.* **2008**, *63*, 657-667.

[11] Deng-lin, S.; Qiang, W.; Bao-yong, Z. *J. Coal Science Engineering.* **2008**, *14*, 280-282.

[12] Buchanan, P.; Soper, A. K.; Thompson, H.; Westacott R. E.; Creek, J. L.; Hobson, G.; Koh, C. A. *J. Chem. Phys.* **2005**, *123*, 164507-1−164507-7.

[13] Lee, J. D.; Susilo, R.; Englezos, P. *Energy Fuels.* **2005**, *19*, 1008-1015.

[14] Jensen, L.; Thomsen, K.; Solms, N. V. *Energy Fuels.* **2011**, *25*, 17-23.

[15] Toschev, S.; Milchev, A.; Stoyanov, S. *J. Cryst. Growth.* **1972**, *13/14*, 123-127.

[16] Alexander Milchev. *Electrocrystallization. Fundamentals of Nucleation and Growth*; Kluwer Ac. Publ.: Norwell, Massachusetts, 2002; p 165.

[17] Jiang, S. and Ter Host, J. H. *J. Cryst. Growth Des.* **2011**, *11*, 256-261.

[18] Frade, J. R.; Queiroz, C. M.; Fernandes, M. H. *J. Non-Cryst. Solids.* **2004**, *333*, 263-270.

[19] Tsuchiyama, A. *Am. Mineral.* **1983**, *68*, 687-698.

[20] Takeya, S.; Hori, A.; Hondoh, T.; Uchida, T. *J. Phys. Chem. B.* **2000**, *104* (17), 4164-4168.

[21] Abay, H. K.; Svartaas, T. M. *Energy Fuels.* **2010**, *24*, 752-757.

[22] Osegovic, J. P.; Tatro, S. R.; Holman, S. A.; Ames, A. L.; Max, M. D. *J. Pet. Sci. Eng.* **2007**, *56*, 42-46.

[23] Parent, J. S.; Bishnoi, P. R. *Chem. Eng. Comm.* **1996**, *144*, 51-64.

[24] Nguyen, T. N. P.; Kim, K.-J. *Int. J. Pharm.* **2008**, *364*, 1-8.

[25] Kashchiev, D.; Firoozabadi, A. *J. Cryst. Growth.* **2003**, *250*, 499-515.

[26] Vehkamaki, H. *Classical Nucleation Theory in Multicomponent Systems*; Springer: Berlin, Heidelberg, 2006; pp 97−113.

[27] Kvamme, B.; Graue, A.; Aspenes, E.; Kuznetsova, T.; Granasy, L.; Toth, G.; Pusztai, T. Tegze, G. *Phys. Chem. Chem. Phys.* **2004**, *6*, 2327-2334.

[28] Wilemski, G. *J. Chem. Phys.* **1983**, *80*, 1370-1372.

[29] Anklam, M. R.; Firoozabadi, A. *J. Chem. Phys.* **2004**, *121* (23), 11867-11875.

[30] Abbas, I. A.; Mohsen, V. S.; Farshad, V. *Iran. J. Chem. Chem. Eng.* **2007**, *26* (2), 63-70.

[31] Oxtoby, D. W.; Kashchiev, D. *J. Chem. Phys.* **1994**, *100* (10), 7665-7671.

[32] Debenedetti, P. G.; Reiss, H. *J. Chem. Phys.* **1998**, *108* (13), 5498-5505.

[33] Laaksonen, A.; McGraw, R.; Vehkamaki, H. *J. Chem. Phys.* **1999**, *111* (5), 2019-2027.

[34] Djikaev, Y. S.; Tabazadeh, A.; Reiss, H. *J. Chem. Phys.* **2003**, *118* (14), 6572-6581.

[35] Nishioka, K.; Kusaka, I. *J. Chem. Phys.* **1992**, *96* (7), 5370-5376.

[36] Kjelstrup, S.; Bedeaux, D.; Johannesen, E. *Elements of Irreversible Thermodynamics for Engineers*; Tapir Academic Press: Trondheim, 2006; p 34.

[37] Onsager, L. Phys. Rev. **1931**, *37*, 405-426.

[38] Onsager, L. Phys. Rev. **1931**, *38*, 2265-2279.

[39] Taylor, R.; Krishna, R. *Multicomponent Mass Transfer*; Willy: New York, 1993.

[40] Chersky, N. J.; Makogon, Y. F. *Oil Gas Int.* **1970**, *10* (8), 82-84.

[41] Makogon, Y. F.; Trebin, F. A.; Trofimuk, A. A.; Tsarev, V. P.; Chersky, N. V. *Dokl. Acad. Sci.: USSR-Earth Sci. Sect.* **1972**, *196*, 197-200.

[42] Peter Englezos. *Ind. Eng. Chem. Res.* **1993**, *32*, 1251-1274.

[43] Kvenvolden, K. A. *Chem. Geol.* **1988a**, 41-51.

[44] Klauda, J. B.; Sandler, S. I. *Energy Fuels.* **2005**, *19*, 459-470.

[45] Prensky S. *A review of gas hydrates and formation evaluation of hydrate-bearing reservoirs*, SPWLA 36th Annual Logging Symposium, 26-29 June 1995, pp 1-12.

[46] Sun, Z. G.; Ma, R. S.; Wang, R. Z.; Guo, K. H.; Fa, S. S. *Energy Fuels.* **2003**, *17*, 1180-1185.

[47] Stern, L. A.; Cirone, S.; Kirby, S. H.; Durham, W. B. *Energy Fuels.* **2001**, *15*, 499-501.

[48] Kvamme, B.; Graue, A.; Buanes, T.; Kuznetsova, T.; Ersland, G. *J. Greenhouse Gas Control I.* **2007**, 236-246.

[49] Gudmundsson, J. S.; Brrehaug, A. In *Proceedings of the 2nd International Conference on Natural Gas Hydrates,* Toulouse, France, June 2-6, 1996; pp 439-446.

[50] Khokhar, A. A.; Sloan, E. D. *Fluid Phase Equilib.* **1998**, *150-151*, 383-392.

[51] Zhong, Y.; Rogers, R. E. *Chem. Eng. Sci.* **2000**, *55*, 4175-4187.

[52] Gudmundsson, J. S. In *Proceedings of the 4th International Conference on Natural Gas Hydrates,* Yokohama, Japan, May 19-23, 2002; pp 997-1002.

[53] Guo, Y. K.; Fan, S. S.; Guo, K. H.; Chen, Y. In *Proceedings of the 4th International Conference on Natural Gas Hydrates,* Yokohama, Japan, May 19-23, 2002; pp 1040-1043.

[54] Lokshin, K. A.; Zhao, Y.; Mao, W. L.; Mao, H.; Hemley, R. J.; Lobanov, M. V.; Greenblatt, M. In *Proceedings of the 5th International Conference on Gas Hydrates,* Trondheim, Norway, June 12-16, 2005.

[55] Strobel, T. A.; Taylor, C. J.; Hester, K. C.; Miller, K. T.; Koh, C. A.; Sloan, E. D. In *Proceedings of the 5th International Conference on Gas Hydrates,* Trondheim, Norway, June 12-16, 2005.

[56] Strobel, T. A.; Kim, Y.; Koh, C. A.; Sloan, E. D. In *Proceedings of the 6th International Conference on Gas Hydrates,* Vancouver, Canada, July 6-10, 2008.

[57] Sugahara, T.; Hashimoto, S.; Mori, H.; Sakamoto, J.; Ogata, K.; Ohgaki, K. In *Proceedings of the 6th International Conference on Gas Hydrates,* Vancouver, Canada, July 6-10, 2008.

[58] Hammerschmidt, E. G. *Ind. Eng. Chem.* **1934**, *26*, 851.

[59] Sloan, E. D. *Hydrate Engineering*, Monograph 21; Society of Petroleum Engineers: Richardson, TX, 2000; p 5.

[60] Cooley, C.; Wallace, B. K.; Gudimetla, R. In the *SPE Annual Technical Conference and Exhibition*, Denver, Colorado, October 5-8, 2003; SPE 84350.

[61] Hammerschmidt, E. G. *Gas* **1939**, *15* (5), 30.

[62] Nielsen, R. B; Bucklin, R. W. *Hydrocarbon Process* **1983**, *62* (4), 71-78.

[63] Kelland, M. A. *Energy Fuels.* **2006**, *20*, 825-847.

[64] Abay, H. K.; Hovring, E.; Svartaas, T. M. In *Proceedings of the 7nd International Conference on Gas Hydrates,* Edinburgh, Scotland, United Kingdom, July 17-21, 2011; pp xxx-yyy.

[65] Karaaslan, U.; Parlaktuna, M. *Energy Fuels.* **2000**, *14*, 1103-1107.

[66] Karaaslan, U.; Parlaktuna, M. *Energy Fuels.* **2002**, *16*, 1387-1391.

[67] Karaaslan, U.; Parlaktuna, M. *Energy Fuels.* **2002**, *16*, 1413-1416.

[68] Sinquin, A.; Arla, D.; Prioux, C.; Peytavy, J. L.; Glenat, P.; Dicharry, C. *Energy Fuels.* **2008**, *22*, 721-728.

[69] Larsen, R.; Lund, A.; Andersson, V.; Hjarbo, K. W. In *The SPE Annual Technical Conference and Exihibition,* New Orleans, Louisiana, Sept. 30 - Oct. 3, 2001; SPE 71550.

[70] Wolden, M.; Lund, A.; Oza, N.; Makogon, T.; Argo, C. B.; Larsen, R. In *Proceedings of the 5th International Conference on Gas Hydrates,* Trondheim, Norway, June 12-16, 2005.

[71] Larsen, R.; Lund, A.; Argo, C.; Makogon, T. In *The 18th International Oil Field Chemistry Symposium,* Geilo, Norway, March 25-28, 2007.

[72] Larsen, R.; Lund, A.; Hjarbo, K. W.; Wolden, M. In *The 20th International Oil Field Chemistry Symposium,* Geilo, Norway, March 22-25, 2009.

[73] Makogon, Y. F. *Hydrates of Natural Gas*; Penn Well Publishing Company: Tulsa, OK, 1981; p 82.

[74] Sloan, E. D.; Koh, C. A. *Clathrate Hydrates of Natural Gases*, 3rd ed.; CRC Press/Tayler & Francis: Boca Raton, FL, 2008; p 180.

[75] Sum, A. K.; Koh, C. A.; Sloan, E. D. *Ind. Eng. Chem. Res.* **2009**, *48*, 7457-7465.

[76] B. Kvamme. In *Proceedings of the 2nd International Conference on Natural Gas Hydrates,* Toulouse, France, June 2−6, 1996; pp 139−146.

[77] B. Kvamme. *Ann. NY Acad. Sci.* **2000**, *912*, 496−501.

[78] Kashchiev, D.; Firoozabadi, A. *J. Cryst. Growth.* **2002**, *243*, 476-489.

[79] B. Kvamme. *Int. J. Offshore Polar Eng.* **2002**, *12* (4), 256−263.

[80] Kashchiev, D.; Firoozabadi, A. *J. Cryst. Growth.* **2002**, *241*, 220-230.

[81] Davies, S. R.; Hester, K. C.; Lachance, J. W.; Koh, C. A.; Sloan, E. D. *Chem. Eng. Sci.* **2009**, *64* , 370-375.

[82] Kashchiev, D.; Borissova, A.; Hammond, R. B.; Roberts, K. J. *J. Cryst. Growth.* **2010**, *312*, 698-704.

[83] Villano, L. D.; Kommedal, R.; Fijten, M.W.M.; Schubert, U. S.; Hoogenboom, R.; Kelland, M. A. *Energy Fuels.* **2009**, *23*, 3665-3673.

[84] Vysniauskas, A.; Bishnoi, P. R. *Chem. Eng. Sci.* **1983**, *38*, 1061-1072.

[85] Skovborg, P.; Ng, H. J.; Rasmussen, P. *Chem. Eng. Sci.* **1993**, *48* (3), 445.

[86] Hemmingsen, P. V.; Li, X.; Kinnari, K. In *Proceedings of the 6th International Conference on Gas Hydrates,* Vancouver, British Columbia, Canada, July 6-10, 2008.

[87] Yousif, M.; Austvik, T.; Berge, L.; Lysne, D. In *Proceedings of the 2nd International Conference on Natural Gas Hydrates,* Toulouse, France, June 2-6, 1996; pp 291-298.

[88] Nakayama, H.; Hashimoto, M. *Bull. Chem. Soc. Jpn.* **1980**, *53* (9), 2427-2433.

[89] Davidson, D. W.; Gough, S. R.; Ripmeester, J. A.; Nakayama, H. *Can. J. Chem.* **1981**, *59*, 2587-2590.

[90] Williams, K. D.; Devlin, J. P. *J. Molecular Structure.* **1997**, *416*, 277-286.

[91] Berecz, E.; Balla-Achs, M. *Studies in Inorganic Chemistry. 4. Gas Hydrates*; Elsevier Science Publishers B. V.: Amesterdam, The Netherlands, 1983; pp 95-109.

[92] Svartaas, T. M.; Fadnes, F. H. In *Proceedings of the 2nd International Offshore and Polar Engineering Conference,* San Francisco, USA, June 14-19, 1992; pp 614-619.

[93] Bobev, S.; Tait, K. T. *Am. Mineral.* **2004**, *89*, 1208-1214.

[94] Alavi, S.; Susilo, R.; Ripmeester, J. A. *J. Chem. Phys.* **2009**, *130*, 174501-1−174501-9.

[95] Nord, L.; Tucker, E. E.; Christian, S. D. *J. Solution Chem.* **1984**, *13* (12), 849-867.

[96] Ohtake, M.; Yamamoto, Y.; Kawamura, T.; Wakisaka, A.; Souza, W. F.; Freitas, A. M. V. *J. Phys. Chem. B* **2005**, *109*, 16879-16885.

[97] Chang, T. M.; Dang, L. X. *J. Phys. Chem. B.* **2005**, *109* (12), 5759-5765.

[98] Chen, P. C.; Huang, W. L.; Stern, L. A. *Energy Fuels.* **2010**, *24*, 2390.

[99] Zeng, H.; Lu, H.; Huva, E.; Walker, V. K.; Ripmeester, J. A. *Chem. Eng. Sci.* **2008**, *63*, 4026-4029.

[100] Zhang, J. S.; Lo, C.; Couzis, A.; Somasundaran, P.; Wu, J.; Lee, J. W. *J. Phys. Chem. C* **2009**, *113*, 17418-17420.

[101] Kvamme, B.; Kuznetsova, T.; Aasoldsen, K. *J. Mol. Graphics and Modeling.* **2005**, 23, 524-536.

[102] Anderson, B. J.; Tester, J. W.; Borghi, G. P.; Trout, B. L. *J. Am. Chem. Soc.* **2005**, *127*, 17852-17862.

[103] Lederhos, J. P.; Long, J. P.; Sum, A.; Christiansen, R. L.; Sloan, E. D. *Chem. Eng. Sci.* **1996**, *51*, 1221-1229.

[104] Larsen, R.; Knight, C. A.; Sloan, E. D. *Fluid Phase Equilibria.* **1998**, *150-151*, 353-360.

[105] Moon, C.; Hawtin, R. W.; Rodger, P. M. *Faraday Discuss.* **2007**, *136*, 367-382.

[106] Buch, V.; Devlin, J. P.; Monreal, I. A.; Cwiklik, B. J.; Aytemiz, N. U.; Cwiklik, L. *Phys. Chem. Chem. Phys.* **2009**, *11*, 10245-10265.

[107] Anderson, G. K. *J. Chem. Thermodyn.* **2004**, *36*, 1119-1127.

[108] Makogon, Y. F. *Hydrates of Hydrocarbons*; PennWell Publishing Company: Tulsa, OK, 1997; pp 65−70.

[109] Song, K. Y.; Feneyrou, G.; Fleyfel, F.; Martin, R.; Lievois, J.; Kobayashi, R. *Fluid Phase Equilib.* **1997**, *128*, 249-260.

[110] Servio, P.; Englezos, P. *Fluid Phase Equilib.* **2001**, *190*, 127-134.

[111] Kashchiev, D. *Nucleation: Basic Theory with Applications*; Butterworth-Heinemann: Oxford, 2000; p 77.

[112] Volmer, M.; Weber, A. *Z. Phys. Chem.* **1926**, *119*, 277-301.

[113] Noyes, R. M. *J. Phys. Chem.* **1990**, *94*, 4404-4412.

[114] Shneidman, V. A. *J. Chem. Phys.* **2007**, *127*, 041102-1-041102-4.

[115] Ma, Q. L.; Chen, G. J.; Guo, T. M. *Fluid Phase Equilib.* **2003**, *205*, 291-302.

[116] Abay, H. K.; Svartaas, T. M. *Energy Fuels.* **2011**, *25*, 41-52.

[117] Subramanian, S.; Kini, R. A.; Dec, S. F.; Sloan Jr., E. D. *Chem. Eng. Sci.* **2000**, *55*, 1981-1999.

[118] Subramanian, S.; Ballard, A. L.; Kini, R. A.; Dec, S. F.; Sloan Jr., E. D. *Chem. Eng. Sci.* **2000**, *55*, 5763-5771.

[119] Ballard, A. L.; Sloan Jr., E. D. *Chem. Eng. Sci.* **2000**, *55*, 5773.

[120] Ballard, A. L.; Sloan Jr., E. D. *Chem. Eng. Sci.* **2001**, *56*, 6883.

[121] Englezos, P. In *Proceedings of the Fifth International Offshore and Polar Engineering Conference,* The Hague, The Netherlands, June 11−16, 1995; pp 289−296.

[122] Ribeiro, C. P.; Lage, P. L. C. *Chem. Eng. Sci.* **2008**, *63*, 2007-2034.

[123] Kuji, Y.; Yamasaki, A.; Yanagisawa, Y. *Energy Fuels.* **2006**, *20*, 2198-2201.

[124] Daimaru, T.; Kuji, Y.; Yanagisawa, Y.; Yamasaki, A. In *Proceedings of the Fifth International Conference on Gas Hydrates,* Trondheim, Norway, June 12−16, 2005.

[125] Okano, T.; Yanagisawa, Y.; Yamasaki, A. In *Proceedings of the Fifth International Conference on Gas Hydrates,* Trondheim, Norway, June 12−16, 2005.

[126] Arjmandi, M.; Tohidi, B.; Danesh, A.; Todd, A. C. *Chem. Eng. Sci.*. **2005**, *60*, 1313-1321.

[127] Happel, J.; Hnatow, M. A.; Meyer, H. *Ann. NY Acad. Sci.* **1994**, *715*, 412-424.

[128] Makogon, Y. F.; Makogon, T. Y.; Holditch, S. A. In *Proceedings of the Japan National Oil Conference*, Japan, October 20-22, 1998; pp 259-267.

[129] Freer, E. M.; Selim, M. S.; Sloan, E. D. *Fluid Phase Equilibria,* **2001**, *185*, 65-75.

[130] Tayer, C. J.; Miller, K. T.; Koh, C. A.; Sloan, E. D. In *Proceedings of the 6th International Conference on Gas Hydrates*, Vancouver, British Columbia, July 6-10, 2008.

[131] Peng, B. Z.; Chen, G. J.; Sun, C. Y.; Yang, L. Y.; Luo, H. In *Proceedings of the 6th International Conference on Gas Hydrates*, Vancouver, British Columbia, July 6-10, 2008.

[132] Turner, D.; Boxall, J.; Yang, S.; Kleehamer, D.; Koh, C.; Miller, K.; Sloan, E. D.; Xu, Z.; Mathews, P.; Tally, L. In *Proceedings of the Fifth International Conference on Gas Hydrates*, Trondheim, Norway, June 12-16, 2005.

[133] Varaminian, F. In *Proceedings of the Fourth International Conference on Gas Hydrates*, Yokohama, Japan, May 19-23, 2002; pp 465-468.

[134] Englezos, P.; Kalogerakis, N. E.; Dholabhai, P. D.; Bishnoi, P. R. *Chem. Eng. Sci.* **1987**, *42* (11), 2647-2658.

[135] Skovborg, P.; Rasmussen, P. *Chem. Eng. Sci.* **1994**, *49* (8), 1131-1143.

[136] Lekvam, K.; Ruoff, P. *J. Am. Chem. Soc.* **1993**, *115*, 8565-8569.

[137] Herri, J.; Gruy, F.; Cournil, M. In *Proceedings of the 2nd International Conference on Natural Gas Hydrates,* Toulouse, France, June 2−6, 1996; pp 243−250.

[138] Parlaktuna, M.; Gudmundsson, J. In *Proceedings of the 2nd International Conference on Natural Gas Hydrates*, Toulouse, France, June 2-6, 1996; pp 439-446.

Appendix A

Paper I

Effects of Ultralow Concentration of Methanol on Methane Hydrate Formation

By:

Hailu K. Abay and Thor M. Svartaas.

Printed in:

Journal of Energy & Fuels, **24**, 752-757, (2010).

The paper is reprinted with permission from the American Chemical Society. Copyright © 2010.

Energy Fuels **2010**, *24*, 752–757 · DOI:10.1021/ef9009422
Published on Web 11/09/2009

energy&fuels
article

Effect of Ultralow Concentration of Methanol on Methane Hydrate Formation

Hailu K. Abay and Thor M. Svartaas*

Department of Petroleum Engineering, Faculty of Science and Technology, University of Stavanger, 4036 Stavanger, Norway

Received August 28, 2009. Revised Manuscript Received October 24, 2009

Methane hydrates were produced in an isochoric high pressure cell in the presence of an ultralow concentration of methanol as an additive. Methanol concentrations examined were in the range 1.5−20 ppm by weight. The real gas equation and the nucleation probability distribution have been used to understand the effect of ultralow concentrations of methanol on the amount of hydrate formation, the rate of nucleation, and the range of probability distribution function in which random nucleation of methane hydrates occur. Comparisons with the pure water baseline experiment showed that an ultralow concentration of methanol exhibits dual effect, both as an inhibitor and as a promoter on structure I methane hydrate formation.

Introduction

Natural gas hydrates are three-dimensional (3D) crystalline ice-like materials. The physical conditions required to form gas hydrates are gas molecules (guests) and water molecules (hosts) with the correct conditions of temperature and pressure. The most common gas hydrate crystal structures are structure I (sI), structure II (sII), and structure H (sH). These structures are composed of cavities formed from hydrogen-bonded water molecules where the guest molecule is trapped in the host. Methane, the main constituent of natural gas, forms sI hydrate. The ideal cubic unit cell of sI hydrate consists of two 5^{12} small cavities and six $5^{12}6^2$ large cavities with a total of 46 water molecules.[1] Methane can stabilize both the smaller and the larger cavities, but has a better fit for the 5^{12} than the $5^{12}6^2$ cavity. Figure 1 illustrates nucleation of methane hydrate in crystallizing the unit cell of sI. During the formation of hydrates, one methane molecule is allocated for 20 water molecules in every smaller cages of the sI unit cell and another methane molecule for 24 water molecules in every 6 larger cavities of the sI unit cell.

Hydrate nucleation and dissociation in oil and gas pipelines are of great industrial and environmental interest since from the first discovery by Hammershmidt that hydrates are capable of blocking transport pipelines.[2] The industrial hydrate concerns have been in flow assurance, which is the major technical problem in offshore development, production, and transportation. In general, the well, the pipeline, and the platform are susceptible portions of the system where hydrate plugs occur.[3] In preventing hydrate blockage, thermodynamic and low dosage hydrate inhibitors have been successfully used. From alcohols, methanol (MeOH) is one of the most widely used thermodynamic hydrate inhibitor (THI) in the gas and oil fields due to its effectiveness. The wellhead jumpers and flow lines are parts of the system where methanol is being added to inhibit the formation of hydrates.[4]

When used in large amounts, methanol prevents hydrate crystallization by shifting the phase boundary thermodynamically to the lower temperature and higher pressure. However, in small amounts, the literature shows contradicting effects—both as an inhibitor and as a promoter. With regard to inhibition, methanol has two effects on hydrate crystallization. The hydroxyl group has the major effect by hydrogen bonding with the water molecules, and the methyl group has the lesser effect by tending to organize the water molecules in direct competition for a hydrate guest. Another effect of methanol is on the surface tension of a gas−solution interface. A molecular dynamics study[5] showed that the surface tension of the liquid−vapor interface of methanol−water mixtures was greatly reduced by adding a small amount of methanol to water.

Experimental studies on the effect of a small amount of methanol with concentration less than 5 wt % have reported on the thermodynamic stability, inhibition, and promotional effect of hydrates. An initially low concentration of methanol was assumed to stabilize both sI and sII structures,[6] but later NMR and dielectric studies verified no sign of enclathration of methanol.[7] Some studies[8,9] showed that a low concentration of methanol in aqueous solution increased hydrate stabilization. In contrary to this, other experimental studies indicated that thermodynamic stability did not increase with the presence of a small amount of methanol, but an inhibiting effect was observed.[10] On the other hand, under-inhibition

---

*To whom correspondence should be addressed. Telephone: +47 51832285. Fax: +47 51832050. E-mail: thor.m.svartas@uis.no.

[1] Sloan, E. D.; Koh, C. A. *Clathrate Hydrates of Natural Gases*, 3rd ed.; CRC Press/Tayler & Francis: Boca Raton, FL, 2008; p 60.

[2] Hammershmidt, E. G. *Ind. Eng. Chem.* **1934**, *26*, 851.

[3] Sloan, E. D. *Hydrate Engineering*, Monograph 21; Society of Petroleum Engineers: Richardson, TX, 2000; p 5.

[4] Cooley, C.; Wallace, B. K.; Gudimetla, R. In *The SPE Annual Technical Conference and Exhibition*, Denver, CO, October 5−8, 2003; SPE 84350.

[5] Chang, T. M.; Dang, L. X. *J. Phys. Chem. B.* **2005**, *109* (12), 5759–5765.

[6] Nakayama, H.; Hashimoto, M. *Bull. Chem. Soc. Jpn.* **1980**, *53* (9), 2427–2433.

[7] Davidson, D. W.; Gough, S. R.; Ripmeester, J. A.; Nakayama, H. *Can. J. Chem.* **1981**, *59*, 2587–2590.

[8] Makogon, Y. F. *Hydrates of Natural Gas*; Penn Well Publishing Company: Tulsa, OK, 1981; pp 133−135.

[9] Berecz, E.; Balla-Achs, M. *Studies in Inorganic Chemistry. 4. Gas Hydrates*; Elsevier Science Publishers B. V.: Amesterdam, The Netherlands, 1983; pp 95−109.

[10] Svartaas, T. M.; Fadnes, F. H. In *Proceedings of the 2nd International Offshore and Polar Engineering Conference*, San Francisco, USA, June 14−19, 1992; pp 614−619.

© 2009 American Chemical Society

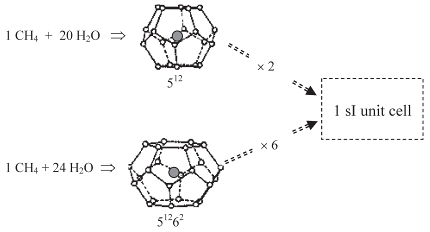

Figure 1. Nucleation of methane hydrate during the crystallization of sI unit cell.

using a small amount of methanol enhanced the rate and amount of hydrates formed in a multicomponent fluid.[11] Promotional effects of deuterated methanol were also clearly observed on the kinetics of hydrate formation.[12]

A recent review shows that the kinetics of hydrate nucleation and growth is much less understood than the thermodynamics.[13] The rate of nucleation and the induction time are the kinetic parameters that are usually associated with nucleation. The rate of hydrate formation (nucleation) can be estimated in different ways. For example, the rate of nucleation could be determined by counting the total number of particles detected by cameras.[14] The rate of change of free gas mole could be utilized as an indicator for the rate of hydrate formation for the study of the promotional effect of polymers and (anionic and nonionic) surfactants.[15,16] The method of laser light scattering could be used by measuring the intensity of the scattered light during hydrate nucleation for the investigation of nucleation behavior.[17] The classical nucleation theory could also be employed for the estimation of the rate of hydrate nucleation.[18] In this paper, the kinetic effects of methanol at four different ultralow concentrations (1.5, 5, 10, 20 ppm) have been examined on methane hydrate formation based on the classical nucleation theory. The theoretical effect of additives (surfactants and polymers) on the rate of nucleation of methane hydrate was discussed previously.[19] According to this theoretical discussion, if the presence of additives increases (decreases) the rate of nucleation, then the additive is acting as a kinetic promoter (inhibitor) of hydrate nucleation. This concept, along with the probability distribution function, has been applied to explain our experimental result and to estimate the kinetic parameters of nucleation in order to understand the effect of the additive on the crystallization of methane hydrate. The amount of hydrate formed was obtained directly from the experimental pressure drop by employing the real gas equation.

Experimental Technique

Isochoric High Pressure Cell Setup. Figure 2 shows the schematic experimental apparatus for ultralow concentration of methanol studies on the induction time of methane hydrate. A similar high-pressure isochoric apparatus was discussed previously for kinetic hydrate inhibitor (KHI) performance test.[20] The cylindrical cell is made of titanium with inner volume of 145 mL, from which 50 mL of the cell volume was filled with distilled water (DIW) with an ultralow concentration of methanol in solution. The rest, 95 mL of the cell volume, was filled with scientific grade 5.5 methane gas with purity 99.9995%. Temperature and pressure sensors had direct access to the inner part of the cell where the sample fluid was present. A 1/10 DIN Pt100 element (accuracy 0.03 °C) connected to a digital signal transmitter was used for temperature measurements, and a Rosemount 3051 TA absolute pressure transmitter was used for pressure readings. The accuracy of the transmitted temperature and pressure signals were ±0.1 °C and ±0.2 bar, respectively.

The cell was equipped with a cylindrical cooling cap, and water from a refrigerated circulator passed through this cap to control the cell temperature. The refrigerated and heating circulator used was Julabo F34 HL "High Tech" Series with integrated programmer. The temperature profile was handled by the integrated programmer, and the internal bath temperature could be logged via an RS 232 interface connection. LabView was used to collect pressure and temperature data, and PT plots were continuously updated by the PC on the LCD screen during the experiment.

Procedure. Small amounts of methanol were dissolved in distilled water to ultralow concentrations of 1.5, 5, 10, and 20 ppm, where 1 ppm corresponds to 3.12×10^{-5} mol/liter. Pure water was considered as 0 ppm baseline for comparison. The lower part of the cell (magnet housing) was filled with the selected methanol solution to displace all dead volume air during mounting of this section. Excess water solution displaced from the magnet housing into the experimental cell section during this mounting was removed prior to filling the desired amount of water into the cell. Thereafter, the top lid was mounted and the cell was closed and centered on the magnet drive (see Figure 2). The bath was adjusted to a temperature of 15.3 °C, which was kept constant at this level during the preparation of the experiment. After mounting, the cell was purged twice with 40 bar of methane gas to remove residual air from the cell (40 × 40 gives 1600× dilution). During this procedure the cell was stirred for a while to purge residual air present in the water solution. The amount of gas used was controlled by two pressure gauges, one gauge from the gas cylinder and another gauge connected to the inlet at the top of the cell. After purging was completed, the cell was pressurized to 93.88 bar, which corresponds to a hydrate equilibrium temperature of 12.6 °C. The system was left without stirring and cooling for the temperature and pressure values to stabilize, and at the same time for a pressure leak test. The stabilized filling pressure and temperature values were taken as the initial condition of the system. The initial condition of temperature and pressure lies in the hydrate-free region approximately 3.3 °C to the right of the hydrate equilibrium curve.

The cell was then cooled down without stirring to 7.8 °C using a cooling rate of 6 °C/h and the bath was programmed to keep this temperature level throughout the continuing part of the experiment. Having obtained a stable temperature and pressure at 7.8 °C and 90 bar, respectively, cell agitation was introduced by start of the stirrer at 750 rpm. Start of stirring was considered as the start of the experiment at time zero. The stabilized values

---

(11) Yousif, M.; Austvik, T.; Berge, L.; Lysne, D. In *Proceedings of the 2nd International Conference on Natural Gas Hydrates*, Toulouse, France, June 2−6, 1996; pp 291−298.

(12) Bobev, S.; Tait, K. T. *Am. Mineral.* **2004**, *89*, 1208–1214.

(13) Sum, A. K.; Koh, C. A.; Sloan, E. D. *Ind. Eng. Chem. Res.* **2009**, *48*, 7457–7465.

(14) Osegovic, J. P.; Tatro, S. R.; Holman, S. A.; Ames, A. L.; Max, M. D. *J. Pet. Sci. Eng.* **2007**, *56*, 42–46.

(15) Karaaslan, U.; Parlaktuna, M. *Energy Fuels.* **2000**, *14*, 1103–1107.

(16) Karaaslan, U.; Parlaktuna, M. *Energy Fuels.* **2002**, *16*, 1413–1416.

(17) Parent, J. S.; Bishnoi, P. R. *Chem. Eng. Commun.* **1996**, *144*, 51–64.

(18) Takeya, S.; Hori, A.; Hondoh, T.; Uchida, T. *J. Phys. Chem. B.* **2000**, *104* (17), 4164–4168.

(19) Kashchiev, D.; Firoozabadi, A. *J. Cryst. Growth.* **2002**, *243*, 476–489.

(20) Villano, L. D.; Kommedal, R.; Fijten, M. W. M.; Schubert, U. S.; Hoogenboom, R.; Kelland, M. A. *Energy Fuels.* **2009**, *23*, 3665–3673.

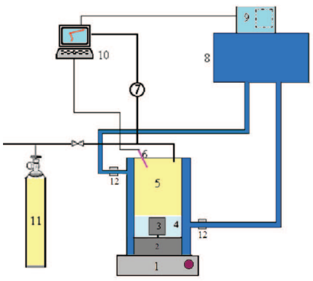

1 = Magnet drive
2 = Cell mount with stirrer magnet
3 = Stirrer blade
4 = DIW with additive
5 = Gaseous phase
6 = Temperature sensor
7 = Pressure sensor
8 = Refrigerated and heating circulator
9 = Programmable temp. control unit
10 = PC with LabView
11 = Gas supply cylinder
12 = Quick fit connections

Figure 2. Experimental setup.

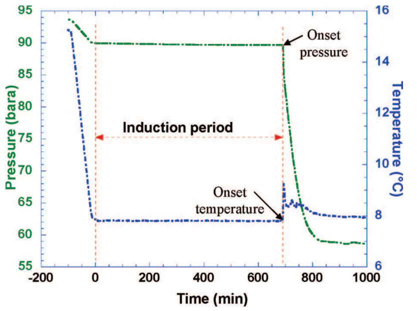

Figure 3. Response of pressure and temperature during hydrate formation.

of temperature and pressure remained constant from time zero to the onset of hydrate formation as shown in Figure 3.

During the onset of hydrate formation, there was a pressure drop accompanied by an increase in cell temperature. The pressure drop was due to the gas consumption when methane gas molecules fills unoccupied water cavities during the process of hydrate formation, and the temperature pulse was due to released heat of formation. As shown in Figure 3, the pressure drop and the temperature variation, and the gas consumption (in Figure 4) attained a constant value when the system reached its equilibrium state where the hydrate, the liquid water, and the methane gas coexist. The time elapsed from the start of the experiment at t_s to the onset of hydrate formation at t_o was taken as the induction time, t_i, which is the major kinetic parameter we measured. The pressure drop was calculated for the analysis of the additive on the amount of methane hydrate formation. The high pressure cell was disassembled and cleaned twice with tap water, distilled water, and dry air prior to the next series of experiments.

Results and Discussion

Amount of Methane Hydrate Formed. Employing the real gas equation for an isochoric system, we have

$$\Delta n = \frac{V}{zRT}\Delta P \qquad (1)$$

where Δn is the amount of gas consumed when hydrates form, ΔP is the measured experimental pressure drop caused by hydrate formation, V is the gas volume, z is the compressibility factor, R is the universal gas constant, and T is the measured experimental temperature. The amount of gas consumed and the pressure drop are directly proportional ($\Delta n \propto \Delta P$) with each other since the term V/zRT could be approximated as the constant of proportionality that does not vary significantly for the experiments. Thus, eq 1 could be utilized to estimate the amount of hydrates formed in every experiment. Figure 5 shows the pressure versus temperature plot during hydrate formation illustrating a typical pressure drop and the degree of subcooling used. As shown in Figure 5, the maximum pressure drop during the experiment was obtained when the cell pressure reached the hydrate equilibrium pressure at the experimental temperature.

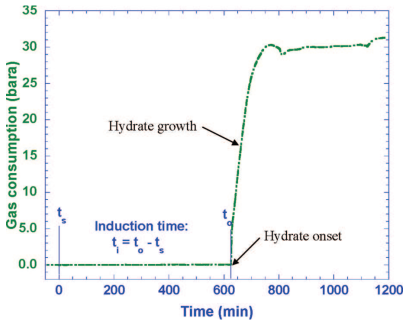

Figure 4. Gas consumption versus time during hydrate nucleation and growth.

Another important approximation is the filling of the 5^{12} and $5^{12}6^2$ cavities by the guest molecules during the process of hydrate formation. Assuming complete filling of cavities, the hydration number should ideally be 5.75 for sI methane hydrate. i.e., 5.75 mols of water for each mole of gas consumed. Such method is not an exact approximation since complete filling of cavities most probably may not be achieved. According to CSMHYD, the hydration number for methane hydrate should be around 5.9 at 90 bar. In addition, all methane molecules that were absorbed from the gaseous phase during hydrate formation may not form hydrates. Some molecules saturate the liquid water at the experimental temperature and pressure, hence the liquid in equilibrium with hydrate is not pure water.[21] In the experiments,

---

(21) Anderson, G. K. *J. Chem. Thermodyn.* **2004**, *36*, 1119–1127.

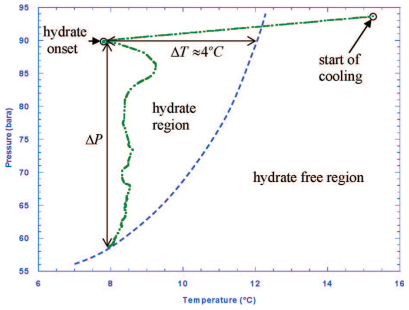

Figure 5. Pressure vs temperature graph during hydrate formation.

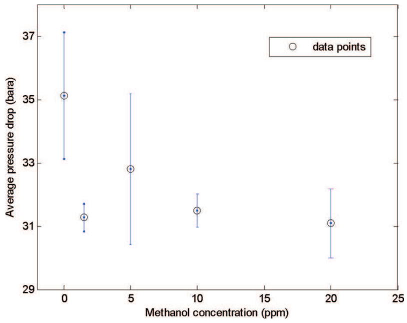

Figure 6. Average pressure drop for ultralow concentration of methanol.

a pressure drop of 0.1−0.2 bar on average was observed in saturating the liquid phase prior to formation of methane hydrates if hydrates were not formed spontaneously at the start of stirring. Thus, saturation had no significant effect in estimating the amount of hydrates formed from the observed pressure drop. A comparison between the total amount of hydrates formed in the system with ultralow concentrations of methanol and the pure water baseline experiment is shown in Figure 6. Each data point represents the average of 6−10 experimental data points with the corresponding error bar (see Table 1). The figure shows that the total amount of gas consumed was significantly reduced for all systems with methanol except the 5 ppm solution (8 data points), where an overlap with the pure water baseline pressure drop exists.

Nucleation Rate and Induction Time Estimation. Nucleation is a stochastic process as shown in Figure 7 of the experimental result. Such stochastic process can be described by the Poisson distribution law, repeating each experiment m times under the same experimental conditions. Thus, the probability distribution of nucleation is

$$P(t_n) = \frac{n}{m} \tag{2}$$

where t_n is the induction time of the nth out of m experiments. All experiments were run at the same initial degree of subcooling. This was done because induction time and formation rate are dependent on the degree of subcooling in both uninhibited and under-inhibited systems.[22] The degree of subcooling, ΔT, at the start of the experiment was on average 4 °C (see Figure 5). Other factors that could affect the induction time were the thermal history of water[8,23] and the degree of agitation.[24] However, the distilled water used in all experiments was fresh and initially at room temperature with the same thermal history prior to loading of the cell. Also, the degree of agitation was kept the same (750 rpm) for all experiments. Experiments that lasted more than 36 h without hydrate formation were terminated (see Table 1). If methanol has an inhibitor effect at ultralow concentrations, the system should be displaced toward longer induction. Thus, terminated experiments would weaken any conclusion on the promotion effect, but strengthen any conclusion on the inhibition effect when observed by the probability function analysis. This is considered in the following discussion of results.

The probability distribution function has been used in determining the probability of finding a nuclei that has reached its critical size within a time interval $(0,t)$. Hence for a given isochoric sample of fluid, the nucleation probability distribution $P(t)$ is expressed as a function of time as

$$P(t) = 1 - e^{-J(t-\tau_0)} \tag{3}$$

where J is the rate of nucleation and τ_0 is the induction time.[18,25] The induction time is also called nonsteady-state time lag, and it is a measure of the time necessary for the nucleation rate to attain a steady-state value.[26] The experimental data has been used to fit the parameters of eq 3. The results for the four different concentrations of methanol are tabulated in Table 1 with 95% confidence intervals.

Comparisons of the induction time of all the nonzero methanol concentrations with the pure water baseline experiment pointed in the direction that the presence of an ultralow concentration of methanol increased the induction time and rate of nucleation of methane hydrate formation. However, within the concentration range examined, the induction time did not show a uniform increase as a function of methanol concentration, but rather some oscillations indicating fluctuation between promotion and inhibition effect, especially for the lower concentrations. The 10 ppm experiment has the least induction time compared to other under-inhibited systems. The negative value for the induction time shows that nucleation is probable before the start of stirring at time zero as shown in Figure 8. The system temperature crossed the hydrate equilibrium curve 53 min prior to the start of stirring in all experiments (i.e., at −53 min with start of stirring defined at zero time for the induction time measurements). Including a probability of nucleation during the sequence of cooling without stirring prior to time zero, the minimum allowed induction time was restricted to −53 min in fitting the experimental data to the parameters of eq 3. Negative values of the induction time

---

(22) Hemmingsen, P. V.; Li, X.; Kinnari, K. In *Proceedings of the 6th International Conference on Gas Hydrates*, Vancouver, British Columbia, Canada, July 6−10, 2008.

(23) Vysniauskas, A.; Bishnoi, P. R. *Chem. Eng. Sci.* **1983**, *38*, 1061.

(24) Skovborg, P.; Ng, H. J.; Rasmussen, P. *Chem. Eng. Sci.* **1993**, *48* (3), 445.

(25) Toschev, S.; Milchev, A.; Stoyanov, S. *J. Cryst. Growth.* **1972**, *13/14*, 123–127.

(26) Tsuchiyama, A. *Am. Mineral.* **1983**, *68*, 687–698.

Table 1. Pressure Drop, Nucleation Rate, and Induction Time for Ultralow Concentrations of Methanol

	number of experiments				
concentration (ppm)	done (< 36 h)	terminated (> 36 h)	ΔP (±std dev[a])	J (min^{-1})	τ_o (min)
0	7	0	35.13 (±2:00)	2.28×10^{-3}	−53
1.5	10	2	31.26 (±0:44)	2.71×10^{-3}	61.18
5	8	1	32.79 (±2:38)	2.43×10^{-3}	27.6
10	10	0	31.49 (±0:53)	3.09×10^{-3}	−32.26
20	6	5	31.08 (±1:09)	6.54×10^{-3}	247.9

[a] Standard deviation.

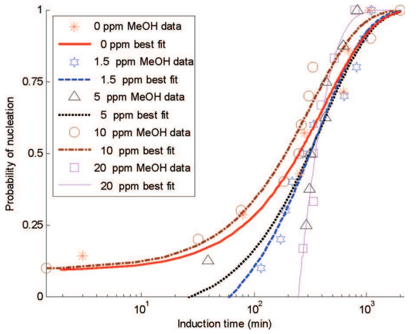

Figure 7. Nucleation probabilities vs induction time for ultralow concentration of methanol.

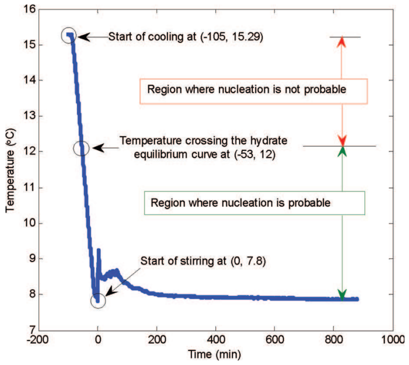

Figure 8. Temperature vs time graph before onset temperature for hydrate formation.

means spontaneous nucleation at the start of stirring or during the cooling sequence prior to start of stirring.

For the 10 ppm concentration, the experimental data and the probability distribution fit show nonzero probability for very short induction time. The S-shaped probability distribution function is shifted to the leftmost side compared to other experiments, including the pure water baseline reference. This shift with the nonzero probability for very short induction time could be an indication that methanol is acting as a promoter at this concentration. Figure 7 also shows that the range of random nucleation of the 10 ppm experiment is as wide as the range of random nucleation of the pure water experiment. However, the rate of nucleation was increased by a factor of 1.4 as compared to that of the pure water baseline value.

Contrary to the 10 ppm solution experiment, the delay of the induction time is more pronounced for the 20 ppm concentration. Unlike the 0 and 10 ppm solutions, the probability of finding nucleation is zero for low induction time, and the range of the probability distribution function is the narrowest compared to others. This considerable increase in induction time and the narrow rightmost probability distribution function could be an indication that the 20 ppm concentration is inhibiting hydrate crystallization. This concentration caused the rate of nucleation to increase by a factor of 2.9, and it is the largest factor compared to others. In addition, the five terminated experiments with measured induction times above 36 h would most probably strengthen an inhibitory effect if included in the analysis.

As compared to the uninhibited system, the 1.5 and 5 ppm solutions show nearly similar effect on the rate of nucleation, that is, it is increased by a factor of 1.2 and 1.1, respectively. However, the induction time was significantly increased. The tabulated results show that increasing the concentration of the additive from 1.5 to 5 ppm did not increase the nucleation rate and the induction time, but rather caused values of J and τ_0 to decrease. In fact, increasing concentration did not show a corresponding increase in nucleation rate and induction time for all under-inhibited systems. In other words, ultralow concentrations of methanol showed two opposing effects on the rate of nucleation of methane hydrate and induction time.

Although opposing effects were observed experimentally on the kinetics of methane hydrates formation, there are still unanswered questions such as why methanol has dual behavior at ultralow concentration and where it is found after hydrate formation. At room temperature, a molecular dynamics study[5] on methanol−water mixtures showed that methanol tends to concentrate at the interface between the liquid and the gas phase in such a way that the hydrophobic (methyl) group is pointing into the vapor phase. On the other hand, the hydrophilic (hydroxyl) group is able to form hydrogen bonding with the water molecules. The interaction of hydrophobic and hydrophilic groups with water and methane molecules may result in deviation from the normal behavior during the nucleation process depending on the experimental conditions.

In a diluted solution of alcohols, previous studies showed[27] that the pairwise interaction between molecules of the alcohol is attractive, triple interactions are repulsive, and higher order interactions are attractive. The magnitudes of these interactions are dependent on the temperature of the system. For example, the repulsive interaction decreases its magnitude when temperature increases. Upon cooling during the course of the experiment and prior to onset temperature for hydrate formation, the temperature of the system was continuously decreasing, which could have resulted in an increase in the magnitude of the repulsive interaction. Temperature-dependent interactions between and among

---

(27) Nord, L.; Tucker, E. E.; Christian, S. D. *J. Solution Chem.* **1984**, *13* (12), 849–867.

methanol molecules in the vicinity of the water and methane molecules could affect the energy barrier (activation energy) the system must cross before a stable nuclei is formed. The activation energy, a function dependent on temperature and pressure, could be easily affected by the attractive and repulsive interactions between and among the molecules of methanol. In fact, the probability of getting two molecules in direct contact with each other at ultralow concentration is zero. Thus, one may speculate that for a possible long-range interactions transmitted (and probably intensified) through the water and methane molecules, ultralow concentration of methanol in solutions may significantly affect the behavior and the role it has on the nucleation process. These interactions could possibly affect the activity of the water and methane molecules in an attempt to rearrange themselves so that they could achieve the critical size for onset of hydrate formation and continued growth. Further investigation using molecular dynamics simulation may reveal why (and how) methanol behaves dually as an inhibitor and as a promoter on the kinetics of methane hydrate formation.

Conclusion

We have performed a series of experiments to investigate the effect of ultralow concentrations of methanol on the amount of methane hydrate formation, the rate of nucleation, and the range of probability distribution in which random nucleation of sI methane hydrates occurs. Compared to the pure water baseline experiment, the presence of ultralow concentrations of methanol in aqueous solution has affected the amount of hydrate formation, the rate of nucleation, and the range of the probability distribution function. The results show that an ultralow concentration of methanol has a dual effect, both as a promoter and as an inhibitor on methane hydrate formation for the specific concentrations considered.

Acknowledgment. The authors thank NFR for the financial support of this work.

Appendix B

Paper II

Multicomponent Gas Hydrate Nucleation: The Effect of the Cooling Rate and Composition

By:

Hailu K. Abay and Thor M. Svartaas.

Printed in:

Journal of Energy & Fuels, **25**, 42-51, (2011).

This paper is reprinted with permission from the American Chemical Society. Copyright © 2011.

Energy Fuels **2011,** *25,* 42–51 · DOI:10.1021/ef1011879
Published on Web 12/29/2010

energy&fuels
article

Multicomponent Gas Hydrate Nucleation: The Effect of the Cooling Rate and Composition

Hailu K. Abay* and Thor M. Svartaas

Department of Petroleum Engineering, Faculty of Science and Technology, University of Stavanger, 4036 Stavanger, Norway

Received September 3, 2010. Revised Manuscript Received November 2, 2010

The effect of the cooling rate and gas composition on the kinetics of hydrate formation and the stochastic nature of nucleation has been examined by forming structure II hydrates from two different synthetic natural gases: one with two components (SNG2) and the other with seven components (SNG7). The hydrate equilibrium properties of SNG2 and SNG7 were comparable, and all experiments were initiated at the same temperature and pressure conditions in an autoclave cell. The initial degree of subcooling and other parameters that could affect the kinetics were, thus, approximately the same during all nucleation experiments. From the experimental results, SNG2 showed an increasing nucleation rate, while SNG7 showed a decreasing effect as the cooling rate increases in steps of 2 °C/h. In addition, it is observed that the rate of nucleation is dependent upon gas compositions, and different gas compositions respond differently on the same cooling rate. In an attempt to understand the experimental results, the classical nucleation theory of multicomponent systems, the probability distribution function, and the principle of irreversible thermodynamics have been employed. The observed effects are, thus, related to the dependence of the critical size upon the temperature and gas composition, chemical oscillations as a result of the change in solubility of the individual gas components, and coupled mass and heat fluxes during cooling. Such findings on system responses are of paramount importance for a reliable evaluation of the effect of additives on hydrate formation processes.

Introduction

Natural gas hydrates are crystalline solid compounds, consisting of a gas molecule (a guest) surrounded by a cage of water molecules (a host). They have attracted significant research since their discovery by Hammershmidt[1] that hydrates were contributing to blockages in oil and gas transmission pipelines. Gas hydrates are known to form different crystal structures, of which structure II (sII) is the commonest. This structure is composed of 16 small (5^{12}) cavities and 8 large ($5^{12}6^{4}$) cavities. Each cavity is formed from hydrogen-bonded water molecules. The smaller cavity can accommodate one guest molecule of suitable size and shape, but the larger cavity can accommodate two guests of suitable combination in size. At high pressures and lower temperatures, the process of filling these cages by a guest molecule starts when hydrates begins to nucleate and grow.

Nucleation is considered as the first step of gas hydrate crystallization. It is a process where small clusters of water and gas grow and disperse to achieve a critical size for a continued growth. Understanding the nucleation process is of paramount importance with regard to hydrate inhibition in pipelines and hydrate promotion in gas storage. A theoretical understanding of one-component hydrate nucleation has been studied.[2−5] The driving force for one-component gas hydrates and its dependence upon the concentration of dissolved gases has been discussed.[6] The effect of the cooling rate on one-component nucleation has also been investigated. For example, the effect of the cooling rate on the hydrate nucleation temperature, the temperature range in which nucleation occurs, has recently been reported[7] by considering the fraction of samples nucleated for three different cooling rates. The effect of the cooling rate on the critical undercooling for crystallization has also been recently reported[8] for single-component crystallites. Unlike single-component nucleation, not much is known about multicomponent nucleation experimentally and how it is affected by the cooling rate and composition. Also, during cooling and just prior to the start of the experiments, the system is subjected to non-equilibrium conditions that could affect the process being studied. For multicomponent mixtures, where individual components respond differently to such effects, the interpretation of results could lead to erroneous conclusions unless the basic mechanisms on pure gas mixtures are better understood. For example, comparing basic effects of kinetic hydrate inhibitors (KHIs) tested under various experimental conditions and in different fluid systems may give contradictory conclusions unless the kinetic response of the uninhibited test system is known.

To the best of our knowledge, no one has reported whether the same cooling rate has the same effect or not on different gas mixtures with regard to nucleation. Besides, there have been no attempts performed in studying multicomponent

---

*To whom correspondence should be addressed. Telephone: +47-51832230. Fax: +47-51832050. E-mail: hailu.k.abay@uis.no.

(1) Hammershmidt, E. G. *Ind. Eng. Chem.* **1934**, *26*, 851.

(2) Kvamme, B. *Proceedings of the 2nd International Conference on Natural Gas Hydrates*; Toulouse, France, June 2−6, 1996; pp 139−146.

(3) Kvamme, B. *Ann. N. Y. Acad. Sci.* **2000**, *912*, 496–501.

(4) Kashchiev, D.; Firoozabadi, A. *J. Cryst. Growth* **2002**, *243*, 476–489.

(5) Kvamme, B. *Int. J. Offshore Polar Eng.* **2002**, *12* (4), 256–263.

(6) Kashchiev, D.; Firoozabadi, A. *J. Cryst. Growth* **2002**, *241*, 220–230.

(7) Davies, S. R.; Hester, K. C.; Lachance, J. W.; Koh, C. A.; Sloan, E. D. *Chem. Eng. Sci.* **2009**, *64*, 370–375.

(8) Kashchiev, D.; Borissova, A.; Hammond, R. B.; Roberts, K. J. *J. Cryst. Growth* **2010**, *312*, 698–704.

© 2010 American Chemical Society

nucleation experimentally and relating to theoretical derivations. Our aim in this paper is, as a first step toward improved understanding of the basic processes involved, to examine effects of the cooling rate and gas composition effects on multicomponent nucleation kinetics. We employ the classical nucleation theory of multicomponent systems and the probability distribution function for the analysis of the experimental results. In addition, we have addressed irreversible (non-equilibrium) thermodynamics in an attempt to explain effects observed in SNG2 because systems during the stagnant cooling sequence may be subjected to coupled heat and mass fluxes in the system. The following section discusses the theoretical background of multicomponent nucleation and coupled heat and mass transfer.

Theoretical Background

Multicomponent Nucleation. For multicomponent nucleation, the general expression for the driving force (per unit cell) in forming a critical hydrate nucleus is given by[9]

$$\Delta g = n_{\mathrm{w}}\left[(v_{\mathrm{w}} - v_{\mathrm{hw}})(P - P_{\mathrm{eq}}) - kT\sum_j v_j \ln\left(\frac{1 - \sum_k \theta_{kj}(T, P, y)}{1 - \sum_k \theta_{kj}(T, P_{\mathrm{eq}}, y)}\right)\right] \tag{1}$$

where n_{w} is the number of water molecules in a unit cell (136 for sII), v_{w} is the molar volume of water molecules in solution, v_{hw} is the molecular volume of water in the hydrate, P is the pressure, T is the temperature, k is the Boltzmann constant, v_j is the number of type j cavities per water molecule, y is the composition in the gas phase, and θ_{kj} is the fractional filling of cavity j by a type k molecule expressed as

$$\theta_{kj} = \frac{C_{kj} f_{gk}}{1 + \sum_i C_{ij} f_{gj}} \tag{2}$$

where C_{kj} is the Langmuir constant for species k in cavity j, f_{gk} is the fugacity of gas component k in the gas phase in equilibrium with the hydrate, and $\sum$ is for all species except water. In eq 1 of the expression for the driving force, it is clear to see that the driving force depends upon the pressure, temperature, and gas-phase composition. In another recent work[10] on the driving force for nucleation of multicomponent gas hydrates, it was also reported that the driving force depends on hydrate phase composition besides temperature, pressure, and gas-phase composition. In general, there are a number of theoretical papers[11−14] on evaluating the work of formation (formation energy) of the critical nucleus, the size of the nucleus, and the thermodynamics of crystal nucleation in multicomponent systems.

In this work, two different synthetic natural gases, SNG2 and SNG7, have been used for the study of the effects of the cooling rate and gas composition in multicomponent kinetics. Table 1 shows the composition of each gas used in mole percentage. Both gases form a sII hydrate. Before sII hydrate growth, there are two hypotheses for the mechanism of hydrate nucleation at the molecular level: labile cluster and local structuring.[15] Our analysis is based on the cluster approach, which is considered as an unstable entity that undergoes a continuous change. The dynamics of clusters play a major role in the kinetics of nucleation.[16] From the classical nucleation theory of multicomponent systems, the dynamics of a cluster is associated with a monomer that leaves a cluster and joins an adjacent cluster during an attempt for a critical size. This results in a variation in the number of clusters grown per unit time. A conceptual picture is drawn in Figure 1 that only shows two newly born unstable clusters that undergo a continuous change and one stable critical nucleus. During the discussion[17] on the composition of the critical nucleus in multicomponent vapor nucleation, it was mentioned that the cluster of the critical nuclei generally contains a few hundred molecules. Such a few hundred molecules do not make a spontaneous steady-state distribution. Before a steady-state regime is attained, the rate of nucleation has a transient regime that corresponds to the time required to attain a steady-state distribution of nuclei.[18] In fact, nucleation in general is a complex process especially before reaching a steady-state regime,[19−23] and hence, we focus on the steady-state regime, where a steady-state nucleation occurs. On the basis of the birth−death equation, which tells us how the concentration of clusters change with time, the steady-state nucleation rate for SNG2 could generally be expressed as[24]

$$J_2 = RN\mathrm{e}^{-\Delta\varphi^*/kT}\frac{W^*}{\sqrt{|\det W^*|}} \tag{3}$$

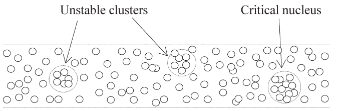

Figure 1. Birth and death of clusters during the formation of a critical nuclei.

Table 1. Composition of SNGs Used

gas component		SNG2 (mol %)	SNG7 (mol %)
CH_4	methane	92.51	80.40
C_2H_6	ethane	0	10.30
C_3H_8	propane	7.49	5.0
iso-C_4H_{10}	isobutane	0	1.65
n-C_4H_{10}	*n*-butane	0	0.72
CO_2	carbon dioxide	0	1.82
N_2	nitrogen	0	0.11

---

(9) Anklam, M. R.; Firoozabadi, A. *J. Chem. Phys.* **2004**, *121* (23), 11867–11875.

(10) Abbas, I. A.; Mohsen, V. S.; Farshad, V. *Iran. J. Chem. Chem. Eng.* **2007**, *26* (2), 63–70.

(11) Oxtoby, D. W.; Kashchiev, D. *J. Chem. Phys.* **1994**, *100* (10), 7665–7671.

(12) Debenedetti, P. G.; Reiss, H. *J. Chem. Phys.* **1998**, *108* (13), 5498–5505.

(13) Laaksonen, A.; McGraw, R.; Vehkamaki, H. *J. Chem. Phys.* **1999**, *111* (5), 2019–2027.

(14) Djikaev, Y. S.; Tabazadeh, A.; Reiss, H. *J. Chem. Phys.* **2003**, *118* (14), 6572–6581.

(15) Sloan, E. D.; Koh, C. A. *Clathrate Hydrates of Natural Gases*, 3rd ed.; CRC Press/Tayler and Francis Group: Boca Raton, FL, 2008; p 180.

(16) Volmer, M.; Weber, A. *Z. Phys. Chem.* **1926**, *119*, 277–301.

(17) Wilemski, G. *J. Chem. Phys.* **1983**, *80*, 1370–1372.

(18) Frade, J. R.; Queiroz, C. M.; Fernandes, M. H. *J. Non-Cryst. Solids* **2004**, *333*, 263–270.

(19) Frade, J. R.; Kharton, V. V.; Lopez, D. M.; Nunez, P.; Abrantes, J. C. C. *Thermochim. Acta* **2005**, *435*, 85–91.

(20) Kelton, K. F.; Geer, A. L.; Thompson, C. V. *J. Chem. Phys.* **1983**, *79*, 6261.

(21) Kelton, K. F.; Narayan, K. L.; Levine, L. E.; Cull, T. C.; Ray, C. S. *J. Non-Cryst. Solids* **1996**, *204*, 13–31.

(22) Davis, M. J. *J. Am. Ceram. Soc.* **2001**, *84*, 492–496.

(23) Frade, J. R.; Queiroz, C. M.; Fernandes, M. H. *J. Non-Cryst. Solids* **2004**, *333*, 271–277.

(24) Vehkamaki, H. *Classical Nucleation Theory in Multicomponent Systems*; Springer: New York, 2006; pp 97−113.

where R is the average growth rate, N is the normalization factor of the cluster size distribution, k is the Boltzmann constant, T is the temperature, $\Delta\varphi^*$ is the activation energy (free energy barrier) for the formation of the critical size cluster, and W^* is the second derivative of the activation energy at the critical size. For SNG7, the general expression for the steady-state nucleation rate could be written as[24]

$$J_7 = \frac{|\lambda|}{2\pi kT} N\mathrm{e}^{-\Delta\varphi^*/kT} \frac{1}{\sqrt{\left|\det\left(\frac{W^*}{2\pi kT}\right)\right|}} \tag{4}$$

where λ is an eigenvalue of the product of the growth matrix. For the detailed derivation of eqs 3 and 4, the reader is advised to read the original work[24] on multicomponent nucleation kinetics. These equations describe the explicit temperature dependence of the steady-state rate of nucleation for multicomponent systems. They also relate the rate of nucleation to the effects of kinetic and thermodynamic barriers to form the nucleus. An implicit dependence of the rate of nucleation upon gas composition is observed from these equations through the formation energy. Unfortunately, the formation energy (nucleation work) cannot be measured experimentally, but the nucleation rate could be measured, in this case, by the help of the data from induction time measurements. The rate of nucleation and the nucleation work are related through a more simplified expression[25]

$$J_{2,7} \sim \mathrm{e}^{-\Delta\varphi^*_{2,7}/kT} \tag{5}$$

where $J_{2,7}$ is the rate of nucleation of SNG2 or SNG7 and $\Delta\varphi_{2,7}$* is the corresponding energy barrier. One can, thus, clearly see the dependence of the nucleation rate upon the gas composition from eq 1, which is the specific expression for a hydrate. This theoretical concept could be employed for investigating the effect of the macroscopic parameters, gas composition and temperature (cooling rate), on the microscopic phenomenon rate of nucleation, keeping other parameters, such as the degree of subcooling and stirring rate, that affect the rate of nucleation the same for both gases.

Although the nucleation step is a microscopic phenomenon involving many molecules and too difficult to observe experimentally, the induction time measurement could be employed to bridge nucleation theory and experimental investigation.[26] This experimentally accessible induction time is the measure of the ability of a system to remain in the state of metastable equilibrium and contains valuable information about the kinetics of nucleation.[27] Because nucleation requires transport of gas molecules, coupled heat and mass transfer may affect the process.

Coupled Heat and Mass Transfer. Mass transport by diffusion in a n-component mixture is described by $n(n-1)/2$ diffusion coefficients. Therefore, the description of coupled heat and mass transfer in multicomponent systems may become complex. For simplicity, we address the SNG2 system and regard the main, reference frame gas (methane) as the solvent and the additional gas (propane) as the solute. Then, mass transport can be described through transport of "solute" gas through "solvent" gas by one single mass transfer (diffusion) coefficient. The entropy production, σ, in the SNG2 system subjected to cooling, pointing in the x direction, can be expressed by[28]

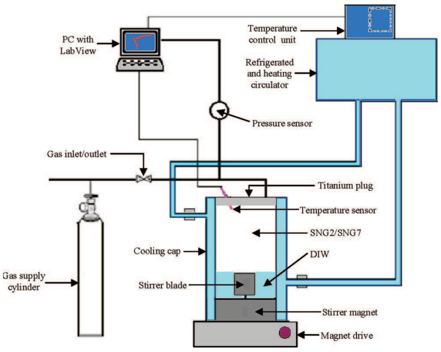

Figure 2. Experimental setup for testing the effect of the cooling rate and gas composition on multicomponent nucleation.

$$\sigma = J_{\mathrm{q}} \frac{\partial}{\partial x}\left(\frac{1}{T}\right) + J_1\left(-\frac{1}{T}\frac{\partial \mu_{1,T}}{\partial x}\right) \tag{6}$$

where J_{q} is the heat flux, J_1 is the mass flux of component 1 (the solute), and $\mu_{1,T} = \mu_1^0 + RT\ln(c_1 y_1)$ is the chemical potential with μ_1^0 as the reference state, c_1 as the concentration, and y_1 as the activity coefficient of component 1. Heat is transported in the system by convection (energy transfer between neighboring molecules) and conduction (i.e., "hot" gas molecules being transported toward the cold surface), and eq 6 tells us that there is a coupled heat and mass transport related to the entropy production in the system.

In our laboratory, we have cylindrical cells (see Figure 2) where the outer part is colder than the inner part because the outer part of the cell has direct contact with the cooling cap. Thus, if we assume transport of heat and mass in the radial direction only, then the entropy production can be described by

$$\sigma = J_{\mathrm{q}} \frac{\partial}{\partial r}\left(\frac{1}{T}\right) + J_1\left(-\frac{1}{T}\frac{\partial \mu_{1,T}}{\partial r}\right) \tag{7}$$

The radial flux−force relations for measurable heat flux and molar flux are

$$J_{\mathrm{q}} = l_{\mathrm{qq}} \frac{\partial}{\partial r}\left(\frac{1}{T}\right) + l_{\mathrm{qu}}\left(-\frac{1}{T}\frac{\partial \mu_{1,T}}{\partial r}\right) \tag{8}$$

$$J_1 = l_{\mathrm{uq}} \frac{\partial}{\partial r}\left(\frac{1}{T}\right) + l_{\mathrm{uu}}\left(-\frac{1}{T}\frac{\partial \mu_{1,T}}{\partial r}\right) \tag{9}$$

where $(\partial/\partial r)(1/T)$ and $(-1/T)(\partial\mu_{1,T}/\partial r)$ describe the forces. The absolute value of these forces will increase by increasing cooling gradients. According to Onsager's reciprocity relations[29,30] the coefficients (conductivities) $l_{\mathrm{qu}} = l_{\mathrm{uq}}$. If the

---

(25) Nishioka, K.; Kusaka, I. *J. Chem. Phys.* **1992**, *96* (7), 5370–5376.

(26) Nguyen, T. N. P.; Kim, K.-J. *Int. J. Pharm.* **2008**, *364*, 1–8.

(27) Kashchiev, D.; Firoozabadi, A. *J. Cryst. Growth* **2003**, *250*, 499–515.

(28) Kjelstrup, S.; Bedeaux, D.; Johannesen, E. *Elements of Irreversible Thermodynamics for Engineers*; Tapir Academic Press: Trondheim, Norway, 2006; p 123.

(29) Onsager, L. *Phys. Rev.* **1931**, *37*, 405–426.

temperature is constant, then $(\partial/\partial r)(1/T) = 0$ and eq 9 can be written as

$$J_1 = -l_{\mathrm{uu}}\frac{1}{T}\frac{\partial \mu_{1,T}}{\partial r}$$

$$= -l_{\mathrm{uu}}\frac{1}{T}\frac{\partial \mu_{1,T}}{\partial c_1}\frac{\partial c_1}{\partial r} = -D_{1,2}\frac{\partial c_1}{\partial r} \qquad (10)$$

where $D_{1,2}$ is the interdiffusion coefficient of component 1 (the solute) in component 2 (the solvent). Interdiffusion coefficients can be measured by spectroscopic and analytical techniques.

Irreversible thermodynamics or non-equilibrium thermodynamics have been applied for several years to describe transport processes in systems that are not in global equilibrium. The need for more accurate flux equations in modeling of chemical processes increases the need for application of irreversible thermodynamics.[31] In the present paper, we have attempted to address irreversible thermodynamics on SNG2 in search for further possible explanations for the observed effects because the initial stage of our experiments with the cooled system without agitation could involve coupled heat- and mass-transfer processes (entropy-driven processes) affecting the results. The following section discusses the experimental setup and procedure that we used and how we carefully measured the induction time for each SNG for the study of the multicomponent nucleation.

Experimental Setup and Procedure

Figure 2 shows the experimental setup for the study of the effect of the cooling rate and gas composition on multicomponent nucleation. The high-pressure cell type had cylindrical geometry with an inner volume of 145 mL, and all main cell parts were made of titanium. Two equal cells with different setups were used: one with one T-sensor in the vapor phase only and the second with two T-sensors, with one sensor in the vapor phase and the second sensor in the aqueous phase. The stirrer blades of the two cells were of different geometry but with comparable area. The cell with one T-sensor in the vapor phase was used for the main series of experiments, and the other cell and setup were used for repeat and verification of observed trends. With respect to nucleation, some response variations between the two cell experiments could be expected because of differences in setup, but trends should be the same.

Refrigerated and heating circulator with a programmable temperature control unit was used for both setups to cool the sample fluid by allowing cold water to pass through the cooling cap surrounding the cell. The sample temperature and pressure changes were monitored and recorded by LabView. The temperature and pressure values were measured to an accuracy of ±0.1 °C and ±0.2 bar, respectively.

Two different gas supply cylinders were used for SNG2 and SNG7. No liquid hydrocarbon phases were present during any of the experiments. A total of 66 experiments were conducted, and the same procedure was followed for each SNG as follows: (i) The bath temperature was adjusted to keep the cell at an initial temperature of 16 °C during filling. At this temperature, the cell was kept outside the hydrate region before the start of cooling the system to the experimental condition inside the hydrate region. (ii) A total of 50 mL of the cell volume was filled with distilled water (DIW). The cell was then closed, and the remaining 95 mL was left for the SNG. Fresh DIW was used for all experiments, and none of the experiments was repeated on water that had previously been in contact with hydrates to avoid memory effects. (iii) The cell is pressure-tight but not vacuum-tight, and the cell was purged with 40 bar of SNG to remove residual air from the cell. After the cell reached 40 bar during purging, it was stirred for a while to saturate the water with SNG and dilute residual air in this phase. The stirrer was then stopped, and the venting valve was opened to bleed the purging gas and let the cell pressure down to atmospheric conditions. The venting valve was then closed, and the stirrer was restarted to remove residual gas from the water. During this process, the cell pressure rose by around 0.5 bar above atmospheric pressure because of the release of residual supersaturated gas from the water. The stirrer was then stopped, and the venting valve was reopened to bleed the residual gas. The purging process was repeated twice. (iv) The cell was then pressurized to 25.16 bar at 16 °C. These conditions lie in the hydrate-free region. The system was stirred to saturate the water phase with the gas, and the pressure was readjusted to keep the pressure in the region of 25.1−25.2 bar at the initial temperature. The cell was closed, and the stirrer stopped when the pressure became stable at this level. (v) The cell was then cooled without stirring from an initial temperature of 16 °C down to 7.8 °C, which lies in the hydrate-forming region. Three different cooling rates of 2, 4, and 6 °C/h were used at a time. (vi) The experiment was initiated by the start of stirring at 750 rpm for 10 min after the bath had reached its stable temperature at the experimental conditions. This time lag was needed for the internal volume of the cell to reach the preset experimental temperature level of 7.8 °C. (vii) At the start of stirring, the pressure in the cell had decreased from initial filling conditions to 24.2−24.3 bar because of the decreased temperature. The initial *T* and *P* conditions at the start of stirring were 7.8 °C and 24.2−24.3 bar during all experiments.

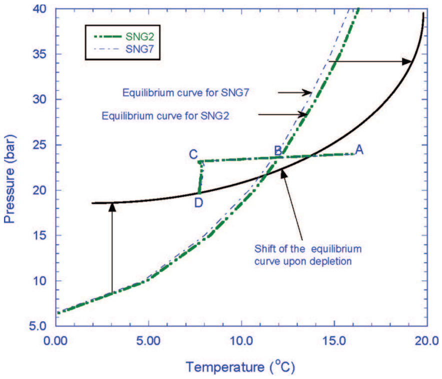

Figure 3. Pressure versus temperature graph during hydrate formation for both SNG2 and SNG7.

Figure 3 shows the pressure versus temperature response during cooling (A−B−C), onset of hydrate formation (C), and growth of hydrate crystals (C−D). The equilibrium curves for both SNG2 and SNG7 were calculated using CSMGEM. Both gases have comparable equilibrium properties, allowing one to investigate the composition effect at nearly the same degree of subcooling (4 °C) for each SNG. The degree of subcooling is defined as the difference between the hydrate equilibrium temperature and the operating temperature. The hydrates formed are enriched on the heavy components (propane and butane), as compared to the feed composition, and in the closed, isochoric system, the composition of the residual gas is gradually changed as the hydrate grows (enriched here in methane). The equilibrium curves

---

(30) Onsager, L. *Phys. Rev.* **1931**, *38*, 2265–2279.

(31) Taylor, R.; Krishna, R. *Multicomponent Mass Transfer*; Wiley: New York, 1993.

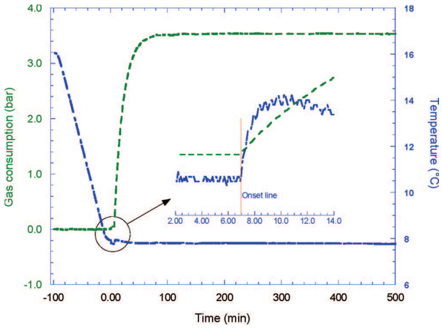

Figure 4. Gas consumption and temperature versus time during multicomponent hydrate formation.

for both SNG2 and SNG7 stay in their positions only before the onset, from point A to point C. At point B, the system temperature crosses the equilibrium curve and enters into the labile region where clustering and rearranging of water molecules begins. Point C is the onset point for hydrate formation, and thereafter, the hydrates start growing fast until the growth stops at point D. During this growth period, the composition of each SNG is depleted on the heavier components because of the "incomplete" filling of the smaller 5^{12} cavities (~65% C_1) and the nearly complete filling of the larger $5^{12}6^4$ cavities (~96.5% C_3 for SNG2 or ~96% $C_2 + C_3 + C_4$ for SNG7) of the sII hydrate in accordance with eq 2 and the CSMGEM hydrate program. This depletion results in a shift of the equilibrium curve from its initial position toward higher pressures, as illustrated in Figure 3. Our analysis of the effect of the composition and cooling rate on multicomponent nucleation is mainly in the region between points B and C, where any effect on composition because of the growth process was assumed negligible.

Figure 4 shows the gas consumption and temperature versus time from the start of the experiment to the end. At the onset of hydrate formation at time zero, the temperature of the system increases because hydrate formation is an exothermic reaction. The onset time is determined by the increase in gas consumption accompanied by the temperature pulse, as shown in the inset of the figure. The time taken by the system from the start of the experiment at time zero to the onset of hydrate formation is defined as the induction time. This induction time is the key parameter that we carefully measured for the investigation of the effect of the cooling rate and gas composition during multicomponent hydrate nucleation.

The induction time and formation rate are affected by the degree of subcooling in uninhibited systems.[32] In fact, the degree of subcooling cannot be considered as the driving force for the investigation of the effect of the composition on the nucleation rate in such systems because of the composition difference between each SNG. The induction time could also be affected by the thermal history of water[33] and the stirring rate.[34] Both SNGs stayed at the same distance and time from the equilibrium curve as described in the procedure. We also kept the same degree of agitation for both SNGs. Thus, for the analysis of the effect of the cooling rate and gas composition on multicomponent nucleation, we used the same degree of subcooling, thermal history, and degree of agitation for both SNG2 and SNG7, enabling us to examine the effect as accurately as possible.

Results and Discussion

Nucleation Rate and Induction Time. Nucleation is a stochastic process[35] requiring many experiments to be performed on a single sample. In fact, attempts[36] have been made recently to limit the stochastic nature of gas hydrate crystallization and increase data repeatability using the persistence of precursory hydrate structures that has previously experienced hydrate formation. However, upon "fresh water" experiments, nucleation of gas hydrate crystallization is a stochastic process in nature that could only be explained in terms of the probability distribution function. The nucleation probability distribution function, $P_{2,7}(t)$, of SNG2 and SNG7 is given by[37−40]

$$P_{2,7}(t) = 1 - e^{-J_{2,7}(t-\tau_{2,7})} \qquad (11)$$

where $J_{2,7}$ is the rate of nucleation of SNG2 or SNG7 and $\tau_{2,7}$ is the corresponding lag time, which is the measure of the time necessary for the nucleation rate to attain a steady-state value. Figures 5 and 6 show the nucleation probabilities versus induction time for three different cooling rates of 2, 4, and 6 °C/h for both SNG2 and SNG7, respectively. Equation 11 has been used to fit the major parameters of the kinetics, and the results are tabulated in Table 2 with 95% confidence bounds.

Effect of the Cooling Rate and Gas Composition. Tabulated results of Table 2 have been analyzed to examine the effect of the cooling rate and gas composition on the rate of nucleation and induction time for each SNG. Each data set contained a total number of seven experiments for the main set and six experiments for the repeat. The repeated values for the slow and fast cooling rates are values using a different experimental setup. For SNG2, increasing the cooling rate from slow (2 °C/h) to fast (6 °C/h) caused the rate of nucleation to increase from 7.2×10^{-2} to 2.8 min^{-1}, respectively, for the first set of experiments and from 4.4×10^{-2} to 2.6 min^{-1}, respectively, for the repeat. The range of the S-shaped probability of nucleation is reduced and shifted from right (higher induction times) to left (lower induction times), as shown in Figure 5 for the main set of experiments. The tabulated values of the induction time for SNG2 indicate that nucleation could have been initiated slightly before or close to the start of stirring. During cooling at 2 °C/h, the P and T conditions of the system cross the hydrate equilibrium curve approximately 2 h prior to the start of stirring; therefore, induction prior to the start of stirring and in the vicinity of the start point is assumed probable. For the faster cooling rates (4 and 6 °C/h), nucleation started at the start of stirring or within the first minute after the start. The results give a strong indication that a 2 °C/h change in the cooling rate has a significant effect on the rate of nucleation for SNG2 and the range of the probability distribution function.

---

(32) Hemmingsen, P. V.; Li, X.; Kinnari, K. *Proceedings of the 6th International Conference on Gas Hydrates*; Vancouver, British Columbia, Canada, July 6−10, 2008.

(33) Vysniauskas, A.; Bishnoi, P. R. *Chem. Eng. Sci.* **1983**, *38*, 1061.

(34) Skovborg, P.; Ng, H. J.; Rasmussen, P. *Chem. Eng. Sci.* **1993**, *48* (3), 445.

(35) Wilson, P. W.; Lester, D.; Haymet, A. D. J. *Chem. Eng. Sci.* **2005**, *60*, 2937–2941.

(36) Duchateau, C.; Peytavy, J. L.; Glenat, P.; Pou, T. E.; Hidalgo, M.; Dicharry, C. *Energy Fuels* **2009**, *23*, 962–966.

(37) Toschev, S.; Milchev, A.; Stoyanov, S. *J. Cryst. Growth* **1972**, *13*/*14*, 123–127.

(38) Tsuchiyama, A. *Am. Mineral.* **1983**, *68*, 687–698.

(39) Takeya, S.; Hori, A.; Hondoh, T.; Uchida, T. *J. Phys. Chem. B* **2000**, *104* (17), 4164–4168.

(40) Abay, H. K.; Svartaas, T. M. *Energy Fuels* **2010**, *24*, 752–757.

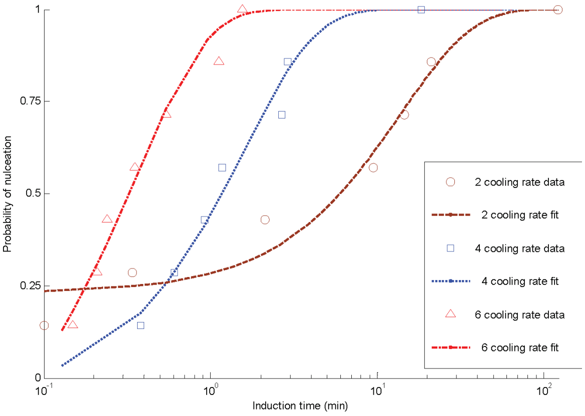

Figure 5. Nucleation probabilities versus induction time for SNG2.

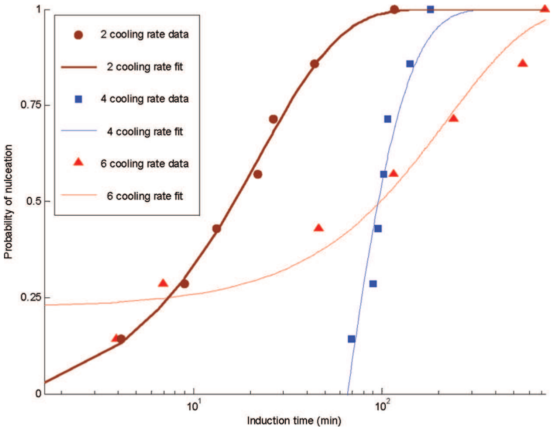

Figure 6. Nucleation probabilities versus induction time for SNG7.

Table 2. Estimated Nucleation Rate and Induction Time for Multicomponent Hydrate Formation

cooling rate (°C/h)	total number of experiments performed	J_2 (min^{-1})	τ_2 (min)	J_7 (min^{-1})	τ_7 (min)	percent difference in the nucleation rate (%)
2	14	7.2×10^{-2}	−3.6	4.5×10^{-2}	1.0	37.5
4	14	6.3×10^{-1}	0.1	2.3×10^{-2}	65.7	96.3
6	14	2.8×10^{-0}	0.2	4.5×10^{-3}	−40.1	99.8
2[a]	12	4.4×10^{-2}	−12.6	2.6×10^{-2}	−5.1	41
6[a]	12	2.6×10^{-0}	0.8	4.9×10^{-3}	−1.4	99.1

[a] Repeat in the other, similar cell, with two T-sensors and a different dimension of stirrer blade.

Contrary to SNG2, the nucleation rate of SNG7 is generally reduced as the cooling rate increases from slow to fast, as shown in Table 2. The induction time showed a different trend, as compared to the SNG2 mixture; i.e., as the cooling rate decreases, the SNG2 nucleates more easily but SNG7 oscillates, indicating that the system has difficulties in attaining a constant rate of nucleation. Figure 7 shows the comparison of the stochastic nature of nucleation for SNG2 and SNG7 when the cooling rate is changed in steps of 2 °C/h from 2 to 6 °C/h during the main set of experiments. For the slow cooling rate, both gases have comparable probability distribution, which could be an indication that, when both of

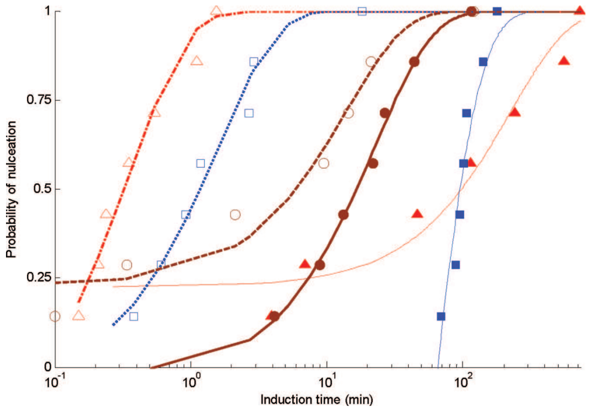

Figure 7. Comparison of the stochastic nature of nucleation for SNG2 (open symbols, dashed lines) and SNG7 (filled symbols, solid lines).

these two sII forming systems are given enough time, the stochastic nature of nucleation is comparable, irrespective of the composition difference. Both gas mixtures contained similar amounts of sII "nucleators" (7.49 mol % C_3 for SNG2 and 7.37 mol % $C_3 + C_4$ mixture for SNG7; see Table 1), which could increase the probability of a similar response at low cooling rates. However, for a fast cooling rate, both systems showed opposing behavior: SNG2 has a probability distribution function shifted toward a shorter induction time, whereas SNG7 has a probability distribution function shifted toward a longer induction time, implying that increasing the number of components in a gas does not reduce the induction time. The observed effect of the reduced nucleation rate by the increased cooling rate for SNG2 could probably be explained by coupled heat and mass fluxes (thermodiffusion) as described by irreversible thermodynamics. In our system, a temperature gradient, $\Delta T = T_c - T_w$, pointing from the center of the cell (T_c) toward the cell wall (T_w) was setup during cooling. The temperature gradient increases by increasing the cooling rate. During 2, 4, and 6 °C/h cooling sequences, the temperature measured in the gas phase close to the cell wall remained stable at a level of 0.17, 0.39, and 0.61 °C above the temperature outside the cell, respectively. For SNG2 stationary systems subjected to a temperature gradient, principles of irreversible thermodynamics suggest that the heavier component will move toward the colder surface to setup a concentration gradient as heat and mass fluxes are coupled through entropy production (change) in the system, as shown in eq 7. Coupled heat and mass fluxes in the SNG2 system are only dependent upon one single interdiffusion coefficient (that of propane in methane), and the apparent correlations between observed effects and mass and heat fluxes can be proposed. If ΔT is sufficiently high, the propane concentration may be sufficiently elevated at the cell wall, thereby affecting the process in the study. Then, if the heterogeneous nucleation in the cell preferentially occurs at the wall−water vapor interface, then an elevated concentration of propane at the cell wall could explain the increased nucleation rate at the highest cooling rate. The SNG7 system is more complex because 21 interdiffusion coefficients are needed to describe mass fluxes in the system. In addition, SNG7 contains CO_2, which is more soluble in water than the hydrocarbon (HC) components.

It is also possible that the cooling rate as well as the individual concentration of components at the site of nucleation affect the critical size during nucleation. In a study[41] of heating rate effects on transient nucleation problems, the survival size dependence upon the heating rate has been discussed. In the discussion, it is pointed out that a critical size depends upon the temperature. The temperature in our case was continuously being changed during cooling that could affect the critical size and, hence, the nucleation process. However, this effect cannot explain the opposite behavior of SNG2 and SNG7 with respect to the nucleation rate. If CO_2, which is easily soluble in water or other sI "preferring" HC components in the mixture, makes the system flicker between sI and sII nucleation during cooling when the system is far from the equilibrium saturation level, this may give a possible explanation of the observed effect for the cooling rate on SNG7. We have to admit that the SNG7 system is complex and that several simpler mixtures between methane and the other components must probably be investigated independently before a reliable explanation of the effect of this mixture can be stated. Ternary mixtures will involve three diffusion coefficients, and quaternary mixtures will involve six coefficients. Thus, gas mixtures containing more than three different gases may probably be too complex if basic mechanisms are going to be revealed by simple experimental investigations.

The rate of nucleation, $J_{2,7}$, versus cooling rate is plotted in Figure 8 for both SNG2 and SNG7. The circle and square symbols represent estimated values of the rate of nucleation for the main set of the experiment. The triangle and diamond symbols represent values of the repeat experiment for the slow and fast cooling rates. All estimated values for all experiments show that the rate of nucleation for SNG7 is lower for all cooling rates used, as compared to results for SNG2. The percentage difference in nucleation rates of SNG2 versus SNG7 at the various cooling rates is listed in Table 2. At the slow cooling rate, the percentage difference is

---

(41) Shneidman, V. A. *J. Chem. Phys.* **2007**, *127*, 041102-1–041102-4.

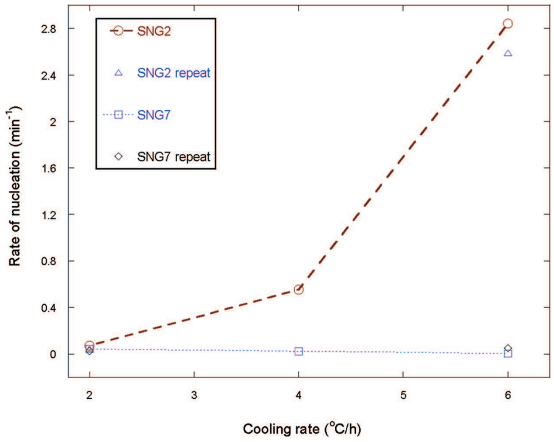

Figure 8. Rate of nucleation versus cooling rate for SNG2 and SNG7.

comparable, but at the fast cooling rate, the difference becomes pronounced.

According to the classical nucleation theory of multicomponent systems, the effects of the rate of nucleation of SNG2 and SNG7 could be described by eq 5. From the equation, we see that the rate of nucleation is dependent upon the activation energy for the critical size nuclei in both cases. The activation energy, in turn, is dependent upon many parameters, of which the composition in the aqueous phase is the most influential according to the specific expression (eq 1) of the activation energy for a multicomponent critical hydrate nucleus. During cooling, the system is stationary without stirring and gas components dissolve in the aqueous phase by diffusion through the gas–water interface. During this period, there is also a temperature gradient between the "high heat capacity" water phase and the "lower heat capacity" vapor phase that could affect the exchange of components between these phases during this "pre-period" of the experiment that makes the system even more complex. The solubility of gas components increases as the temperature decreases, and the abilities of the various gas types to enter the water phase are dependent upon various parameters, such as solubility, diffusivity, concentration (i.e., partial pressure/fugacity), etc. Thus, fluctuations in the concentration may be expected during the non-stirred cooling sequence. In addition, CO_2 is more soluble in water than the HC components and N_2, so that CO_2 may play an important role in the nucleation process prior to obtaining equilibrium concentrations (supersaturation) of the various gas components in the aqueous phase after the start of stirring.

For SNG7, the relatively high solubility of CO_2 in water may be of more importance for effects on nucleation than coupled mass and heat fluxes toward the cold wall surface. Possible additional effects of coupled heat and mass fluxes toward the cold cell wall during cooling are difficult to evaluate for the more complex SNG7 mixture because 21 interdiffusion coefficients are required. In this mixture, ethane, propane, and butane have the highest molecular weights and heat capacities and would probably all be the major components if coupled heat and mass flux processes toward the cold surface are important factors for the effect on nucleation. Ethane, having a heat capacity comparable to propane and the lowest molecular weight and, thus, the highest diffusivity of these three gas components and also because of its concentration level in SNG7, may balance mass fluxes and any concentration buildup of the sII, forming components propane and butane at the cell wall. All of these factors may give some additional contribution to increased activation energy for sII hydrate nucleation in the SNG7 system together with the far more water-soluble CO_2 gas. On the other hand, an increased concentration of propane at the cell wall for the SNG2 system through coupled heat and mass fluxes may give reduced activation energy through the metal surface, acting as a kind of catalyst for the process. Other parameters, such as the temperature, pressure, stirring rate (after the start of experiments), apparatus, and degree of subcooling used, could be considered the same for both multicomponent gases, contributing no or negligible effect on the rate of nucleation.

According to Makogon,[42] methane hydrate nucleation preferentially took place at the gas–water interface away from the wall because of capillary forces from the meniscus existing at the gas–water–cell wall interface. However, at cooling rates higher than 1–3 K/h, he observed an increased tendency of nucleation at the gas–water–metal boundary (i.e., at the cell wall). He assumed this because of a lower temperature at the meniscus than at the interface closer to the cell center. Such an effect could not help explain the observed difference between our SNG2 and SNG7 mixtures, but temperature effects and an increased propane concentration at the gas–water–cell wall (meniscus) interface may both be factors responsible for the increased nucleation rate at a high cooling rate during our SNG2 nucleation experiments. Another factor could be the extra molecules present in SNG7. In comparison to SNG2, SNG7 has extra molecules (ethane,

---

(42) Makogon, Y. F. *Hydrates of Hydrocarbons*; PennWell Publishing Company: Tulsa, OK, 1997; pp 65–70.

Table 3. Molar Composition of Phases Present after Nucleation

	SNG2			SNG7		
component	aqueous	vapor	sII hydrate	aqueous	vapor	sII hydrate
methane	0.000653	0.923944	0.0810	0.000585	0.808215	0.078435
ethane	0	0	0	0.000087	0.103250	0.005838
propane	0.000064	0.075369	0.0494	0.000043	0.050140	0.030863
isobutane	0	0	0	0.000002	0.007535	0.010852
n-butane	0	0	0	0.000011	0.016537	0.002240
carbon dioxide	0	0	0	0.000224	0.012604	0.001096
nitrogen	0	0	0	0	0.001075	0.000025
water	0.999283	0.000687	0.8696	0.999048	0.000645	0.870653
phase fraction	0.963666	0.036334	0	0.963133	0.036867	0

isobutane, *n*-butane, and carbon dioxide), which are competitors for the larger $5^{12}6^4$ cavity during the formation of sII hydrates. However, the competition for this cavity is affected by the solubility of each gas, which, in turn, is affected by the cooling rate and the changing temperature that alters the solubility of every gas molecule during the course of nucleation upon cooling.

Table 3 shows the molar composition of phases present after nucleation, which is calculated using CSMGEM. Three phases (aqueous, vapor, and hydrate) are available in the system. A total of 87% of the sII hydrate is composed of water in both SNG2 and SNG7. The molar composition of the vapor phase could be used to indirectly estimate components that are involved during the process of sII formation. The components in the aqueous and hydrate phases could inform which molecules are key factors for the process. As shown in the table, methane and propane are the key elements in the structure formation for both SNG2 and SNG7. In SNG7, almost all components contributed for the formation of sII hydrate, except nitrogen. Nitrogen is a simple sII hydrate former that can stabilize both the small 5^{12} and the large $5^{12}6^4$ cavities of the sII structure. Propane and isobutane are sII hydrate formers, stabilizing only the larger $5^{12}6^4$ cavity. For SNG7, Table 3 shows that the gas composition in the aqueous phase is dominated by methane and CO_2 despite a relatively low CO_2 concentration in the vapor phase, as compared to methane, ethane, and propane. CO_2 is primarily a sI hydrate former, and the high concentration of CO_2 in the water phase may affect the activation energy for the formation of the given sII hydrate, although CO_2 fits into the sII cavities and gives contribution to its stability. Such factors may delay the nucleation rate of SNG7, as compared to SNG2, which has only two gases that could fit into two different cavities without any competition.

Natural gases actively dissolve in water even at low pressures. Generally, the solubility of natural gases decreases with an increasing molecular weight of hydrocarbons, and the presence of inorganic gases, such as carbon dioxide and nitrogen, could affect the solubility of the natural gas in water.[42] The presence of the acid gas CO_2 in SNG7 increases the solubility of the hydrocarbon gases in water, whereas the presence of the other inorganic gas N_2 decreases the gas solubility in water. However, the amount of N_2 is low and could be assumed negligible. Besides, upon cooling to attain the desired temperature for the operating condition using the three different cooling rates, the system temperature changes with time. The system pressure also changes in accordance with the real gas equation. The change in the temperature and pressure of the system induces a change in the solubility of the components in both SNG2 and SNG7. The main reason is that the solubility of gas in water depends upon the temperature, the partial pressure of the gas over the liquid water, the nature of the solvent (in this work, DIW), and the nature of the gas from Henry's solubility law. The hydrate formation process could change the solubility of the organic gases and may show divergence from the normal Henry's law of solubility.[43] Inorganic gases may also change solubility. For example, the solubility of CO_2 increases with a decreasing temperature in the absence of gas hydrate, but this trend becomes reversed in the presence of gas hydrate; i.e., the solubility of CO_2 decreases with a decreasing temperature in the hydrate formation region.[44] The solubility change in SNG7 is assumed more complex than the process for SNG2 because of the extra molecules that are subjected to change their solubility of the individual gas components continuously upon cooling. In addition, the relatively high concentration of CO_2 in the water phase, as compared to the other gas components, may affect sII nucleation, as mentioned above.

The chemical potential of each molecule in the cluster will also affect the solute concentration at which the *n*-sized cluster can coexist with the solution, cluster solubility.[45] All of these conditions make SNG7 difficult to equilibrate the system easily, as compared to SNG2, where only two hydrocarbon molecules are present. Because hydrate formation in the bulk water is like "vacuuming" dissolved gas from the water phase to the region of the growing cluster in the water phase, solubilities of SNG2 and SNG7 play the major role for the rate of nucleation. Besides, the hydrate nucleation rate in the water phase is determined mainly by the flux of dissolved gas to the surface of a growing cluster in the water phase. These dissolved gases may show an oscillating reaction during nucleation. Chemical oscillations involving nucleation and growth of bubbles from a solution in other systems were reported,[46] and their mechanisms were discussed. Chemical oscillations because of the solubility of components in SNG7 could possibly result in a reduced nucleation rate, as compared to SNG2.

Knowing the effect of the gas component on the rate of nucleation without any additive is of paramount importance in laying the foundation for testing the effect of additives on the rate of nucleation. The effect of the cooling may be different in a continuously stirred system during cooling; therefore, the choice of the test method and the effect of the test method are also important for the evaluation of the effect of additives. One has to take into consideration the effect of

---

(43) Song, K. Y.; Feneyrou, G.; Fleyfel, F.; Martin, R.; Lievois, J.; Kobayashi, R. *Fluid Phase Equilib.* **1997**, *128*, 249–260.

(44) Servio, P.; Englezos, P. *Fluid Phase Equilib.* **2001**, *190*, 127–134.

(45) Kashchiev, D. *Nucleation: Basic Theory with Applications*; Butterworth-Heinemann: Oxford, U.K., 2000; p 77.

(46) Noyes, R. M. *J. Phys. Chem.* **1990**, *94*, 4404–4412.

the gas composition as well as the test method before testing the effect of additives, such as KHIs, on different multicomponent gas hydrate nucleations. In a non-stirred system during cooling, the effect of the same additive on nucleation of two different multicomponent gas mixtures could be different because the component itself plays its own role during the nucleation process. Besides cooling, the presence of an additive could also change the solubility of gas species,[47] which, in turn, may affect the rate of nucleation in the region of the growing cluster, leading to even more complex processes that are challenging to describe.

Conclusion

Two different gas mixtures, SNG2 and SNG7, have been used in studying the effect of the gas composition and cooling rate on the kinetics of sII hydrate formation and the stochastic nature of nucleation. The systems were cooled without stirring at three different cooling rates of 2, 4, and 6 °C/h, keeping other parameters that could affect the kinetics the same for both SNG2 and SNG7. The experimental results showed that the rate of nucleation is dependent upon gas composition and different gas compositions respond differently on the same cooling rate. For the slower cooling rate of 2 °C/h, the rates of nucleation in both systems were of comparable magnitude at the selected *P* and *T* conditions. However, for the faster cooling rate of 6 °C/h, SNG2 gave an increased nucleation rate by a factor of 38.9, while the nucleation rate was reduced by a factor of 10 for SNG7.

The classical theory of nucleation in multicomponent systems, the probability distribution function, and the principle of irreversible thermodynamics have been employed in an attempt to understand the experimental results. The dependence of the critical size upon the temperature and gas composition, chemical oscillations because of the solubility change of individual gas components, and coupled mass and heat fluxes during cooling were the possible explanations for the observed effects. Such information on system responses is of paramount importance for reliable evaluation of effects of low-dosage hydrate inhibitors, such as KHIs.

Acknowledgment. The authors thank NFR for the financial support of this work.

---

(47) Ma, Q. L.; Chen, G. J.; Guo, T. M. *Fluid Phase Equilib.* **2003**, *205*, 291–302.

Appendix C

Paper III

Effect of Gas Composition on sII Hydrate Growth Kinetics

By:

Hailu K. Abay, Thor M. Svartaas and Ke Wei.

Printed in:

Journal of Energy & Fuels, **25**, 1335-1341, (2011).

The paper is reprinted with permission from the American Chemical Society. Copyright © 2011.

energy&fuels ARTICLE
pubs.acs.org/EF

Effect of Gas Composition on sII Hydrate Growth Kinetics

Hailu K. Abay,* Thor M. Svartaas, and Wei Ke

Department of Petroleum Engineering, Faculty of Science and Technology, University of Stavanger, 4036 Stavanger, Norway

ABSTRACT: Kinetics of hydrate formation is of paramount importance for hydrate prevention in pipelines and gas storage in a hydrate state. The effect of gas composition on the kinetics of structure II (sII) hydrate growth has been examined by using two different synthetic natural gases, one with two components (SNG2) and the other with seven components (SNG7). The hydrate equilibrium properties of SNG2 and SNG7 were comparable and the initial degree of subcooling was thus approximately the same during all growth experiments. The same PT conditions and stirring rate were also set for both SNGs enabling us to examine the effect of gas composition on the growth behavior of the same crystal structure. The amount of gas consumed and the structure of the growth curves have been investigated to understand the effect of gas composition on the kinetics of sII hydrate formation. In addition, several chemicals (MeOH, PVP, PVCap) have been tested for their effects on the amount of hydrate formation and structure of the growth curves. The results showed that the amount of sII hydrate formed from SNG7 was doubled as compared to SNG2 with and without the additives. This could be explained by the higher amount of large cavity preferring gas components in SNG7 as compared to SNG2. On the other hand, the growth rate of sII hydrate made from SNG7 first increased toward a maximum value after hydrate onset, and then decreased toward zero at the end of experiment. This growth behavior was not observed for sII hydrate structure produced from SNG2. The SNG2 growth rate showed a maximum at onset and then decreased toward zero eventually. The addition of the chemicals did not change the characteristic growth behavior produced by the individual gas mixtures. The chemicals had an effect in shifting the initial growth rates either up or down based on concentration and type of the chemicals used while the structure of growth rate versus time was kept the same. This study confirmed that gas composition alone is an important parameter for sII hydrate growth kinetics, and the same hydrate structure produced from different gas compositions does not necessarily show the same growth behavior.

■ INTRODUCTION

Gas hydrates are nonstoichiometric crystalline compounds that are composed of water molecules as hosts with encaged gas molecules as guests. The process of encaging a guest into a host starts under suitable low temperature and high pressure conditions. Such process of hydrate formation has two major stages, nucleation and growth, that has drawn considerable attention in the petroleum industry since the discovery[1] that gas hydrates plug pipelines and cause costly operations. On the other hand, studying gas hydrate nucleation and growth is of great importance in relation to various aspects of hydrate production such as gas storage and transportation. Thus, knowledge of the dynamics of gas hydrate formation could be important in determining the parameters for production of gas hydrates and in understanding plug conditions in pipelines.[2] Despite many attempts to understand nucleation and growth kinetics, still little is known about the process as compared to hydrate thermodynamics because time-dependent processes of hydrate nucleation and growth are challenging with regard to measurement and modeling.[3]

In studying the effect of gas composition on the kinetics of hydrate growth, SNG2 and SNG7 multicomponent gases were selected. Both gases form sII hydrates which is the most common structure formed in oil and gas pipelines. A sII unit cell consists of sixteen small (5^{12}) cages and eight large ($5^{12}6^4$) cages. The cages are formed from hydrogen-bonded water molecules in which one single guest molecule is located at or near the center of the host. The smaller cage accommodates only the smaller guest molecule such as, e.g., methane and nitrogen. The larger cage accommodates all gas components in the mixture, but is preferentially occupied by propane, butane, and ethane.

The effects of three different chemicals on the growth kinetics of sII hydrates formed from SNG2 and SNG7 were also tested. Methanol (MeOH), polyvinylpyrrolidone (PVP), and polyvinylcaprolactum (PVCap) were selected for the study of their effects on sII hydrate growth rate curves. The chemicals represent two classes of inhibitors: thermodynamic hydrate inhibitors (THIs) and kinetic hydrate inhibitors (KHIs). As a THI, methanol shifts the phase boundary thermodynamically to the lower temperature and/or higher pressure when used at high concentrations. At low concentrations, MeOH shows inhibition, promotion, or dual effects on hydrate formation process.[4−7] Unlike the conventional THIs, a recent method of retarding crystal growth was achieved by using water-soluble polymers like PVP and PVCap. These polymers are well-known KHIs that belong to the class of low dosage hydrate inhibitors (LDHIs).[8] Experimental[9,10] and simulation[11,12] studies showed that, compared to PVP, PVCap is a more effective kinetic inhibitor. It has a better attachment to the surface of a growing crystal resulting in retardation of hydrate formation. The optimal performance depends on a certain concentration at a given pressure,[13] i.e., increasing concentration of KHIs does not always increase inhibition performance. Such effects of THIs and KHIs on the kinetics of hydrate formation have been a focus, whereas gas

Received: December 14, 2010
Revised: February 15, 2011
Published: March 10, 2011

ACS Publications © 2011 American Chemical Society

Table 1. Composition of SNGs Used

component		SNG2 (mol %)	SNG7 (mol %)
CH_4	methane	92.50	80.40
C_2H_6	ethane	0	10.30
C_3H_8	propane	7.50	5.0
i-C_4H_{10}	i-butane	0	1.65
n-C_4H_{10}	n-butane	0	0.72
CO_2	carbon dioxide	0	1.82
N_2	nitrogen	0	0.11

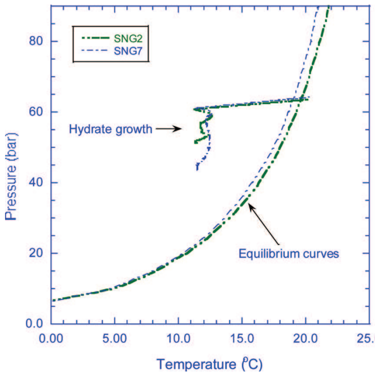

Figure 1. Pressure vs temperature graph during sII crystal growth for both SNG2 and SNG7.

composition itself as a kinetic parameter has never been investigated with and without additives. In this paper, the main focus is investigating the effect of gas composition on sII hydrate growth kinetics in addition to studying the effects of low concentrations of MeOH, PVP, and PVCap on the kinetics.

Table 1 shows the compositions in mol percentage of SNG2 and SNG7 gases used in the investigation of the effect of gas composition on sII hydrate growth kinetics. SNG2 and SNG7 experiments were done at the same PT conditions. Moreover, the equilibrium curves of each SNG based on predictions using CSMGem were comparable as shown in Figure 1 enabling us to keep approximately the same degree of subcooling. The degrees of subcooling for both gases are more comparable during the first stages of hydrate growth than the later stages. Investigating the effect of gas composition requires operation at similar degree of subcooling, as studies[14−22] on formation rates indicated that growth kinetics are dependent on the degree of subcooling used. Besides, the degree of agitation has an effect[14,16,23] on the rate of hydrate crystallization, and hence the experiments were performed for a constant stirring rate of 750 rpm for both SNGs. Thus, by keeping these parameters that could affect the kinetics approximately the same, we investigated the effect of gas composition on sII hydrate growth kinetics with and without the additives. Growth kinetics could be determined by using the rate of change in moles of free gas,[24−26] or equivalently, directly from the gas consumption plots by applying the principle of mass conservation as mass is conserved in an isochoric cell system.

■ EXPERIMENTAL SETUP AND PROCEDURE

The effect of gas composition on sII hydrate growth kinetics was investigated in the high pressure cell apparatus shown in Figure 2. The autoclave cell is cylindrical with an inner volume of 145 mL, of which 50 mL was filled with distilled water (DIW) with or without the additives and 95 mL was filled with SNG2/SNG7. The temperature of the cell was controlled by the refrigerated and heating circulator with programmable temperature control unit. Two temperature sensors were used, one in the vapor phase and the other in the aqueous phase. This enabled us to track the temperature pulse in the vapor phase and aqueous phase during gas consumption and hydrate growth as shown in Figure 3. Each temperature sensor had an accuracy of ±0.03 °C (Pt-100 1/10 DIN elements) and the temperature was measured within an accuracy of ±0.1 °C. The pressure was measured with an accuracy of ±0.2 bar. The system temperature and pressure changes were monitored and recorded using LabView.

Two different gas supply cylinders with two different synthetic natural gases of SNG2 and SNG7 (see Table 1) were used for the study of the effect of gas composition on sII hydrate growth kinetics. Both gases form sII hydrates with no liquid hydrocarbon phases. A total of 32 experiments were run for both SNG2 and SNG7 with and without the additives MeOH, PVP, and PVCap. MeOH (liquid), PVP (dry powder, $M_w \approx 15{,}000$) and PVCap (dry powder, $M_w \approx 6{,}000$) were prepared in distilled water in the range 0−100 ppm by weight. The pure water was considered as 0 ppm baseline for comparison. The system was then cooled from an initial temperature of 20 °C to an experimental temperature of 11 °C using a cooling gradient of 2 °C/h. The system pressure was 60 bar at the end of the cooling sequence and the start of the experiments. After attaining a stable temperature and pressure at the experimental conditions, cell agitation was introduced. The start of cell agitation was considered as the start of the experiment for studying the growth kinetics of sII hydrates.

■ RESULTS AND DISCUSSION

Amount of sII Hydrate Formation. Figure 1 shows the pressure drop for both SNG2 and SNG7. Such pressure drop gives an estimation of the amount of sII hydrates formed from each SNG by employing the real gas equation for the isochoric system as

$$\Delta n = \frac{V}{zRT}\Delta P \tag{1}$$

where Δn is the amount of gas consumed during sII hydrate formation, V is SNG2/SNG7 volume, z is the compressibility factor which is slightly different for both SNGs but with comparable value, R is the universal gas constant, T is the measured experimental temperature, and ΔP is the measured experimental pressure drop caused by sII hydrate formation. Approximating the term V/zRT as the constant of proportionality which does not change significantly for all the experiments of each SNG, we have

$$\Delta n \propto \Delta P$$

indicating that the amount of gas consumed and the pressure drop are directly proportional with each other. Alternatively, employing the gas consumption vs time plot of both SNG2 and SNG7, one can estimate the amount of hydrate formation. Figure 4 shows the gas consumption vs time for the baseline and the 50 ppm experiments for both SNG2 and SNG7. The induction time, the time taken by the system from the start of stirring (cell agitation) to onset of hydrate formation, was reset to

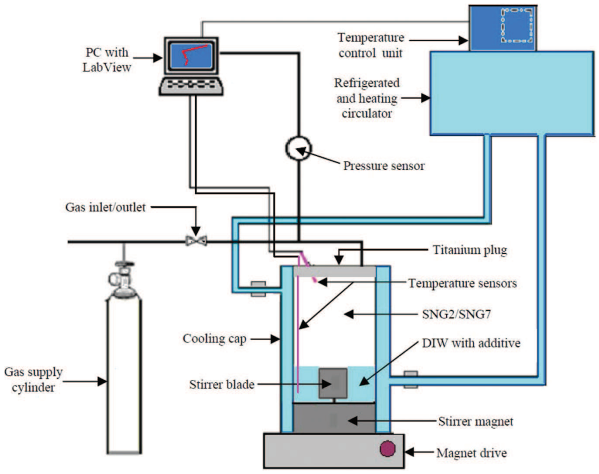
PC with LabView
Temperature control unit
Refrigerated and heating circulator
Pressure sensor
Gas inlet/outlet
Titanium plug
Temperature sensors
SNG2/SNG7
DIW with additive
Cooling cap
Stirrer blade
Gas supply cylinder
Stirrer magnet
Magnet drive

Figure 2. Experimental setup used for studying the effect of SNG2/SNG7 on sII hydrate growth kinetics.

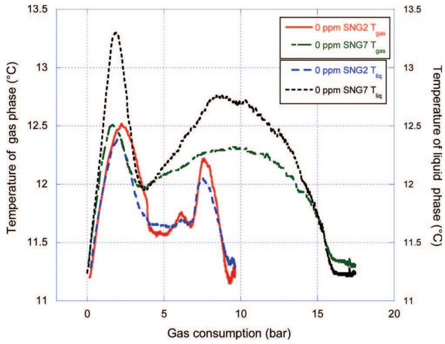

Figure 3. Temperature pulse of the gas and liquid phase during gas consumption. The lower curves are SNG2 temperature profiles and the upper curves are SNG7 temperature profiles.

count zero at hydrate onset for each parallel. Either from the pressure drop (Figure 1) or from the gas consumption (Figures 3 or 4), one can clearly see that the amount of sII hydrate formed from SNG7 was nearly twice of the amount of hydrate formed from SNG2 with and without the additives. A similar difference was observed for experiments with 100 ppm additives in solution implying that difference in gas composition matters for the amount of hydrate formation. The main reason SNG7 produced more hydrates than SNG2 and thus gave greater pressure drop could be explained by the gas compositions and the individual content of large cavity preferring components in the mixtures. Both systems are water excess and the conversion of water into sII hydrate is limited by the amount of sII formers available.

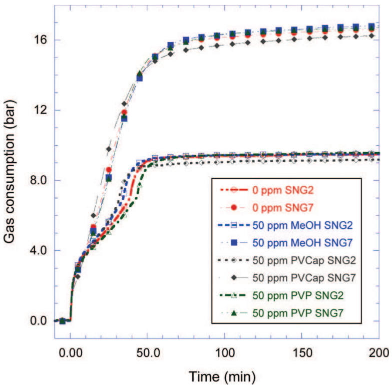

Figure 4. Gas consumption vs time for 50 ppm additives. The amount of sII hydrate formed from SNG7 (filled symbols) is nearly double that of SNG2 (open symbols), regardless of the additives.

Flash calculations conducted by CSMGem on SNG2 system suggested a phase fraction of hydrate equal with 0.185 at the experimental "equilibrium". The simulated compositions and phase fractions are shown in Table 2. This Table shows flash results at the initial equilibrium conditions (left 3 columns) and final experimental conditions (right 3 columns). Mass balance calculations based on simulated phase fractions and compositions indicated that the phase fraction of hydrate could be slightly overestimated. However, the residual gas fraction was considerably depleted in sII former (here propane) at the end of the experiment as demonstrated by the flash calculation. This

Table 2. Molar Composition of Phases Present at the Initial and Final Conditions of SNG2 System from CSMGem Flash Calculations

	T = 19.32 °C			T = 11.21 °C		
	P = 60.29 bar			P = 50.73 bar		
	stable convergence			stable convergence		
component	aqueous	vapor	sII hydrate	aqueous	vapor	sII hydrate
methane	0.001242	0.924295	0.090209	0.001364	0.992204	0.103750
propane	0.000073	0.075206	0.047970	0.000010	0.007451	0.035492
water	0.998685	0.000499	0.861820	0.998626	0.000345	0.860759
phase fraction	0.906768	0.093232	0.000000	0.747385	0.067615	0.185000

Table 3. Molar Composition of Phases Present at the Initial and Final Conditions of SNG7 System from CSMGem Flash Calculations

	T = 18.73 °C			T = 11.49 °C		
	P = 60.64 bar			P = 40.0 bar		
	stable convergence			metastable convergence		
component	aqueous	vapor	sII hydrate	aqueous	vapor	sII hydrate
methane	0.001111	0.806024	0.087476	0.000987	0.882158	0.090336
ethane	0.000123	0.103435	0.006148	0.000103	0.085679	0.018724
propane	0.000046	0.050341	0.025199	0.000009	0.007796	0.017537
i-butane	0.000005	0.016704	0.016627	0.000001	0.001332	0.006402
n-butane	0.000004	0.007267	0.000730	0.000004	0.004366	0.001623
carbon dioxide	0.000421	0.014643	0.001311	0.000448	0.016851	0.001579
nitrogen	0.000001	0.001112	0.000033	0.000001	0.001395	0.000035
water	0.998289	0.000475	0.862475	0.998448	0.000424	0.863762
phase fraction	0.900882	0.099118	0.000000	0.680173	0.064827	0.255000

explains why the hydrate formation process stops at some defined P and T conditions inside the hydrate region of the initial gas composition.

For SNG7, CSMGem failed during calculation of phase fractions and compositions at the final experimental pressure and temperature conditions due to problems with convergence or number of iterations. Some flash results with metastable convergence were obtained at temperatures far above the final temperature of the experiments at the given pressure, and mass balance calculations suggested that the indicated phase fraction of hydrate was considerably underestimated. However, the flash showed that the residual gas fraction will be considerably depleted of large cavity fillers (here ethane, propane, and butane) when sufficient amount of hydrate is formed under isochoric conditions. This demonstrates that hydrate formation process will stop at some defined P and T conditions inside the hydrate region of the initial gas composition. Results from the CSMGem flash simulations on SNG7 are shown in Table 3.

Growth Rate Curves of sII Hydrates. The gas consumption curves in Figure 4 have been used to investigate the structure of the growth rate curves of sII hydrate crystals with and without the additives for both SNG2 and SNG7. The gas consumption plots were fitted with a polynomial of degree 9 given by

$$p = a_0 + a_1 t + a_2 t^2 + ... + a_7 t^7 + a_8 t^8 + a_9 t^9 \qquad (2)$$

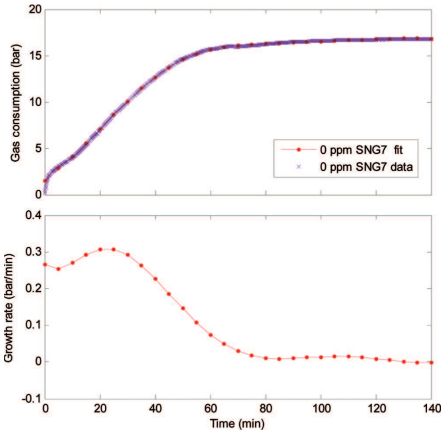

Figure 5. Gas consumption, polynomial fit, and growth rate vs time curves for 0 ppm SNG7. The upper figure shows the gas consumption vs time for the gas consumption data and the corresponding polynomial fit. The lower figure shows the growth rate curve vs time calculated from the polynomial fit.

where p is the gas consumption in bar, t is the time in min, and a_i where i = 0,1,...,8,9 are coefficients which were fit with 95% confidence bounds. The first derivative of eq 2 gives the slope of a line that is tangent to the gas consumption curve at each time. This slope estimates the global growth rate of sII hydrate formation for both the SNG2 and SNG7 systems in bar/min. The gas consumption plot, the polynomial fit, and the corresponding growth rate curves were plotted as a function of time in Figure 5 for the 0 ppm SNG7 experiment. The initial growth rates at onset of hydrate formation and the structures of the growth rate curves were analyzed in detail for the investigation of the effect of gas composition on sII hydrate growth kinetics with and without the additives present. For SNG7, Figure 5 shows that the growth process is nearly finished after 80 min when the system is close to the local equilibrium between the phases present in the system. During the first 20 min of sII hydrate growth, the system showed some oscillations which can be related to heat release from the exothermic process and temperature fluctuations that affected the degree of subcooling part of the driving force. The temperature fluctuations during the growth process as shown in Figure 3 will most probably affect the observed global growth rate and give fluctuations. For both SNG2 and SNG7 systems, the temperature profiles of Figure 3 showed two peaks, one with a maximum close to onset.

Figure 6 shows the growth rate curves of sII hydrates produced from SNG2. Time zero represents onset for hydrate formation. For SNG2 maximum growth rate occurred at onset, and then growth rates for all SNG2 systems decayed over the next 18−20 min after onset. In this period, the rates showed fluctuations before finally decaying toward zero value at the end of the process. The temperature profile for SNG2 reaction as shown in Figure 3 “reflects” the growth profile as shown in Figure 4 and rate oscillations as shown in Figure 6. The growth curves for the

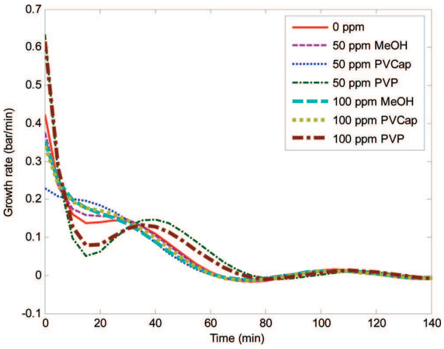

Figure 6. Growth rate vs time curves of SNG2 experiments for 50 and 100 ppm concentrations of MeOH, PVP, and PVCap. 0 ppm curve is the pure water baseline experiment.

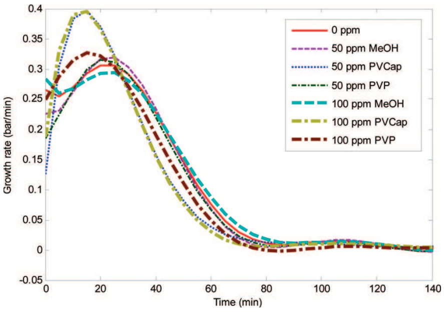

Figure 7. Growth rate vs time curves of SNG7 experiments for 50 and 100 ppm concentrations of MeOH, PVP, and PVCap including the reference curve.

PVP experiments showed higher initial rates and stronger fluctuations than the pure water, MeOH, and PVCap systems. It has a minimum growth rate near 19 min after onset. After this minimum value, the growth rates increased and then decayed to zero. The initial growth rate of sII hydrate formed from SNG2 was in the range between 0.2−0.7 bar/min for all the aqueous solutions examined. The maximum initial growth rate for SNG2 system was more than twice the maximum initial growth rate observed for the SNG7 system as shown in Figure 7. The range of the initial growth rate of sII hydrate formed from SNG7 was between 0.1 and 0.3 bar/min. The increased initial growth rate of sII hydrate produced from SNG2 as compared to the hydrate produced from SNG7 could be due to the large number of critical nuclei in SNG2 as compared to SNG7. In a multicomponent gas hydrate nucleation study[27] of sII hydrates from both SNG2 and SNG7, it was shown that SNG2 system nucleates more easily than SNG7 system. Moreover, as discussed before on the difference of the total amount of hydrate formation from SNG2/SNG7, more options of guest molecules for $5^{12}6^{4}$ cage fillings may contribute to an increased overall hydrate formation. Despite its promotion on hydrate formation, more options of guest molecules available in SNG7, however, may reduce the growth rate, especially during the starting period of the growth process. With abundant guest molecules in both SNGs for $5^{12}6^{4}$ cage fillings, $5^{12}6^{4}$ cage fillings may become the rate-limiting step in hydrate formation. The multiple $5^{12}6^{4}$ cage filling molecules (ethane, propane, *i*-butane, *n*-butane, carbon dioxide, and nitrogen) in SNG7 may compete with each other in occupying $5^{12}6^{4}$ cages and thus reduce the initial growth rate in an observable manner.

The structure of the growth curves of SNG7 was also different as compared to the structure of the growth curves of SNG2. As shown in Figure 7, the growth rates of sII hydrate produced from SNG7 initially increased to attain a maximum value, and then decreased to zero. Such differences in growth patterns for the same hydrate structure could be considered as a fingerprint of the effect of gas composition on growth kinetics. These sII hydrate growth curve structures were unique for each SNG, and the effects of the additives on these growth curves were shifting the curves up or down based on the concentration and type of the chemicals used while the unique structure remained the same.

The additives used play different roles for the growth kinetics of the system. MeOH may act on the surface tension. During a molecular dynamics study[28] on methanol−water mixtures it was observed that the surface tension of the solution was greatly reduced by adding a small amount of methanol to water. As hydrate formation requires transporting of guest molecules from the gas phase to the growing cluster in the liquid phase, the reduction in surface tension may have an effect on the growth process. Experimental work on methanol shows contradicting results with regard to hydrate cavity stabilization. FTIR spectra study[29] on thin-film vapor deposits of methanol with water showed that methanol can readily form sII mixed clathrate hydrates within a certain temperature range. Another experimental study[30] also showed that methanol has the potential to form and stabilize sII hydrate at low concentrations. On the other hand, further investigations using NMR and dielectrics proved that methanol cannot stabilize sII structure.[31] Despite such contradicting reports of methanol on forming and stabilizing hydrate cages, its presence in hydrate forming systems has some effects on hydrate formation. The hydroxyl group of methanol has an effect by hydrogen bonding with the water molecules, whereas the methyl group tends to organize the water molecules in direct competition for a hydrate guest. This may cause a lattice defect as lattice defects caused by guest−water hydrogen bonding in other systems have been reported[32] and a distorted lattice structure may enhance diffusion that could possibly affect the growth.

Another possible explanation of methanol effect on the kinetics could be through the temperature-dependent attractive and repulsive forces that could disturb the system's behavior. In a dilute aqueous solution of alcohols, a study[33] showed that alcohol molecules have temperature-dependent attractive and repulsive forces that affect the activity coefficient of alcohol and water. This may have an effect on the kinetics of sII hydrate formation since the kinetic rate is dependent on the temperature of the system described by the Arrhenius equation. In an investigation[34] on the influence of ethanol in optimizing formation rates, trace amounts of ethanol dramatically enhanced the formation of methane hydrate aggregates. Although the formation process and the hydrate structure was different from ours, it is an indication that trace amounts of alcohols in general can play a role in the kinetics of hydrate formation.

The effects of PVP and PVCap on hydrate growth are not by changing the thermodynamic phase boundary for the hydrate stability, but by delaying the growth of gas hydrate crystals. The growth inhibition by PVCap is a result of polymer adsorption to an active growing crystal surface where the adsorbed molecule is acting as a barrier for further growth.[35] PVP does not adsorb to the surface of a hydrate crystal, but only increases the surface energy of the interfacial region as a molecular dynamics study[36] showed. Achieved level of inhibition for such KHIs depends on degree of subcooling, type of polymer, molecular weight of polymer, and degree of agitation in solution. The initial degree of subcooling (8 °C), type of KHI (PVP or PVCap), molecular weight (15 000 for PVP and 6000 for PVCap), and solution agitation (750 rpm) were kept constant in all PVP and PVCap experiments to examine the effect of the additives on the structure of the growth rate curves. All the results showed that changing concentration and type of the chemicals has an effect in shifting the growth rate curves of sII hydrate. Because transporting the reactants to the growing product is a significant factor[37] for hydrate growth kinetics, PVP could easily affect this factor by increasing the surface energy of the interfacial region and PVCap by binding to an actively growing structure and result in delay for the growth process.

■ CONCLUSION

The effect of gas composition on the kinetics of sII hydrate formation has been investigated by using two different multicomponent gases: SNG2 and SNG7. Other factors that could affect the kinetics such as initial degree of subcooling, operating T and P, stirring rate, and type and molecular weights of the chemicals used were all kept constant to examine the effect of gas composition alone. The effects of the additives MeOH, PVP, and PVCap on the structure of the growth curves have also been studied. For all aqueous solutions the amount of hydrate formed from SNG7 was twice the amount of hydrate formed from SNG2 due to concentration differences in the large $5^{12}6^4$ cavity preferring gas components in the mixtures. Growth rate curves of sII hydrates produced from SNG2 and SNG7 were also different. SNG2 had a higher growth rate at onset of hydrate formation which then reduced to zero. SNG7 started with a lower growth rate at onset which then increased to a maximum value and then decayed to zero at the end of the experiment. The additives only shifted the growth curves of sII hydrates formed from both SNG2 and SNG7. The growth curves of SNG2 and SNG7 were unique for each composition, and this unique curve structure was not affected by the presence of the additives. This study confirmed that gas composition itself plays a major role in sII hydrate growth kinetics.

■ AUTHOR INFORMATION

Corresponding Author

*E-mail: hailu.k.abay@uis.no Telephone: +47 51832230. Fax: +47 51832050.

■ ACKNOWLEDGMENT

We thank NFR for the financial support of this work.

■ REFERENCES

(1) Hammerschmidt, E. G. *Ind. Eng. Chem.* **1934**, *26*, 851–855.

(2) Makogon, Y. F. *Hydrates of Natural Gas*; Penn Well Publishing Company: Tulsa, OK, 1981; p 82.

(3) Sloan, E. D.; Koh, C. A. *Clathrate Hydrates of Natural Gases*, 3rd ed.; CRC Press/Tayler Francis: Boca Raton, FL, 2008; p 180.

(4) Svartaas, T. M.; Fadnes, F. H. In *Proceedings of the 2nd International Offshore and Polar Engineering Conference*, San Francisco, USA, June 14−19, 1992; pp 614−619.

(5) Yousif, M.; Austvik, T.; Berge, L.; Lysne, D. In *Proceedings of the 2nd International Conference on Natural Gas Hydrates*, Toulouse, France, June 2−6, 1996; pp 291−298.

(6) Bobev, S.; Tait, K. T. *Am. Mineral.* **2004**, *89*, 1208–1214.

(7) Abay, H. K.; Svartaas, T. M. *Energy Fuels* **2010**, *24*, 752–757.

(8) Kelland, M. A. *Energy Fuels* **2006**, *20*, 825–847.

(9) Zeng, H.; Lu, H.; Huva, E.; Walker, V. K.; Ripmeester, J. A. *Chem. Eng. Sci.* **2008**, *63*, 4026–4029.

(10) Zhang, J. S.; Lo, C.; Couzis, A.; Somasundaran, P.; Wu, J.; Lee, J. W. *J. Phys. Chem. C* **2009**, *113*, 17418–17420.

(11) Kvamme, B.; Kuznetsova, T.; Aasoldsen, K. *J. Mol. Graphics Modell.* **2005**, *23*, 524–536.

(12) Anderson, B. J.; Tester, J. W.; Borghi, G. P.; Trout, B. L. *J. Am. Chem. Soc.* **2005**, *127*, 17852–17862.

(13) Lederhos, J. P.; Long, J. P.; Sum, A.; Christiansen, R. L.; Sloan, E. D. *Chem. Eng. Sci.* **1996**, *51*, 1221–1229.

(14) Vysniauskas, A.; Bishnoi, P. R. *Chem. Eng. Sci.* **1983**, *38*, 1061–1072.

(15) Happel, J.; Hnatow, M. A.; Meyer, H. *Ann. N.Y. Acad. Sci.* **1994**, *715*, 412–424.

(16) Parlaktuna, M.; Gudmundsson, J. In *Proceedings of the 2nd International Conference on Natural Gas Hydrates*, Toulouse, France, June 2−6, 1996; pp 439−446.

(17) Makogon, Y. F.; Makogon, T. Y.; Holditch, S. A. In *Proceedings of the Japan National Oil Conference*, Japan, October 20−22, 1998; pp 259−267.

(18) Freer, E. M.; Selim, M. S.; Sloan, E. D. *Fluid Phase Equilib.* **2001**, *185*, 65–75.

(19) Varaminian, F. In *Proceedings of the Fourth International Conference on Gas Hydrates*, Yokohama, Japan, May 19−23, 2002; pp 465−468.

(20) Turner, D.; Boxall, J.; Yang, S.; Kleehamer, D.; Koh, C.; Miller, K.; Sloan, E. D.; Xu, Z.; Mathews, P.; Tally, L. In *Proceedings of the Fifth International Conference on Gas Hydrates*, Trondheim, Norway, June 12−16, 2005.

(21) Tayer, C. J.; Miller, K. T.; Koh, C. A.; Sloan, E. D. In *Proceedings of the 6th International Conference on Gas Hydrates*, Vancouver, British Columbia, July 6−10, 2008.

(22) Peng, B. Z.; Chen, G. J.; Sun, C. Y.; Yang, L. Y.; Luo, H. In *Proceedings of the 6th International Conference on Gas Hydrates*, Vancouver, British Columbia, July 6−10, 2008.

(23) Herri, J.; Gruy, F.; Cournil, M. In *Proceedings of the 2nd International Conference on Natural Gas Hydrates*, Toulouse, France, June 2−6, 1996; pp 243−250.

(24) Karaaslan, U.; Parlaktuna, M. *Energy Fuels* **2000**, *14*, 1103–1107.

(25) Karaaslan, U.; Parlaktuna, M. *Energy Fuels* **2002**, *16*, 1387–1391.

(26) Karaaslan, U.; Parlaktuna, M. *Energy Fuels* **2002**, *16*, 1413–1416.

(27) Abay, H. K.; Svartaas, T. M. *Energy Fuels* **2011**, *25*, 42–51.

(28) Chang, T. M.; Dang, L. X. *J. Phys. Chem. B* **2005**, *109*, 5759–5765.

(29) Williams, K. D.; Devlin, J. P. *J. Mol. Struct.* **1997**, *416*, 277–286.

(30) Nakayama, H.; Hashimoto, M. *Bull. Chem. Soc. Jpn.* **1980**, *53*, 2427–2433.

(31) Davidson, D. W.; Gough, S. R.; Ripmeester, J. A.; Nakayama, H. *Can. J. Chem.* **1981**, *59*, 2587–2590.

(32) Alavi, S.; Susilo, R.; Ripmeester, J. A. *J. Chem. Phys.* **2009**, *130*, 174501-1–174501-9.

(33) Nord, L.; Tucker, E. E.; Christian, S. D. *J. Solution Chem.* **1984**, *13* (12), 849–867.

(34) Chen, P. C.; Huang, W. L.; Stern, L. A. *Energy Fuels* **2010**, *24*, 2390.

(35) Larsen, R.; Knight, C. A.; Sloan, E. D. *Fluid Phase Equilib.* **1998**, *150*—*151*, 353–360.

(36) Moon, C.; Hawtin, R. W.; Rodger, P. M. *Faraday Discuss.* **2007**, *136*, 367–382.

(37) Buch, V.; Devlin, J. P.; Monreal, I. A.; Cwiklik, B. J.; Aytemiz, N. U.; Cwiklik, L. *Phys. Chem. Chem. Phys.* **2009**, *11*, 10245–10265.

Appendix D

Paper IV

On the Kinetics of Methane Hydrate Formation: A Time-dependent Kinetic Rate Model

By:

Hailu K. Abay and Thor M. Svartaas.

Printed in:

Proceedings of the 7th International Conference on Gas Hydrates, Edinburgh, United Kingdom, July 17-21, 2011.

Proceedings of the 7th International Conference on Gas Hydrates (ICGH 2011),
Edinburgh, Scotland, United Kingdom, July 17-21, 2011.

ON THE KINETICS OF METHANE HYDRATE FORMATION: A TIME-DEPENDENT KINETIC RATE MODEL

Hailu K. Abay[1*] and Thor M. Svartaas[1]
Department of Petroleum Engineering[1]
Faculty of Science and Technology
University of Stavanger
4036, Stavanger
NORWAY

ABSTRACT

The kinetics of hydrate formation is of paramount importance for hydrate prevention and gas storage in a hydrate state. Methane hydrates were produced in a high pressure autoclave cell and kinetic rates were investigated in the presence of low concentrations of methanol (MeOH) and polyvinylcaprolactam (PVCap). The degree of subcooling has been used as the driving force for hydrate formation. A detailed analysis of the dynamics of the free gas content and the principle of mass conservation have been employed to understand the growth behavior in the liquid phase by considering a constant kinetic rate, and its limitations are discussed. The results show that kinetic rates in an isochoric cell system are not generally constant during the whole growth period of hydrate formation, and a time-dependent model is proposed. The model could also be utilized for testing the effect of other additives on the rate of growth of methane hydrates.

Keywords: crystallization, diffusion, heat transfer, kinetics, mass transfer, nucleation

NOMENCLATURE

k kinetic rate constant [mol/min, bar/min]
M_w molecular weight
n number of moles of free gas
P pressure [bar]
r growth rate [mol/min, bar/min]
T temperature [^oC]
ΔT degree of subcooling [^oC]
V gas volume [mL]
z compressibility factor

INTRODUCTION

Hydrate formation has two major steps, nucleation and growth. Contrary to hydrate thermodynamics, the time-dependent processes of hydrate nucleation and growth are challenging with regard to measurement and modelling [1]. The knowledge of the dynamics of hydrate formation and build-up of gas hydrates may be important in determining the parameters for production of gas hydrates, and in understanding plug conditions in the gas pipeline and/or the equipment [2]. The former has an advantage for gas storage in a hydrate state and the later has an advantage for the prevention of hydrate blockage in offshore processing, production, and transportation of natural gas and oil.

Two additives, methanol (MeOH) and polyvinylcaprolactum (PVCap), were selected for the study of methane hydrate formation. The two chemicals were selected to represent the two classes of inhibitors, thermodynamic and kinetic. Methanol is a thermodynamic hydrate inhibitor when used in large amounts. The method of prevention is by shifting the phase boundary thermodynamically to the lower temperature and/or higher pressure. In small amounts, methanol shows both inhibition and promotion effect. During hydrate crystallization process, an

---

[*] Corresponding author: Phone: +47 51 83 22 30 Fax +47 51 83 20 50 E-mail: hailu.k.abay@uis.no

experimental study [3] showed that methanol has an inhibition effect, whereas other experimental studies [4, 5] showed that it has promotional effect. Even at ultralow concentrations, methanol has a dual effect on the nucleation of methane hydrate formation [6].

PVCap is water-soluble polymer capable of delaying the growth of gas hydrate crystals. It is a kinetic hydrate inhibitor (KHI) that belongs to the class of low dosage hydrate inhibitors (LDHIs). A comprehensive review [7] on the history of LDHIs was given previously. PVCap has a higher free energy of binding (or more attractive interaction) with the hydrate indicating that it has a better attachment than other inhibitors. Such binding of an inhibitor to the surface of a growing crystal slows down hydrate formation. In addition to investigating the effect of low concentrations of PVCap and MeOH on the growth of methane hydrate formation, the main aim of this work is proposing a time-dependent kinetic rate model that could be employed for testing the effect of other additives on methane hydrate formation.

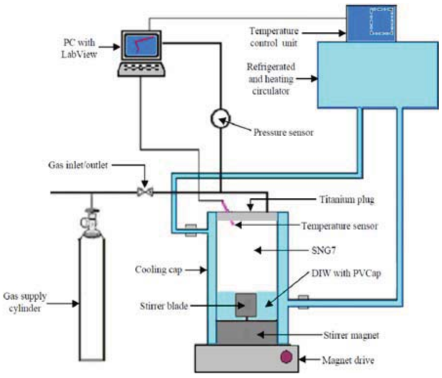

Figure 1. High pressure autoclave cell experimental setup.

Experimentally, the rate of hydrate formation could be determined by the thermodynamic conditions during the course of the experiment and the gas composition used. The change in the rate of moles of free gas has been used as an indicator of the rate of hydrate formation in an isochoric cell system during the study of promotional effect of polymers and surfactants [8-10]. These papers and another work [11] considered the rate constants and rates as a constant parameter for the analysis of the effect of additives on hydrate formation kinetics. On the other hand, studies [12-14] on methane hydrate formation indicated that formation rates are dependent on the degree of subcooling besides other factors such as stirring rate. Methane hydrate film growth studies [15-18] on the rate of formation also showed the dependence of the rate of hydrate growth on the degree of subcooling used. A flow loop experiment study [19] also used the degree of subcooling as the driving force for hydrate formation, and the formation rate was found proportional to the driving force. In addition to these studies, a heat transfer modelling study [20] showed an explicit dependence of the rate of methane hydrate formation on the degree of subcooling.

In this work, the variation of the degree of subcooling during hydrate formation is investigated in detail within every single experiment. The rate of change of the free gas mole and the principle of mass conservation are used for the analysis of the effect of MeOH and PVCap on the kinetics of methane hydrate formation. The usual trend of applying a constant kinetic rate parameter is used, and its limitations are discussed. In subcooled systems, energy is suddenly released when hydrates form, giving temperature increase which affects the degree of subcooling over a period of time until the experimental preset temperature is reestablished. In addition, in an isochoric cell system a pressure drop during hydrate formation also affects the driving force. Since the degree of subcooling varies with time during the build-up of methane molecules into the hydrate surface, a time-dependent model is proposed for the kinetic rate during the growth of methane hydrate formation.

EXPERIMENAL SETUP AND PROCEDURE

Growth kinetics were investigated in the high pressure autoclave cell apparatus shown in Fig. 1. A cylindrical high pressure autoclave cell of inner volume 145 mL was used as a reactor. The reactor had a magnetic stirring plate rotating at 750 rpm. The temperature of the cell was controlled by the refrigerated and heating circulator with programmable temperature control unit. The temperature was measured to an accuracy of ±0.1 ^{o}C, and the pressure was measured to an accuracy of ±0.2 bar. The system temperature and pressure changes were monitored and recorded using LabView. Similar procedures with different conditions were used for each additive as follows: (i) Ultralow concentrations of methanol were prepared in distilled water (DIW) in the range 1.5-20 ppm by weight. 50 mL of test solution was filled in the cell, the cell was closed and then purged twice with 40 bar methane gas, accessed directly from the gas supply cylinder. The methane gas used was 5.5 scientific grade with purity 99.9995% supplied by Yara. The system was then forced to enter the hydrate forming region by cooling it down from an initial temperature of 15.3 ^{o}C to an experimental temperature of 7.8 ^{o}C. The cooling rate used was 6 ^{o}C /h. In accordance with the real gas equation, the pressure of the isochoric system was reduced from an initial value of 93.9 bar to 90 bar. Thereafter, the main experiment was initiated by the start of stirring at time zero. A total number of 6-10 experiments were run on each methanol solution including baseline experiments. (ii) For the model validation, a similar procedure with PVCap at different conditions was used. PVCap (dry powder, $M_w \approx 6{,}000$) solutions were prepared in distilled water in the range 20-100 ppm by weight. The system was cooled from an initial temperature of 13.7 ^{o}C to an experimental temperature of 4 ^{o}C that makes the degree of subcooling 8 ^{o}C. The cooling rate and the experimental pressure used were 10 ^{o}C /h and 90 bar, respectively. Other factors such as the type of gas, stirring rate and volume of test solutions used were similar to the methanol experiments. A total of 6-8 runs were made on each PVCap solution including the pure water baseline experiments.

Fig. 2 shows the time evolution of the number of moles of the free gas (red curve) and the temperature of the system (blue curve) from the start of the experiment to the end for a system with methanol in solution. The number of moles of the free gas (free gas content) was calculated by employing the real gas equation

$$n = \frac{PV}{zRT} \qquad (1)$$

where P is the cell pressure, V is the gas volume (assumed constant = 95 mL), z is the compressibility factor, n is the number of moles of the gas, R is the universal gas constant, and T is the cell temperature. The compressibility factor was calculated using the FORTRAN code of AGA8PROG. As shown in Fig. 2, the free gas content is constant from the start of the experiment to the onset of hydrate growth. After hydrate onset, the number of moles of free gas initially shows a linear reduction as function of time and then decays exponentially until it again becomes constant at the cell pressure and temperature in the vicinity of hydrate equilibrium conditions (see Fig. 9). The detailed investigation of the rate of formation has been done only for the linear and exponential part of the experiment where very rapid growth is observed.

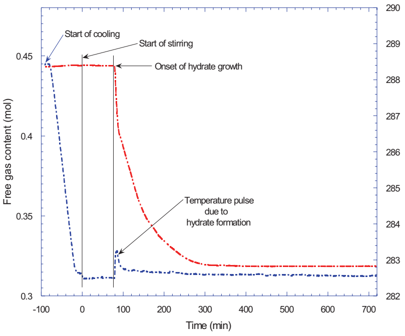

Figure 2. Gas content and temperature vs time for a system with methanol.

RESULTS AND DISCUSSION

Rate of Methane Hydrate Formation in Systems with Methanol:

Fig. 3 shows gas consumption and pressure drop as a function of time. The growth and gas consumption region shows two symmetric plots that could be interpreted as conservation of mass during the course of hydrate growth. In fact, the mass conservation holds true only after the water in the liquid state is saturated with methane gas and cooled to the desired temperature prior to time zero as shown in Fig. 3. The pressure drop prior to time zero is due to the temperature drop during the cooling cycle, and a minor drop at start of stirring due to re-saturation of methane in the water, but not due to any gas consumption by hydrate formation. Taking the pressure drop due to re-saturation of methane in the water phase at start of stirring into consideration, the mass conservation holds true throughout the whole experiment.

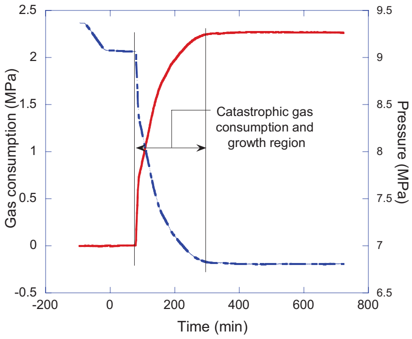

Figure 3. Gas consumption (red curve) and cell pressure (blue curve) vs time for a system with methanol

Focusing only on the growth and consumption region, and assuming that gas accumulation in the liquid water saturated with methane gas is unlikely, the number of methane molecules leaving the gas phase are represented by the pressure drop, whereas the number of methane molecules entering in the hydrate cages are represented by the gas consumption plot. Since mass must be conserved in an isochoric system, the two plots shows symmetry about an axis passing through the intersection of the two plots and parallel to the time axis. Thus, the dynamics of the number of moles of methane in the gas phase could give information on the rate of hydrate formation in the liquid phase.

With the dynamics of the number of moles of the free gas content as an indicator of the growth rate in the liquid phase, we closely investigate the structure of the gas consumption curves during the growth period. As shown in the dynamics of the free gas content of Fig. 2, at the onset of hydrate formation, there is a strong exothermic reaction leading to a sudden temperature increase. In this experiment, a peak temperature value is obtained approximately 4 min after onset. During this period the free gas content shows a sudden drop indicating a high hydrate formation rate. When the initial exothermic reaction decreased, the hydrate formation rate appeared to obtain a reduced, but constant level during the next 38 min of the experiment. Thereafter the formation rate appeared to fall exponentially towards completion of the cell reaction. This suggested 3 different regions where growth kinetics are controlled or dominated by different proportions of heat and mass transfer, and decreasing driving force as the cell PT conditions approached hydrate equilibrium.

Fig. 4 shows the structure of the growth in 3 different regions for representative plots of ultralow concentrations of methanol with different onset time. All the representative plots show distinct features i.e., the slope of the curve change after some time, which is marked by the boundary lines of region 1, 2 and 3. For comparison, the time axis of Fig. 4 is reset to count zero at hydrate onset for all systems as shown in Fig. 5. This figure clearly shows that all systems have very steep slope during the very early stage of the hydrate growth that changes to another slope after a certain turning point. During the first part of the reaction (region 1), there is a sudden temperature increase due to released dissociation energy from hydrates formed in subcooled, non-equilibrium system. Removing the first non-equilibrium excess heat of reaction by the cooling, local equilibria will be reestablished throughout the system, and growth rate is determined by subcooling, pressure (i.e., concentration), temperature and heat transfer (region 2). In region 3, the main effect on growth rate is dominated by decreasing concentration of reacting species i.e., pressure approaching equilibrium conditions.

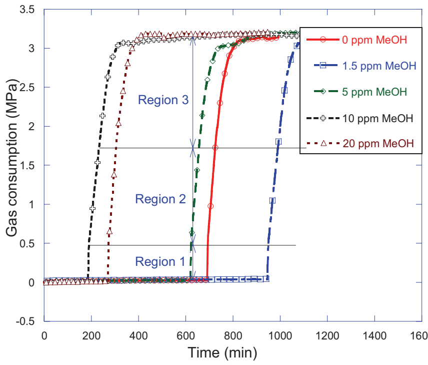

Figure 4. Representative plots of gas consumption vs time.

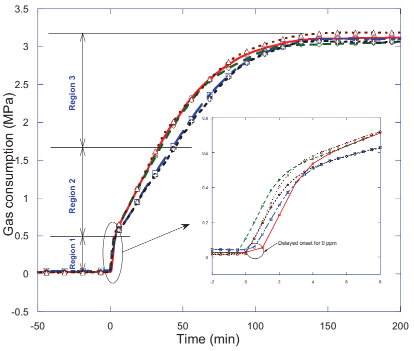

Figure 5. Representative plots of gas consumption vs time (t_{onset}=0) for a system with methanol.

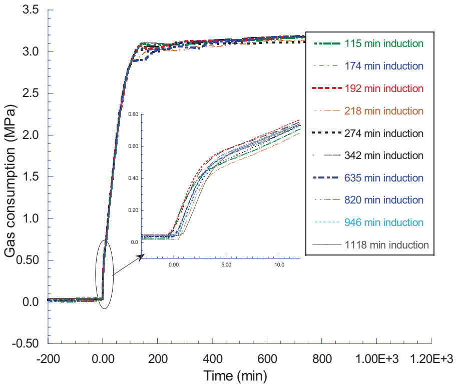

Figure 6. Gas consumption vs time (t_{onset}=0) for 1.5 ppm methanol experiment.

Except the pure water experiment which has an apparently slow initial growth period of short duration prior to onset of catastrophic growth, all under-inhibited experiments have spontaneous and fast growth at onset as shown in the inset of Fig. 5. This could be an indicator that an ultralow concentration of methanol may affect (trigger) the onset of methane hydrate formation. Similar structure was observed in every experiment of ultralow concentrations of methanol including the pure water reference. For example, Fig. 6 shows the structure of gas consumption vs time plots for 10 parallel experiments with 1.5 ppm methanol in solution. The inset of the figure shows the slope change going from region 1 to region 2.

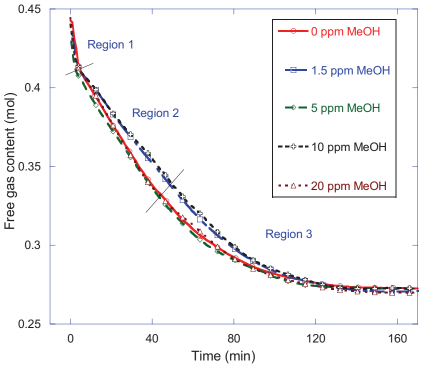

Figure 7. The dynamics of free gas content during the hydrate growth period.

The dynamics of the number of moles of the free gas in the cell is shown in Fig. 7 for the whole period of the reaction. One could notice the structural similarity of this figure with Fig. 5, which is the result of mass conservation. This suggests that one may use either the gas consumption plots, or equivalently, the free gas content plots for studying and understanding growth behaviours in isochoric cell experiments. Region 1 of Fig. 7 represents the very early stage of rapid hydrate growth. Regions 2 and 3 represent the early and late growth periods, respectively. Regions 1 and 2 show apparently linear behavior from which zero-order reactions could be assumed. The zero-order reaction is defined by

$$n = n_o - k_i t \tag{2}$$

where n_o is the initial amount of free gas (mol), k_i is a kinetic rate constant (mol/min), t is the time (min), and i=1, 2. The time derivative of the zero-order reaction is

$$\frac{dn}{dt} = -k_i \tag{3}$$

which gives a growth rate equal with the kinetic rate constant. Methane hydrate growth rate in regions 1 and 2 could be estimated using Eq. (3), where each region has different initial number of moles and growth rates. For region 1, the initial number of moles of the free gas content, n_{o1}, is the free gas content at time zero (t=0). For region 2, the initial content of the free gas, n_{o2}, is taken as the final content of the free gas when the system transforms from a steep slope of k_1 in region 1 to a reduced slope of k_2 in region 2. The steep slope transformation ends when the temperature pulse attains its peak value and starts falling as shown in Fig. 2. Tables 1 and 2 give the calculated values of the kinetic constants, growth rates, and deviation factor from the reference pure water experiment value. The last column of the tables represents average values for all experiments at each concentration. In region 1, the results show that all nonzero ultralow concentrations of methanol gave growth rate increase of 9% (i.e., factor +1.09) or less as compared to the pure water baseline. Such low increase could be ignored concluding that an ultralow concentration of methanol has no effect in the very early growth period of methane hydrate formation. But it may trigger onset of region 1 as described before. In region 2, the solution in the range 1.5-10 ppm methanol showed growth rate reduction of 29% or less. However, experiments with 20 ppm methanol showed that growth rate was increased by 4% as compared to the pure water baseline. Fluctuations within the range of 23-29% on growth rates as for 1.5 and 10 ppm MeOH are not negligible for systems with methanol at ultralow concentrations.

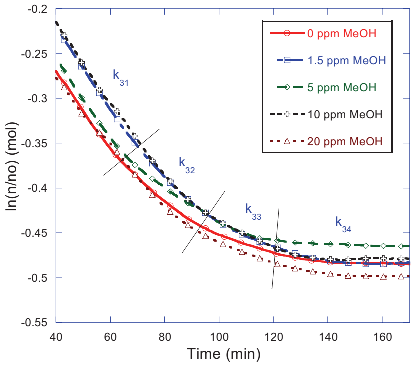

Figure 8. The natural logarithm of the relative free gas vs time for the late growth region.

Conc. (ppm)	**n_{01} (mol)**	**k_1 (mol/min)**	**Increasing factor**
0	0.44284	8.36×10^{-3}	
1.5	0.43929	8.54×10^{-3}	+1.02
5	0.43360	8.90×10^{-3}	+1.06
10	0.44016	8.46×10^{-3}	+1.01
20	0.44434	9.10×10^{-3}	+1.09

Table1: Kinetic rate constants and growth rates of region 1 in systems with methanol for the representative plots.

Conc. (ppm)	**n_{02} (mol)**	**k_2 (mol/min)**	**deviation factor**
0	0.41049	2.07×10^{-3}	
1.5	0.41011	1.68×10^{-3}	-1.23
5	0.40545	1.95×10^{-3}	-1.06
10	0.41020	1.60×10^{-3}	-1.29
20	0.41003	2.15×10^{-3}	+1.04

Table 2: Kinetic rate constants and growth rates of region 2 in systems with methanol for the representative plots.

As seen in Fig. 7, region 3 shows exponential time variation of the free gas content. This exponential variation could be assumed by a first-order reaction [9, 10] of the form

$$n = n_o e^{-k_3 t} \tag{4}$$

where n_o is the initial number of moles of the free gas, k_3 is a kinetic rate constant for region 3 with unit min^{-1}, and t is the time in min. The rate constant could easily be determined by plotting the natural logarithm of the free gas content vs time, and fitting a straight line provided that the plot gives a straight line. The slope of the straight line is the kinetic rate constat, k_3. The growth rate is then determined by taking the time derivative of Eq. (4) as

$$r = -r_o e^{-k_3 t} \tag{5}$$

where r is the growth rate dn/dt at any time, and r_o is the initial rate $n_0 k_3$. The growth rate is usually expressed through the rate by which the amount of methane molecule is converted to hydrate [21]. Fig. 8 shows the natural logarithm of the relative free gas content as function of time (only 50% of the data points are displayed). As shown in the figure, the whole range of the curves cannot be fit with a single straight line. However, it could be possible to divide the curves into different straight line sections with rate constants

$$k_{31}, k_{32}, k_{33}, \ldots$$

where the final segment depends on the number of straight lines available for each plot. Each value of k_3 represents the kinetic rate constant during different regions of the growth period implying that k_3 in the whole range of region 3 is not a constant, but a function of time.

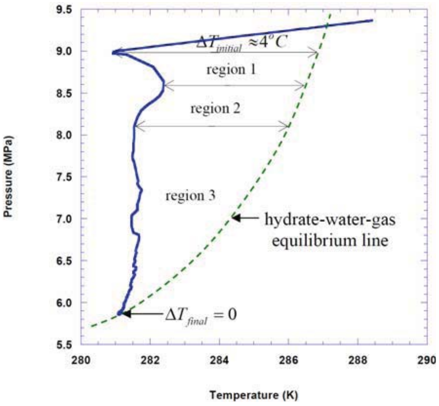

Figure 9. Graph showing variation of ΔT during hydrate growth for a system with methanol.

Kinetic Rate Model for Hydrate Formation: A comprehensive review [22] on modelling of hydrate formation kinetics shows that growth models considered a constant kinetic rate parameter for many reasons. The straight line fit method works well, and it gives a fair estimation of the kinetic rate constants. However, the visual inspection of Fig. 8 shows that the late growth section cannot be fit by a straight line to represent all data in this region. Thus, this method may not be the best way to determine the kinetic rate constant. Hence, calculating k at any instantaneous time during the growth period would be a much better approach. This leads one to consider a time-dependent kinetic rate based on the experimental conditions.

The reason for having time-dependent kinetic rate could be explained in terms of the driving force of the system, which is the degree of subcooling in this case. Some studies [11, 23, 24] used the difference in the chemical potential (or fugacity) of the guest gas between in the gas phase and in the hydrate phase to calculate formation rates and the kinetic rate constants. In fact, the degree of subcooling does not represent the real driving force in all systems, but in systems with one type of guest molecule like the methane gas under consideration, the driving force for hydrate formation is proportional to the degree of subcooling over a wide pressure range [25]. Thus, the degree of subcooling can be a good representative of the driving force, but it is not constant during the growth period of hydrates, and the rate of growth is a function of the degree of subcooling.

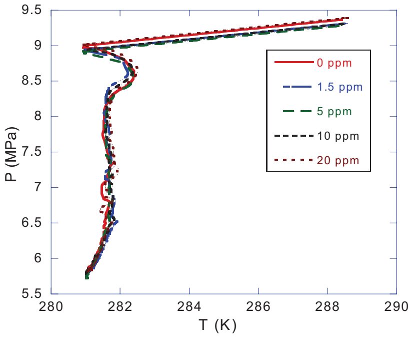

Figure 10a. Graph showing PT path for systems with MeOH in solution.

Fig. 9 shows the PT path from onset of hydrate growth at a subcooling of 4 ^oC ($\Delta T_{initial}$), to the end of the growth process in the vicinity of the hydrate equilibrium curve at $\Delta T_{final} = 0$ ^oC. The temperature is measured in the gas phase for practical reasons while the hydrate formation process takes place in the liquid phase at a temperature closer to equilibrium. Thus, quantification of the exact subcooling along the PT path from the start to the end of growth is difficult. However, all experiments did follow comparable PT paths from start to end as shown in Fig. 10a. Fig. 10b shows similar plots for systems with PVCap which has a stronger effect on the conversion of water into hydrates resulting in reduced gas consumption and hydrate growth. The reduced conversion of water into hydrates and the effect on growth could easily be seen from the pressure drop reading of each concentration in Figure 10b.

Both chemicals (MeOH and PVCap) have shown their own distinct PT structure. Thus, it is assumed that the driving force followed the same decaying path for a given chemical during all experiments. This time-dependent driving force may suggest a time-dependent kinetic rate k(t), which could be derived from the PVT relation of the gas phase using Eq. (1). Equating the right-hand sides of Eqs. (1) and (4), and after rearranging terms we get

$$k_3 = -\frac{1}{t}\ln\left(\frac{PV}{zn_oRT}\right) \qquad (6)$$

which gives the kinetic rate of hydrate formation at any time for the first-order reaction in the late growth region. Fig. 11 shows the kinetic rate in region 3 as a function of time for the pure water experiment and experiments with ultralow concentrations of methanol.

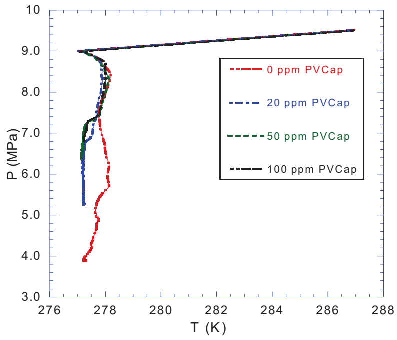

Figure 10b. Graph showing PT path for systems with PVCap in solution.

Originally, the kinetic rate parameter based on the theories of crystallization and mass transfer at a gas-liquid interface [26] accounts for the combined diffusion and reaction of the guest molecule during the modelling of hydrate formation. Another paper [27] indicated that changing the magnitude of the kinetic rate parameter has an effect on the rate and gas consumption. During mechanistic model study [28] for hydrate formation, different rate constants within a single experiment were reported. Hence, a good advantage of the proposed model may be that it gives information about the kinetic rate from the easily accessible thermodynamic conditions of the system at any time during hydrate formation. However, the present model was tested for a stirring rate of 750 rpm, and it does not include the effect of rpm on the rate constant. It is reported [12, 14, 29, 36] that stirring rate has an effect on the rate of methane hydrate crystallization and growth.

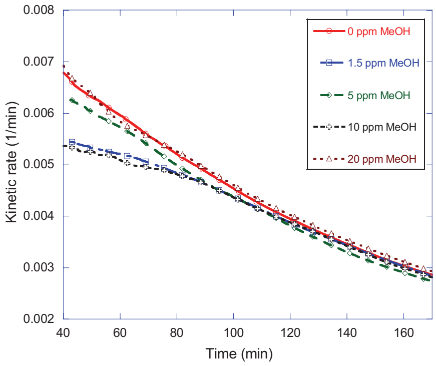

Figure 11. Graph showing kinetic rate vs. time in region 3.

The inverse time dependence of Eq. (6) shows that the kinetic rate decreases as time increases, which could be explained by the reduction in the driving force with time. As an alternative to Eq. (5), which tells that the rate of hydrate formation decreases from its initial rate by an exponential decaying factor, one could equivalently express the decreasing hydrate growth in the liquid water phase by employing the time-dependent rate as

$$r = -n_o k_3 \qquad (7)$$

where k_3 is given by Eq. (6). This model predicts the hydrate growth rate for the pure water reference and for the four different ultralow concentrations of methanol as shown in Fig. 12. As shown in this figure, there is a difference in the rates of hydrate growth at the beginning of region 3, but finally the rates seem to obtain comparable values as time increases and the systems approach their final equilibrium when all the water is converted into hydrates. The growth model shows that the growth rate is dependent on the temperature, pressure, initial amount of free gas, the compressibility factor, and time. The growth model in Eq. (5) lacks this detailed information, and one possible reason could be the parameter k may not be a constant, but a function dependent on the experimental conditions as proposed by Eq. (6).

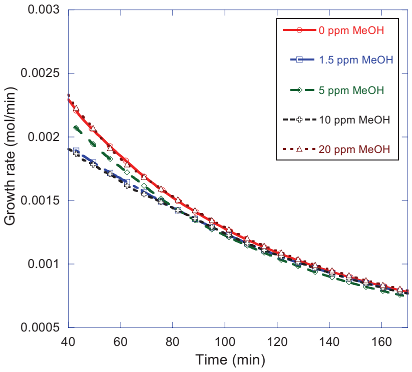

Figure 12. Growth rate vs. time graph in region 3.

The role of an ultralow concentration of methanol on the growth period of methane hydrate formation is not clearly understood. The effect could be that methanol can reduce the surface tension [30] or affect the activity coefficient of water [31] or optimize formation rates [32].

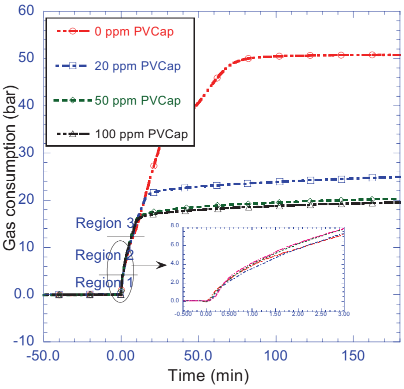

Figure 13. Representative plots of gas consumption vs time (t_{onset}=0)

Model Validation on Systems with PVCap: Fig. 13 shows gas consumption vs. time curves for the representative plots of PVCap experiments at four different concentrations including the baseline experiment. The structure of the growth curves in these systems have also shown the three different regions (region 1, 2 and 3) in a different way as compared to those which were observed in systems with methanol in solution. The inset figure in Figure 13 shows growth details during the 3 first minutes after onset where the slope change between regions 1 and 2 occurs at 0.5 to 0.7 minutes. Region 2 has a reduced slope as compared to region 1. In these regions, a straight line fit could be used to estimate the growth of methane hydrate formation just like the experiments in the presence of methanol as an additive. Tables 3 and 4 show the kinetic rate constant and growth rate with the corresponding deviation factor from the reference pure water experiment for regions 1 and 2, respectively (cf. Eqs. 2 and 3). In region 1, an average growth rate reduction of 32-66 % was observed, and this average reduction increased to a value of 41-75 % in region 2. Unlike the methanol experiments, PVCap showed a clear and significant effect on the rate of growth of methane hydrates based on concentration in both regions. With respect to the calculated rate constants and growth rates for each region the difference between 50 and 100 ppm PVCap was small. This could be due to the fact that PVCap has an optimal performance at a certain concentration, and increasing concentration does not always increase PVCap performance [33].

Conc. (ppm)	**k_1 (bar/min)**	**decreasing factor**
0	6.65	
20	5.04	-1.32
50	4.13	-1.61
100	4.01	-1.66

Table 3: Kinetic rate constants and growth rates of region 1 for the representative plots of PVCap.

Conc. (ppm)	**k_2 (bar/min)**	**decreasing factor**
0	5.12	
20	3.63	-1.41
50	2.98	-1.72
100	2.93	-1.75

Table 4: Kinetic rate constants and growth rates of region 2 for the representative plots of PVCap.

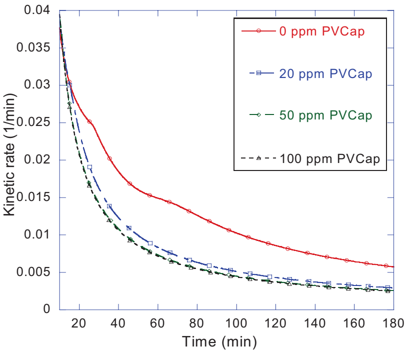

Figure 14. Kinetic rate vs. time graph in region 3.

In region 3, Eqs. (6) and (7) are employed to compare the kinetic and growth rates as a function of time for each concentration. The kinetic rate and the growth rate are plotted as function of time in Figs. 14 and 15, respectively. Both figures show a clear effect of PVCap on methane hydrate formation and growth as is also seen from the gas consumption graph in Fig. 13. The effect of PVCap on methane hydrate growth is not by changing the thermodynamic phase boundary for the hydrate stability, but by reducing / preventing continuing growth on the crystal surface. Growth inhibition by PVCap is due to adsorption of the polymer to a growing crystal surface thereby acting as a barrier for further growth, and achieving full inhibition depends on subcooling, type of polymer, molecular weight of polymer, and solution agitation [34]. The initial degree of subcooling (8 °C), type of polymer (PVCap), molecular weight (6000), and solution agitation (750 rpm) were kept constant and the same in all PVCap experiments to examine the effect of concentration on growth kinetics. The results show that changing concentration of PVCap has a reduction effect on the growth of methane hydrates. Transporting hydrate forming molecules to an active growing site is a significant factor [35] for hydrate growth kinetics. Thus, PVCap could easily affect this factor by binding to the active growing structure and result in delay for the process. The delaying effect on the growth of methane hydrates by the presence of PVCap could easily be identified either from the gas consumption plot (Fig. 13) or from the plots made on the basis of the proposed model (Figs. 14 and 15).

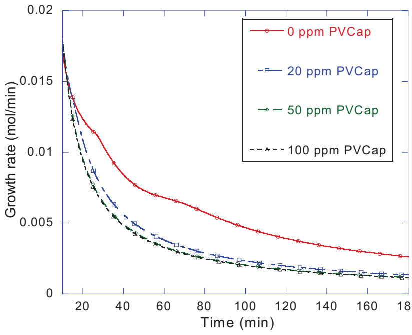

Figure 15. Growth rate vs. time graph in region 3.

CONCLUSION

A high pressure autoclave cell was used to produce methane hydrates in the presence of low concentrations of MeOH and PVCap. A detailed analysis on the dynamics of the number of moles of free gas and the principle of mass conservation have been used to understand the effect of the additives on the growth kinetics of methane hydrates. The usual method of using a constant kinetic rate has been utilized and its limitations are discussed. Based on the thermodynamics of the system, a time-dependent model for the kinetic rate has been proposed, by which instead of considering a decaying initial rate of hydrate formation, one could equivalently consider a time varying kinetic rate for the time evolution of methane hydrate formation. The time-dependent model reflects effects of decreasing concentration (pressure) and driving force during the experiments. The model could also be applied for testing the effect of other additives on the rate of growth of methane hydrates.

ACKNOWELGMENTS

NFR is greatly acknowledged for the financial support of this work.

REFERENCES

[1] Sloan ED, Koh CA. *Clathrate Hydrates of Natural Gases*. FL: Boca Raton, 2008.

[2] Makogon YF. *Hydrates of Natural Gas*. OK: Penn Well Publishing Company, 1981.

[3] Svartaas TM, Fadnes F H. *Methane hydrate equilibrium data for the methane-water-methanol system upto 500 bara. In: Proceedings of the 2nd*

International Offshore and Polar Engineering Conference, San Francisco, 1992.

[4] Yousif M, Austvik T, Berge L, Lysne D. *The effects of low concentration methanol on hydrate formation. In: Proceedings of the 2nd International Conference on Natural Gas Hydrates, Toulouse, 1996.*

[5] Bobev S, Tait KT. *Methanol-inhibitor or promoter of the formation of gas hydrates from deuterated ice?* Am. Mineral 2004; 89: 1208-1214.

[6] Abay HK, Svartaas TM. *Effect of ultralow concentration of methanol on methane hydrate formation.* Energy Fuels 2010; 24: 752-757.

[7] Kelland MA. *History of the development of low dosage hydrate inhibirors.* Energy Fuels 2006; 20: 825-847.

[8] Karaaslan U, Parlaktuna M. *Surfactants as hydrate promoters?* Energy Fuels 2000; 14: 1103-1107.

[9] Karaaslan U, Parlaktuna M. *PEO-a new hydrate inhibitor polymer.* Energy Fuels 2002; 16: 1387-1391.

[10] Karaaslan U, Parlaktuna M. *Promotion effect of polymers and surfactants on hydrate formation rate.* Energy Fuels 2002; 16: 1413-1416.

[11] Kuji Y, Yamasaki A, Yanagisawa Y. *Effect of cyclodextrins on hydrate formation rates.* Energy Fuels 2006; 20: 2198-2201.

[12] Vysniauskas A, Bishnoi PR. *A kinetic study of methane hydrate formation.* Chem. Eng. Sci. 1983; 38: 1061-1072.

[13] Happel J, Hnatow MA, Meyer H. *The study of separation of nitrogen from methane by hydrate formation using a novel apparatus.* Ann. N.Y. Acad. Sci. 1994; 715: 412-424.

[14] Parlaktuna M, Gudmundsson J. *Formation rate of methane and mixture hydrate. In: Proceedings of the 2nd International Conference on Natural Gas Hydrates, Toulouse, 1996.*

[15] Makogon YF, Makogon TY, Holditch SA. *Several aspects of the kinetics and morphology of gas hydrates. In: Proceedings of the Japan National Oil Conference, Japan, 1998.*

[16] Freer EM, Selim MS, Sloan ED. *Methane hydrate film growth kinetics.* Fluid Phase Equilibria 2001; 185: 65-75.

[17] Tayer CJ, Miller KT, Koh CA, Sloan ED. *Macroscopic investigation of hydrate film growth at the hydrocarbon/water interface. In: Proceedings of the 6th International Conference on Gas Hydrates, Vancouver, 2008.*

[18] Peng BZ, Chen GJ, Sun CY, Yang LY, Luo H. *Is the gas hydrate film growth controlled by intrinsic kinetic or heat transfer? In: Proceedings of the 6th International Conference on Gas Hydrates, Vancouver, 2008.*

[19] Turner D, Boxall J, Yang S, Kleehamer D, Koh C, Miller K, Sloan ED, Xu Z, Mathews P, Tally L. *Development of a hydrate kinetic model and its incorporation into the OLGA2000 transient multiphase flow simulator. In: Proceedings of the Fifth International Conference on Gas Hydrates, Trondheim, 2005.*

[20] Varaminian F. *The role of heat transfer in kinetics of hydrate formation. In: Proceedings of the Fourth International Conference on Gas Hydrates, Yokohama, 2002.*

[21] Englezos P. *Kinetics of gas hydrate formation and kinetic inhibition in offshore oil and gas operations. In: Proceedings of the Fifth International Offshore and Polar Engineering Conference, the Hague, 1995.*

[22] Ribeiro CP, Lage PLC. *Modelling of hydrate formation kinetics: State-of-the-art and future directions.* Chem. Eng. Sci. 2008; 63: 2007-2034.

[23] Daimaru T, Kuji Y, Yanagisawa Y, Yamasaki A. *Effect of the structure of surfactants on the hydrate formation kinetics of methane and xenon - effect of the carbon chain length. In: Proceedings of the Fifth International Conference on Gas Hydrates, Trondheim, 2005.*

[24] Okano T, Yanagisawa Y, Yamasaki A. *Development of a new method for hydrate formation kinetics measurements – a breakthrough method. In: Proceedings of the Fifth International Conference on Gas Hydrates, Trondheim, 2005.*

[25] Arjmandi M, Tohidi B, Danesh A, Todd AC. *Is subcooling the right driving force for testing low-dosage hydrate inhibitors?* Chem. Eng. Sci. 2005; 60: 1313-1321.

[26] Englezos P, Kalogerakis NE, Dholabhai PD, Bishnoi PR. *Kinetics of formation of methane and ethane gas hydrates.* Chem. Eng. Sci. 1987; 42: 2647-2658.

[27] Skovborg P, Rasmussen P. *A mass transport limited model for the growth of methane and ethane gas hydrates.* Chem. Eng. Sci. 1994; 49 (8): 1131-1143.

[28] Lekvam K, Ruoff P. *A reaction kinetic mechanism for methane hydrate formation in liquid water.* J. Am. Chem. Soc. 1993; 115: 8565-8569.

[29] Herri J, Gruy F, Cournil M. *Kinetics of methane hydrate formation. In: Proceedings of the*

2nd International Conference on Natural Gas Hydrates, Toulouse, 1996.

[30] Chang TM, Dang LX. *Liquid-vapor interface of methanol-water mixtures: A molecular dynamics study.* J. Phys. Chem. B 2005; 109: 5759-5765.

[31] Nord L, Tucker EE, Christian SD. *Liquid-vapor equilibrium of dilute aqueous solutions of ethanol and 2-propanol.* J. Solution Chem. 1984; 13: 849-867.

[32] Chen PC, Huang WL, Stern LA. *Methane hydrate synthesis from ice: Influence of pressurization and ethanol on optimizing formation rates and hydrate yield.* Energy Fuels 2010; 24: 2390-2403.

[33] Lederhos JP, Long JP, Sum A, Christiansen RL, Sloan ED. *Effective kinetic inhibitors for natural gas hydrates.* Chem. Eng. Sci. 1996; 51: 1221-1229.

[34] Larsen R, Knight CA, Sloan ED. *Clathrate hydrate growth and inhibition.* Fluid Phase Equilibria 1998; 150-151: 353-360.

[35] Buch V, Devlin JP, Monreal IA, Cwiklik BJ, Aytemiz NU, Cwiklik L. *Clathrate hydrates with hydrogen-bonding guests.* Phys. Chem. Chem. Phys. 2009; 11: 10245-10265.

[36] Wei Ke, Svartaas TM. *Effects of Stirring and Cooling on Methane Hydrate Formation in High-Pressure Isochoric Cell. In: Proceedings of the 7th International Conference on Gas Hydrates*, *Edinburgh, 2011.*

Appendix E

Paper V

Does PVCap Promote Nucleation of Structure II Hydrate?

By:

Hailu K. Abay, Eirik Hovring and Thor M. Svartaas.

Printed in:

Proceedings of the 7th International Conference on Gas Hydrates, Edinburgh, United Kingdom, July 17-21, 2011.

Proceedings of the 7th International Conference on Gas Hydrates (ICGH 2011),
Edinburgh, Scotland, United Kingdom, July 17-21, 2011.

DOES PVCAP PROMOTE NUCLEATION OF STRUCTURE II HYDRATE?

Hailu K. Abay[1*], Eirik Hovring[1] and Thor M. Svartas[1]
Department of Petroleum Engineering[1]
Faculty of Science and Technology
University of Stavanger
4036, Stavanger
NORWAY

ABSTRACT

A seven-component synthetic natural gas has been used to produce structure II (sII) hydrates in an isochoric high pressure cell with PVCap as an additive. The effect of the additive on nucleation of sII hydrate has been investigated at different concentrations in the range 50–3000 ppm by weight (i.e., 0.005–0.3 wt%). The nucleation probability distribution function has been employed to understand the stochastic experimental result. The rate of nucleation and the range of the probability distribution function in which random nucleation of sII hydrates occur have also been investigated for each concentration. The results show that all the concentration in the range 50–500 ppm (0.005–0.05 wt%) increased the rate of nucleation as compared to the pure water baseline experiment. The probability distribution functions are also found to be displaced towards shorter nucleation times as compared to the pure water distribution function indicating a promotional effect of PVCap at these concentrations. However, the concentration range between 1000–3000 ppm (0.1–0.3 wt%) reduced the rate of nucleation, and all the probability distribution functions are found to be displaced towards longer induction times as compared to the pure water distribution function indicating inhibition of nucleation. The promotional effect of PVCap on nucleation of sII hydrate is, thus, concentration dependent.

Keywords: nucleation, gas hydrates, kinetic inhibitors, thermodynamic inhibitors

NOMENCLATURE

J	nucleation rate [min^{-1}]
p	probability of nucleation
P	pressure [bar]
ΔP	pressure drop [bar]
T	temperature [^oC]
ΔT	degree of subcooling [^oC]
t_o	induction time [min]
τ	lag time [min]

INTRODUCTION

Gas hydrates are clathrates in which a gas molecule is in captivity in hydrogen-bonded water molecules. The entrapped gas molecule is referred as the guest and the lattice of water molecules as the host. The process of encaging a guest into a host requires favourable conditions such as high pressure, low temperature, liquid water and the nature of the guest. The study of gas hydrates has attracted the interest of scientists because of technologies related to gas hydrates are very important for industrial applications such as prevention of gas hydrate formation during oil and gas production in pipelines. Gas hydrates were reported [1] as problems that could plug production pipelines and hence are nuisance for the oil and gas industries.

Inhibition of gas hydrates could be performed using thermodynamics inhibitors (THIs) such as

---

[*] Corresponding author: Phone: +47 51 83 22 30 Fax +47 51 83 20 50 E-mail: hailu.k.abay@uis.no

methanol or kinetic hydrate inhibitors (KHIs) such as polyvinylcaprolactum (PVCap). PVCap belongs to the class of low dosage hydrate inhibitors (LDHIs). A comprehensive review [2] on the history of LDHIs was given previously. THIs inhibit hydrate formation by shifting the equilibrium curve from right to left allowing a narrow region for hydrate formation, whereas, KHIs like PVCap inhibit hydrate formation by slowing down the growth of hydrate crystal by attaching to an active growing site [3, 4]. In this paper, we investigate the effect of PVCap on the nucleation of structure II (sII) hydrates produced from a seven-component synthetic natural gas (SNG7). The molar composition of SNG7 is shown in Table 1. The concentration of the PVCap was varied at the same experimental conditions, and the rate of nucleation was calculated for each concentration by employing the probability distribution function.

Component of SNG7		Composition in mol%
CH_4	Methane	80.40
C_2H_6	Ethane	10.30
C_3H_8	Propane	5.0
i-C_4H_{10}	i-butane	1.65
n-C_4H_{10}	n-butane	0.72
CO_2	Carbon dioxide	1.82
N_2	Nitrogen	0.11

Table 1. Composition of SNG7 used for studying the effect of PVCap on the nucleation of sII hydrates.

The nucleation probability distribution function is given by [5-10]

$$p(t) = 1 - e^{-J(t_0 - \tau)} \qquad (1)$$

where $p(t)$ is the probability to measure an induction time, t_o, between zero and time t, J is the rate of nucleation per unit volume, and τ is the lag time. The measured induction times are stochastic and such nondeterministic problems of nucleation kinetics could only be approached using probability distribution functions. The following section discusses the experimental section used and how the induction time was measured.

EXPERIMENAL METHODS

Experimental setup: Figure 1 illustrates the high-pressure experimental setup we used for the investigation of the effect of PVCap on the nucleation of sII hydrate kinetics. The cylindrical cell was made of titanium with inner volume of 145 mL. 50 mL of the cell volume was filled with distilled water (DIW) with PVCap in solution. The rest 95 mL of the cell volume was filled with SNG7. The system (DIW with PVCap and SNG7) had a direct contact with a cooling cap by which the system is allowed to cool to a desired experimental temperature. The temperature profile was controlled by the refrigerated and heating circulator with interfaced temperature control unit. The cell was equipped with a stirrer blade that is connected to a magnet house in the bottom end piece via an axle. A stirring rate of 750 rpm was used for all experiments of PVCap including the pure water base line experiments.

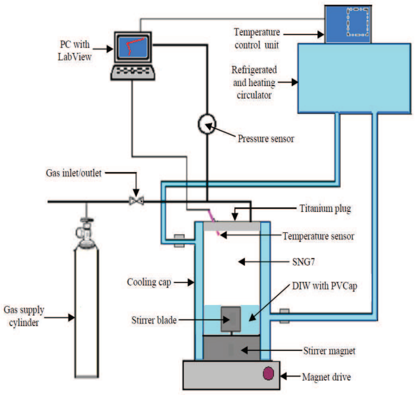

Figure 1. High-pressure experimental setup.

Experimental procedure: Dry powder PVCap of molecular weight 6000 (M_w, weight average) was dissolved in DIW at concentrations of 50, 100, 500, 1000, 2000, and 3000 ppm. 0 ppm DIW experiments were considered as the baseline for comparison. The lower part of the cell was filled with PVCap in solution and the upper part of the cell with 99 bar of SNG7. The system temperature was then cooled from an initial temperature of 22 °C down to 9 °C. At a temperature of 9 °C, a corresponding pressure of 90 bars was attained as the operating pressure before onset of hydrate formation. The corresponding sub-cooling at the experimental conditions was approx. 12 °C. The cooling rate used was 8.3 °C/h. The path from point A to point C of Figure 2 shows this cooling sequence. After attaining a stable temperature and pressure at point C, cell agitation is introduced by start of stirring. From point C to E the figure shows the PT path during hydrate formation. A pressure drop of 28.5 bar was observed in this specific experiment which could estimate the amount of hydrate formation as pressure drop is directly proportional to the amount of gas consumed from the real gas equation.

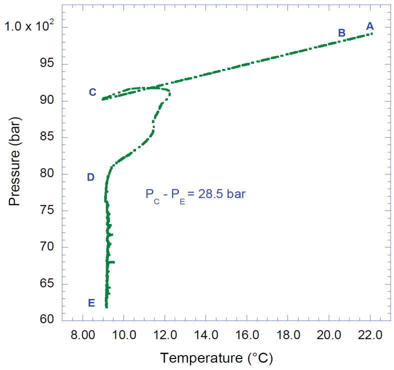

Figure 2. Pressure versus temperature graph during nucleation and growth of sII hydrate.

At point C, the system takes some time before onset of hydrate growth. The time taken by the system from the start of stirring to the onset of hydrate formation is called the induction time. This induction time has been measured by plotting the gas consumption and temperature as a function of time from the start of the experiment to the end. Figure 3 shows the gas consumption and temperature plots as a function of time. The inset of the figure shows how the induction time is determined from the temperature pulse of the system during onset of hydrate formation. The temperature pulse confirms that hydrate formation is an exothermic reaction releasing energy as a form of heat during hydrate formation. This released energy is measured by the temperature sensor in the gas phase. The gas consumption plot in the figure also shows some gas release by a negative peak on the gas consumption curve right after onset. This phenomenon was observed for all experiments and we do not have a clear explanation for why the system releases gas immediately after onset.

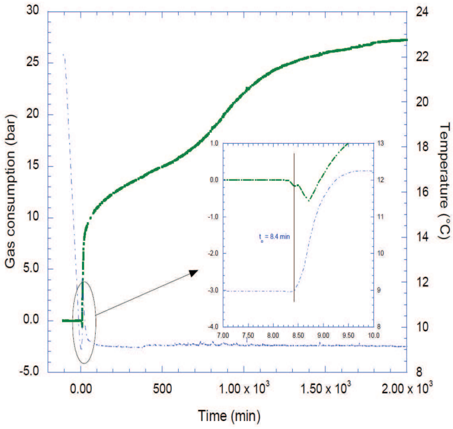

Figure 3. Gas consumption and temperature response plots during onset of sII hydrate formation.

RESULTS AND DISCUSSION

The experimental data points have been fitted with the theoretical probability distribution function given by Eq. (1). The results are plotted in two figures, Figures 4 and 5. Figure 4 shows the probability distribution versus induction time for the PVCap concentration in the range 0 – 500 ppm And Figure 5 shows results for experiments with PVCap in the range 1000 to 3000 ppm. The 0 ppm is the base line for comparison and the same baseline curve has been used in Figures 4 and 5. As shown in Fig. 4, all the PVCap concentrations less than 500 ppm are found to the left of the pure water base line curve. Such shift to the left of the reference experiment shows that all the induction times are found in the shorter induction time region. Table 2 shows the estimated nucleation rate and lag time from the theoretical probability distribution function. From the Table, it is shown that the nucleation rate increases by reducing concentration in the region between 50 and 500 ppm PVCap and that the nucleation rate at 500 ppm is close to that of the baseline. The corresponding lag time oscillates around zero for all these systems including the baseline. The negative value in the lag time indicates that the system reaches constant rate of nucleation before the start of stirring at time zero. The increase in the nucleation rate by decreasing concentration in the range 50 – 500 ppm indicates that PVCap is acting as a promoter at these low concentrations.

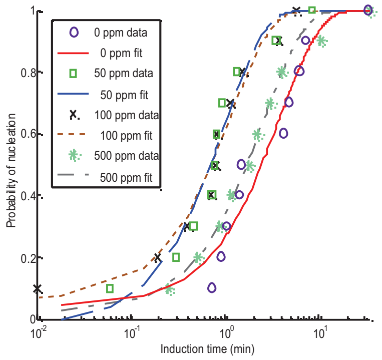

Figure 4. Probability of nucleation versus induction time for 0, 50, 100 and 500 ppm PVCap.

However, at concentrations in the range 1000-3000 ppm, a different effect was observed. Figure 5 shows the probability of nucleation versus induction time for this range. As shown in the figure, all the probability distributions have been found to the right of the pure water experiment. Clear effect of concentration is observed in the figure i.e., as concentration increases, the distribution functions shifted to the right toward a region of increased induction time as compared to the baseline. Table 2 shows the estimated rate of nucleation and lag time and Figure 6 shows experimental values and corresponding 4th order polynomial fits of nucleation rate and lag time as function of PVCap concentration. From Figure 6 it can be seen that the rate of nucleation decreases as function of increasing concentration in the region between 50 and 1000 ppm. For all concentrations of PVCap in this range the lag time remains low and oscillates around values in the vicinity of zero. In the region between 1000 and 2000 ppm the rate of nucleation approaches a minimum value while the lag time showed a markedly increase. Both nucleation rate and lag time increase with increasing concentration of PVCap in the region between 2000 and 3000 ppm. The effect on the nucleation rate seems to reach an optimum for concentrations in the region between 1000 and 2000 ppm, while the effect on the lag time (i.e. the inhibitors ability to delay nucleation) increases as function of concentration in the range between 1000 and 3000 ppm. At concentrations less than 1000 ppm catastrophic fast growth (i.e. fast, exothermic reaction) occurred immediately after onset. At 1000 ppm the initial growth rate was considerably reduced and the catastrophic growth was delayed by approx. 1 minute. At 2000 ppm the catastrophic growth was delayed by approx. 10 minutes and at 3000 ppm catastrophic growth was not reached within the normal duration of the experiments (between 15 and 24 hours). In one experiment with 3000 ppm run over a weekend catastrophic growth occurred after 67.8 hours.

The effect of PVCap is threefold; 1) reduced nucleation rate, 2) increased lag time before nucleation and 3) reduced initial growth with delay of catastrophic growth. In this paper we have focused effects of PVCap on nucleation rate and lag time only. The degree of sub-cooling was 12 °C at start of the experiments. This level of sub-cooling could be a little too high to detect effects on lag time at PVCap concentrations below 1000 ppm. However, as compared to the pure water baseline the nucleation rates showed significant increases as function of decreasing concentration at concentrations below 500 ppm.

Figure 6 indicates that nucleation rate has a minimum in the region between 1000 and 2000 ppm. This could be due to the fact that PVCap at concentrations in the range 1000 to 2000 ppm at 90 bars is a good inhibitor with respect to nucleation for our system. In a previous study [11] on effective inhibitors for natural gas hydrates, it was reported that optimal performance of PVCap depends on a certain concentration at a given pressure. In other words, increasing concentration from 2000 ppm to 3000 ppm, doesn't increase inhibition performance with respect to nucleation, but there was a tremendous increase in the prevention of growth. In general, increasing the concentration of PVCap doesn't always increase inhibition performance. Achieving full inhibition also depends on the degree of subcooling, type of polymer, molecular weight of polymer, and solution agitation [12]. The initial degree of subcooling (12 °C), type of polymer (PVCap), molecular weight (6000), and solution agitation (750 rpm) were all kept the same in all PVCap experiments to examine the effect of concentration change on nucleation of sII hydrates as accurately as possible. Because transporting the reactants to the growing product is a significant factor [13] for hydrate kinetics, PVCap at these concentrations could easily affect this factor by binding to an actively nucleating structure and result in delay for the process.

With regard to inhibition, PVCap was reported to be the best inhibitor as compared to other LDHIs such as polyvinylpyrrolidone (PVP). Experimental [14, 15] and molecular dynamics simulation [16, 17] studies have reported the good performance of PVCap as compared to PVP. Despite its good performance as an inhibitor at high concentrations, it is also a good promoter of sII hydrates at low concentrations. But the promotional effect of PVCap is only at low concentrations depending on system pressure and volume. In our system at 90 bars, PVCap was found to be a good promoter in the range 50 – 500 ppm, and a good inhibitor in the range 1000 – 3000 ppm.

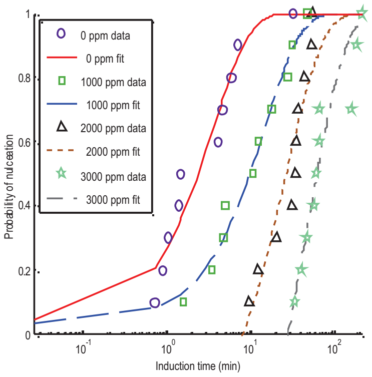

Figure 5. Probability of nucleation versus induction time for 0, 1000, 2000 and 3000 ppm PVCap.

Concentration (ppm)	Nucleation rate (1/min)	Lag time (min)
0	0.27	-0.16
50	1.01	0.02
100	0.88	-0.07
500	0.39	-0.05
1000	0.07	-0.52
2000	0.04	8.27
3000	0.61	29.56

Table 2: Estimated nucleation rate and induction time for 0 – 3000 ppm PVCap.

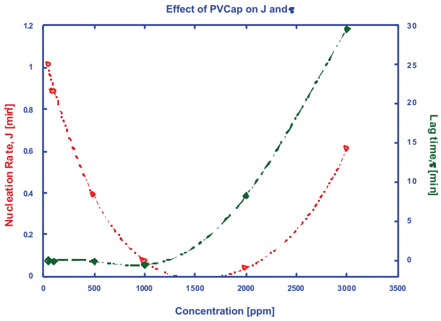

Figure 6. Nucleation rate (left axis, red curve), and lag time (right axis, green curve) as function of PVCap concentration.

CONCLUSION

Structure II gas hydrates were produced from a seven-component synthetic natural gas (SNG7) in the presence of PVCap as an additive. Several concentrations of PVCap in the range between 50 - 3000 ppm were investigated on the effect of sII hydrate nucleation. The experimental results were used to fit the theoretical nucleation probability distribution function. The rate of nucleation and the lag times were estimated for all concentrations of PVCap used. The results showed that PVCap in the range 50-500 ppm has increased rate of nucleation, whereas, the range 1000-2000 ppm has reduced rate of nucleation as compared to the pure water base line experiment. For concentrations in the range 2000 to 3000 ppm, the lag time was considerably increased as compared to the DIW base and all lower concentrations of PVCap. This leads to the conclusion that PVCap at low concentration promotes sII hydrate nucleation but at higher concentrations it inhibits. Thus, the promotional effect of PVCap on sII hydrate nucleation is concentration dependent.

ACKNOWELGMENTS

NFR is greatly acknowledged for the financial support of this work.

REFERENCES

[1] Hammershmidt EG. *Formation of Gas Hydrates in Natural Gas Transmission Lines.* Ind. Eng. Chem. 1934; 26: 851-855.

[2] Kelland MA. *History of the development of low dosage hydrate inhibirors.* Energy Fuels 2006; 20: 825-847.

[3] Sloan E D, Koh CA. *Clathrate Hydrates of Natural Gases.* FL: Boca Raton, 2008.

[4] Larsen R, Knight CA, Sloan ED. *Clathrate Hydrate Growth and Inhibition*. Fluid Phase Equilibria 1998; 150-151: 353-360.

[5] Toschev S, Milchev A, Stoyanov SJ. *On Some Probabilistic Aspects of the Nucleation Process.* Cryst. Growth 1972; 13/14: 123-127.

[6] Tsuchiyama A. *Crystallization Kinetics in the System* $CaMgSi_2O_6$-$CaAl_2Si_2O_8$*: the delay in nucleation of diopside and anorthite*. Am. Mineral 1983; 68: 687-698.

[7] Takeya S, Hori A, Hondoh T, Uchida T. *Freezing-Memory Effect of Water on Nulceation of* CO_2 *Hydrate Crystals.* J. Phys. Chem. B. 2000; 104 (17): 4164-4168.

[8] Abay HK, Svartaas TM. *Effect of Ultralow Concentration of Methanol on Methane Hydrate Formation*. Energy Fuels 2010; 24: 752-757.

[9] Jiang S, Ter Host JH. *Crystal Nucleation Rates from Probability Distributions of Induction Times.* J. Cryst. Growth Des. 2011; 11: 256-261.

[10] Abay HK, Svartaas TM. *Multicomponent Gas Hydrate Nucleation: The Effect of the Cooling Rate and Composition*. Energy Fuels 2011; 25: 42-51.

[11] Lederhos JP, Long JP, Sum A, Christiansen RL, Sloan ED. *Effective kinetic inhibitors for natural gas hydrates.* Chem. Eng. Sci. 1996; 51: 1221-1229.

[12] Larsen R, Knight CA, Sloan ED. *Clathrate hydrate growth and inhibition.* Fluid Phase Equilibria 1998; 150-151: 353-360.

[13] Buch V, Devlin JP, Monreal IA, Cwiklik BJ, Aytemiz NU, Cwiklik L. *Clathrate hydrates with hydrogen-bonding guests.* Phys. Chem. Chem. Phys. 2009; 11: 10245-10265.

[14] Zeng H, Lu H, Huva E, Walker VK, Ripmeester JA. *Differences in nucleator adsorption may explain distinct inhibition activities of two gas hydrate kinetic inhibitors.* Chem. Eng. Sci. 2008; 63: 4026-4029.

[15] Zhang JS, Lo C, Couzis A, Somasundaran P, Wu J, Lee JW. *Adsorption of kinetic inhibitors on clathrate hydrates.* J. Phys. Chem. C 2009; 113: 17418-17420.

[16] Kvamme B, Kuznetsova T, Aasoldsen K. *Molecular dynamics simulations for selection of kinetic hydrate inhibitors.* J. Mol. Graphics and Modeling 2005; 23: 524-536.

[17] Anderson BJ, Tester JW, Borghi GP, Trout BL. *Properties of inhibitors of methane hydrate formation via molecular dynamics simulations.* J. Am. Chem. Soc. 2005; 127: 17852-17862.

Appendix F

Paper VI

The Effect of PVCap on Methane Hydrate Nucleation and Growth

By:

Hailu K. Abay, Jonas Hovland and Thor M. Svartaas.

Printed in:

Proceedings of the 7th International Conference on Gas Hydrates, Edinburgh, United Kingdom, July 17-21, 2011.

Proceedings of the 7th International Conference on Gas Hydrates (ICGH 2011),
Edinburgh, Scotland, United Kingdom, July 17-21, 2011.

THE EFFECT OF PVCAP ON METHANE HYDRATE NUCLEATION AND GROWTH

Hailu K. Abay[1*], Jonas Hovland [1] and Thor M. Svartas[1]
Department of Petroleum Engineering[1]
Faculty of Science and Technology
University of Stavanger
4036, Stavanger
NORWAY

ABSTRACT

PVCap is a kinetic hydrate inhibitor which has recently attracted many researchers as it is an alternative method to the conventional thermodynamic inhibitors such as MeOH and MEG. Six different concentrations of PVCap in the range 20 to 2000 ppm (i.e. 0.002 to 0.2 wt %) were used to investigate the effect on both nucleation and growth of sI hydrate. The hydrates were formed at 90 bars from a pure methane gas (99.9995 %) and distilled water in an isochoric high pressure cell. The probability distribution function and the real gas equation have been used to investigate the effect on nucleation and growth during hydrate formation, respectively. The results show that PVCap has a clear effect on growth based on concentration. However, its effect on the nucleation was not found to be concentration dependent as promotional and inhibition effects were observed which were not as a function of concentration. This could possibly be due to the random phenomenon of newly born critical nuclei in the aqueous phase that could easily attract the PVCap during the nucleation process.

Keywords: gas hydrates, nucleation, growth, kinetic inhibitors, thermodynamic inhibitors

NOMENCLATURE

J	nucleation rate [min^{-1}]
Δn	amount of hydrates formed [mol]
p	probability of nucleation
P	pressure [bar]
ΔP	pressure drop [bar]
T	temperature [^{o}C]
ΔT	degree of subcooling [^{o}C]
t_o	induction time [min]
τ	lag time [min]

INTRODUCTION

Polyvinylcaprolactum (PVCap) is a water-soluble polymer which has been used as a kinetic hydrate inhibitor (KHI). KHIs belong to the class of low-dosage hydrate inhibitors (LDHIs) that have been in commercial use in the oil and gas industry for more than a decade [1]. KHIs work by delaying hydrate nucleation and crystal growth so that there will be plenty of time to transport the hydrate forming fluid to the process facilities before hydrates nucleate, grow and plug the pipeline. PVCap, as one of the most effective KHI, prevents hydrate growth by attaching to a growing crystal surface and preventing further growth. The pendant group of PVCap is very important in achieving strong adsorption [2]. Molecular dynamics simulation studies [3] on selection of kinetic hydrate inhibitors also indicated that the active inhibitor molecules of PVCap that attaches themselves to the hydrate surface are the double-bonded oxygens, the hydroxyle groups, and the nitrogen. Figure 1 shows the chemical structure of PVCap possessing all the inhibitor molecules. A

---

[*] Corresponding author: Phone: +47 51 83 22 30 Fax +47 51 83 20 50 E-mail: hailu.k.abay@uis.no

seven-member lactam ring is attached to a carbon backbone. The lactam ring is characterized by an amide group (-N-C=O) which protrudes from the polymeric backbone. In another study [4] on the adsorption of KHIs on clathrate hydrates, PVCap was also reported as a more effective inhibitor by reducing the diffusion of hydrate formers (gases) from the bulk phase to the hydrate surface where the hydrate growth prefers to proceed.

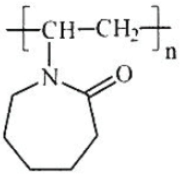

Figure 1. Chemical structure of PVCap.

The inhibition effect of PVCap on hydrate growth has been reported extensively as discussed above, whereas the effect on nucleation was not addressed adequately. In this paper we address the effect of PVCap on the nucleation of methane hydrate. In addition to the major focus on nucleation, the effect of PVCap on the total growth of methane hydrates has been also investigated. The data on the effect of PVCap on the total growth of methane hydrate has been analysed by employing the real gas equation. From the real gas equation, one can easily derive the direct relationship between the amount of hydrates formed and the pressure drop in the system as

$$\Delta n = \frac{V}{zRT}\Delta P \qquad (1)$$

where Δn is the amount of gas consumed when hydrates form, V is the gas volume, z is the compressibility factor, R is the universal gas constant, T is the experimental temperature, and ΔP is the measured experimental pressure drop caused by hydrate formation. Equation (1) could be used to estimate the amount of hydrates formed in an isochoric system [5] by assuming that V/zRT is a constant of proportionality that does not vary much for all PVCap experiments. For the analysis of the data to investigate the effect of PVCap on the nucleation of sI hydrates, the classical theory of nucleation has been employed. According to this theory, the nucleation probability distribution function is given by [5-10]

$$p(t) = 1 - e^{-J(t_0-\tau)} \qquad (2)$$

where $p(t)$ is the probability to obtain an induction time equal with or less than the measured time, t_o, between time zero and time t. J is nucleation rate per unit volume, and τ is the lag time. For the nucleation stage of the process induction time was the major parameter, and for the growth the amount of gas consumed, measured from the pressure drop reading, was the main parameter studied. The following section discusses the experimental setup and procedure for measuring induction time and pressure drop in systems in the presence of PVCap as an additive.

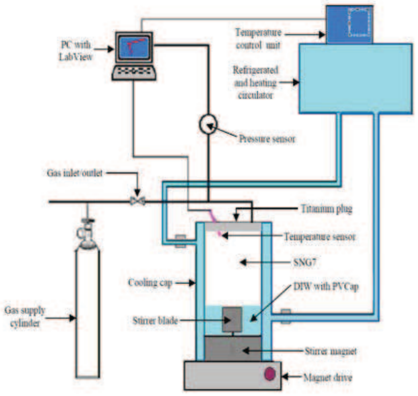

Figure 2. Autoclave cell experimental setup.

EXPERIMENAL METHODS

Experimental setup and procedure: The experimental setup we used for the investigation of PVCap on the nucleation and growth of sI hydrates is illustrated in Figure 2. The major components are the cylindrical cell, the cooling bath, PC, and gas supply cylinder. The cylindrical cell, with inner volume of 145 mL, was used in holding the hydrate forming fluid - distilled water (DIW) and PVCap. PVCap, dry powder with molecular weight 6000, was dissolved in DIW at concentrations of 0, 20, 50, 100, 500, 1000, and 2000 ppm. Pure DIW system without PVCap in solution was considered as the baseline for comparison. In each experiment 50 mL of the cell volume was filled with the actual aqueous solution leaving 95 mL of the cell volume for pressurized methane gas (~90 bars).

The methane gas was accessed directly from the gas supply cylinder whose pressure was controlled by the pressure gauge on the gas cylinder and by another external pressure sensor. After mounting the cell as shown in Figure 2, the cell was charged with test solution and methane to the desired pressure and the system was cooled from an initial temperature of 13.7 °C down to 4 °C with a cooling rate of 10 °C/h. At 4 °C and 90 bar the sub-cooling, ΔT, with reference to hydrate equilibrium is approximately 8 °C. All experiments were initiated at this degree of sub-cooling. The temperature profile was controlled by the refrigerated and heating circulator with interfaced temperature control unit. Figure 3 shows the pressure versus temperature plot of the system during the cooling sequence. Point 1 of the figure represents the initial condition of the system. This initial temperature was about 1.7 °C outside the hydrate equilibrium region of the system at the experimental pressure. The system crosses hydrate equilibrium at point 2, and from point 2 to point 3, the system temperature is inside the hydrate forming region. Once the desired operating temperature at point 3 was attained by cooling, cell agitation was introduced by the start of stirring. The start of stirring was considered as the start of the experiment. A stirring rate of 750 rpm was used for all experiments of PVCap including the pure water base line experiments.

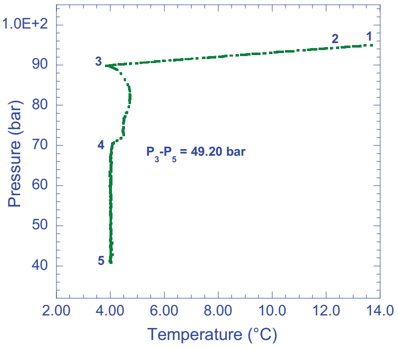

Figure 3. Pressure versus temperature curve during nucleation and growth of sI hydrate.

At point 3, the system may take some time before onset for hydrate formation occurred. Path 3-4-5 shows the hydrate growth region after onset and between points 3 and 4 along this path, the system couldn't restore the operating temperature of the cooling bath because hydrate formation is a fast exothermic reaction releasing heat energy in this section of the experiment. But the system recovers its operating temperature after a while as indicated by path 4-5. The pressure drop from point 3 to point 5 (49.2 bar in this specific graph) has been used to estimate the amount of hydrates formed in the presence of different concentrations of PVCap in accordance with Equation (1). The effect of the additive on the nucleation time was measured at point 3 prior to hydrate formation and growth.

Figure 4 shows the gas consumption and temperature as a function of time from the start of the experiment to the end. During the first step, the gas consumption plot shows a very fast gas intake because of methane gas molecules leaving the gas phase and entering into the liquid phase and filling sI hydrate cavities. This fast growth period is followed by a slow growth period where the system continues to build up gas hydrates slowly.

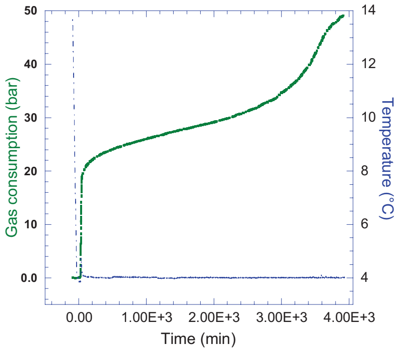

Figure 4. Gas consumption and temperature plots from the start of the experiment to the end illustrating onset and growth of sI hydrates.

The gas consumption onset, or equivalently hydrate formation onset, is accompanied by a temperature pulse. Figure 5 shows the magnified section of Figure 4 during onset. The induction time, the time from the start of stirring at time zero to the onset of hydrate formation (28.12 min in this specific figure), is determined from both the gas consumption plot and the temperature pulse that reflects the exothermic reaction of hydrate formation.

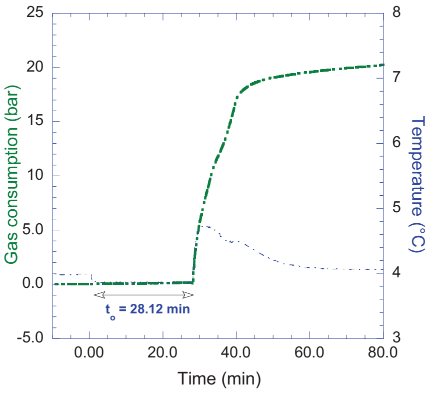

Figure 5. Measurement of induction time from gas consumption curve and temperature pulse at onset of hydrate formation.

RESULTS AND DISCUSSION

Equations (1) and (2) have been respectively used to calculate the amount of sI hydrate formation and the rate of nucleation for each concentration of PVCap. For the estimation of the amount of sI hydrates formation, average pressure drop of each concentration is calculated. This average pressure drop is assumed to be directly proportional with the average amount of gas consumed during the filling of hydrate cavities in the bulk liquid phase. The results are tabulated in the last column of Table 2. The amount of sI hydrates formed for 20 ppm PVCap is nearly the same as the amount of hydrates formed for the pure water system. This shows that PVCap at very low concentrations doesn't affect hydrate growth. However, PVCap concentrations in the range 50-2000 ppm have shown significant differences in the amount of hydrate formation as compared to the 0 ppm PVCap average pressure drop. This indicates that PVCap at higher concentrations affect sI hydrate growth in some way. It is not known whether this effect of PVCap is due to morphological changes affecting the consistency (mechanical strength) leading to stirrer blockage or other factors affecting the conversion of water into hydrates. However, the maximum effect on total gas consumption at 90 bars operating pressure was found at 100 ppm for the cell volume we used. According to the study [11] on effective inhibitors for natural gas hydrates, it was reported that optimal performance of PVCap depends on a certain concentration at a given pressure. The lactam rings of PVCap are believed to adsorb on the growing hydrate crystal. Hydrogen bonding by the amide group plays the major role in blocking further hydrate growth. But increasing the polymer network does not always provide better inhibiting performance though this may depend on system and cell sizes. It is difficult to suggest a reliable explanation of the pressure drop response based on "blind cell" PT studies only. PVCap is known to affect morphology as well as hydrate consistency and apparent hardness (mechanical strength) of the formed hydrates. During experiments with PVCap in another cell (1000 ppm) we observed that reduced pressure drop during hydrate formation could be correlated with stirrer blockage and stop of stirring. For the cell used in the present study there was no free insight into the stirring mechanism, but sensing the magnet field surrounding the stirrer from outside the cell at end of experiment showed that stirrer was blocked. It is therefore believed that the reduced pressure drop is due to formation of a hydrate of a consistency that is harder to crush and stir as compared to the baseline hydrate.

For investigating the effect of PVCap on sI hydrate nucleation, the classical nucleation probability distribution function given by Equation (2) has been employed to fit the experimental data points. Figure 6 shows the probability of nucleation versus induction time for all concentrations of PVCap used including the pure water baseline experiment. As shown in the figure, 20 and 1000 ppm PVCap nucleation probability distribution functions are shifted to the left of the pure water reference distribution curve. The 2000 ppm PVCap probability distribution function is comparable with the pure water baseline experiment. The rest 50, 100, and 500 ppm PVCap concentrations were found to the right of the reference distribution function. The estimated nucleation rate and lag time for all concentrations of PVCap are tabulated in Table 2. The 20, 1000, and 2000 ppm PVCap has increased the rate of nucleation as compared to the 0 ppm PVCap experiments. The 20 ppm PVCap nucleation rate has shown a significant difference from the pure water base line nucleation rate unlike the 1000 and 2000 ppm PVCap experiments. The 50, 100, and 500 PVCap experiments have reduced the rate of nucleation from which the 500 PVCap experiment has shown the significant reduction.

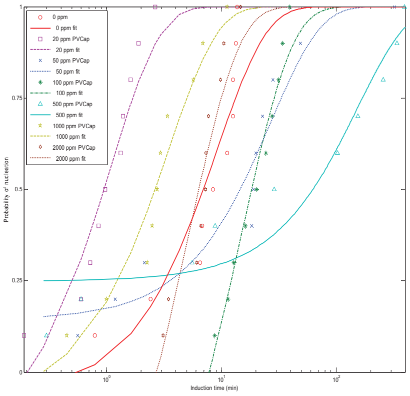

Figure 6. Probability of nucleation versus induction time for all concentrations of PVCap.

The time the system takes to attain a constant rate of nucleation is called the lag time. This lag time is tabulated in Table 2 for all concentrations of PVCap used. For the 50 and 500 ppm solutions a negative lag time as suggested by the analysis means that nucleation has occurred and a constant rate of nucleation is reached before start of stirring. During all experiments the system crosses the hydrate equilibrium curve approx. 82.5 minutes prior to start of stirring and at -44.1 minutes (i.e., lag time of 500 ppm experiments) the system is 6 °C inside the hydrate region. A negative lag time and a low nucleation rate as for the 50 and 500 ppm experiments means that the nucleation process may take place over a broad time span as indicated by the corresponding graphs.

Concentration (ppm)	**Nucleation rate (1/min)**	**Lag time (min)**	**Average P drop (bar)**
0	0.11	0. 60	51.43
20	0.94	0.21	51.15
50	0.04	-4.16	42.05
100	0.07	7.80	25.30
500	0.01	-44.1	29.20
1000	0.29	0.28	29.50
2000	0.19	2.74	28.06

Table 2: Estimated nucleation rate, induction time, and pressure drop for 0 – 2000 ppm PVCap.

The 100 ppm experiments have taken the longest time to attain a constant rate of nucleation. Both the lag time and the rate of nucleation have shown concentration independent effect of PVCap on the nucleation of the system. This could be due to the random nucleation phenomenon occurring in the liquid phase that could easily get the attention of PVCap upon molecule rearrangement for a cavity. Hawtin et. al. [12] observed from MD simulation that long-lived 5^{12}-like cage structure did not exist before the first $5^{12}6^2$ cavity was formed. Thus, it appears that formation of the $5^{12}6^2$ cavity is essential for the methane nucleation process. Increase in the rate of nucleation in the presence of additives has also been reported [13] from molecular dynamics simulation studies on methane hydrate systems. This study shows that LDHIs increase the rate of nucleation when crystals are observed. Once the crystal structures are observed in the bulk volume, they could easily get the attention of the additive and the additive starts promoting the nucleation process. Thus, the promotional effect of PVCap on the nucleation phase is primarily dependent on the random phenomenon of restructuring of water molecules for a crystal. When stable nuclei are formed, the inhibitor can block hydrate growth by adsorbing onto the surface. Thus, the effect on nucleation and growth is part of different mechanisms.

During our experiments no effect on growth rates were observed for PVCap concentrations of 100 ppm or below. At 500 ppm the initial growth rate was considerably reduced over the first 30 seconds from start of growth. At 1000 ppm the exothermic fast growth was delayed by 1 minute and at 2000 ppm the catastrophic growth process was delayed by 2 minutes. Thus the effect on the growth of sI hydrate was found to be concentration dependent. Unlike the nucleation phase, the growth phase of methane hydrates require fast transporting of methane molecules in the active site of the growing crystal. Such transporting of methane molecules to the growing crystal is a major parameter for hydrate kinetics [14]. This major factor could easily be affected by the presence of PVCap in the crystal forming region. Subramanian and Sloan [15] showed the formation of the large $5^{12}6^2$ cavity of sI methane hydrate during the post nucleation growth stage is the time limiting step and that 200 ppm (i.e., 0.02 wt%) PVCap significantly reduced the formation of hydrate cavities, especially the large $5^{12}6^2$ cavity. So, on one hand PVCap may promote methane hydrate nucleation and on the other hand reduce growth probably blocking growth sites involved in the formation of the large $5^{12}6^2$ cavity.

CONCLUSION

Methane hydrates were produced in a stirred high pressure cell apparatus. Polyvinylcaprolactam (PVCap) has been used to study its effect on both nucleation and growth of sI hydrates. The real gas equation and the classical probability distribution functions have been employed to analyze the experimental data. The analysis showed that PVCap has a clear effect on the growth part of methane hydrate formation depending on concentration. However, on the nucleation phase of methane hydrate formation, the promotion or inhibition effects of PVCap were primarily dependent on the random nature of newly born critical nuclei that could make the PVCap start acting on the system. The latter result was also supported by molecular dynamics simulation studies.

ACKNOWELGMENTS

We are thankful to NFR for the financial support of this work.

REFERENCES

[1] Kelland MA. *History of the development of low dosage hydrate inhibitors.* Energy Fuels 2006; 20: 825-847.

[2] Larsen R, Knight CA, Sloan ED. *Clathrate Hydrate Growth and Inhibition*. Fluid Phase Equilibria 1998; 150-151: 353-360.

[3] Kvamme B, Kuznetsova T, Aasoldsen K. *Molecular dynamics simulations for selection of kinetic hydrate inhibitors.* J. Mol. Graphics and Modeling 2005; 23: 524-536.

[4] Zhang JS, Lo C, Couzis A, Somasundaran P, Wu J, Lee JW. *Adsorption of kinetic inhibitors on clathrate hydrates.* J. Phys. Chem. C 2009; 113: 17418-17420.

[5] Abay HK, Svartaas TM. *Effect of Ultralow Concentration of Methanol on Methane Hydrate Formation*. Energy Fuels 2010; 24: 752-757.

[6] Toschev S, Milchev A, Stoyanov SJ. *On Some Probabilistic Aspects of the Nucleation Process*. Cryst. Growth 1972; 13/14: 123-127.

[7] Tsuchiyama A. *Crystallization Kinetics in the System $CaMgSi_2O_6$-$CaAl_2Si_2O_8$: the delay in nucleation of diopside and anorthite*. Am. Mineral 1983; 68: 687-698.

[8] Takeya S, Hori A, Hondoh T, Uchida T. *Freezing-Memory Effect of Water on Nucleation of CO_2 Hydrate Crystals*. J. Phys. Chem. B. 2000; 104 (17): 4164-4168.

[9] Shanfeng J, Joop HTH. *Crystal Nucleation Rates from Probability Distributions of Induction Times*. Cryst. Growth & Design. 2010; Inpress.

[10] Abay HK, Svartaas TM. *Multicomponent Gas Hydrate Nucleation: The Effect of the Cooling Rate and Composition*. Energy Fuels 2011; 25: 42-51.

[11] Lederhos JP, Long JP, Sum A, Christiansen RL, Sloan ED. *Effective kinetic inhibitors for natural gas hydrates.* Chem. Eng. Sci. 1996; 51: 1221-1229.

[12] Hawtin RW, Quigley D, Rodger PM, *Gas hydrate nucleation and cage formation at a water/methane interface*. Phys. Chem. Chem. Phys. 2008; 10: 4853-4864.

[13] Hawtin JM, Rodger PM. *Polydispersity in Oligomeric Low Dosage Gas Hydrate Inhibitors*. J. Mater. Chem. 2006; 16:1934-1942.

[14] Buch V, Devlin JP, Monreal IA, Cwiklik BJ, Aytemiz NU, Cwiklik L. *Clathrate hydrates with hydrogen-bonding guests.* Phys. Chem. Chem. Phys. 2009; 11: 10245-10265.

[15] Subramanian S, Sloan ED. *Molecular measurements of methane hydrate formation*. Fluid Phase Equilibria. 1999; 158-160: 813- 820.